Republic of Iraq
Ministry of Higher Education
and Scientific Research

DEVELOPING A MODEL FOR THERMODYNAMIC ANALYSIS OF A HYDROGEN-OXYGEN FUEL CELL

A Thesis

Submitted to the College of Engineering of the University of Babylon in Partial Fulfillment of the Requirements for the Degree of Master of Science in Mechanical Engineering (Power)

By

QUSAY RASHID AL- HAGAG

(B.Sc. , 1996)

May , 2005

بسم الله الرحمن الرحيم

اقرأ باسم ربك الذي خلق * خلق الإنسان من علق* اقرأ وربك الأكرم * الذي علم بالقلم * علم الإنسان ما لم يعلم *

صدق الله العظيم
العلق (الآية ١-٥)

Acknowledgements

First of all, all thanks are due to **ALLAH** who gave me the ability and desire to complete this research work.

I would like to express my deepest appreciation to **Dr. Haroun A.K. Shahad** for his guidance and supervision throughout the duration of this project. I would also like to express my appreciation to the staff of the Department of Mechanical Engineering in the college of Engineering at Babylon University.

Furthermore, deepest thanks to my friends for their help to accomplish this study, especially Nawras, Mraoui and Maher.

Last but not least, I would like to thank **my parents** for making my education is possible. They have supported me in everything that I have done and I am grateful for that.

Qusay

2005

EXAMINING CERTIFICATE

We certify that we have read this thesis entitled "***DEVELOPING A MODEL FOR THERMODYNAMIC ANALYSIS OF A HYDROGEN-OXYGEN FUEL CELL***" and as an examining committee, examined the student, " ***QUSAY RASHID ABD AL- AMER***", in its contents and that in our opinion it meets standard of a thesis for the degree of Master of Science in Mechanical Engineering.

Signature:
Name: Asst. Prof.
Dr. Haroun A.k. Shahad
(Supervisor)
Date: / / 2005

Signature:
Name:
Dr.
(Member)
Date: / / 2005

Signature:
Name:
Dr.
(Member)
Date: / / 2005

Signature:
Name:
Dr.
(Chairman)
Date: / / 2005

Approval of the Mechanical Engineering Department.
Head of the Mecanical Engineering Department.

Signature:
Name:
Dr.
Date: / / 2005

Approval of College of Engineering.
Dean of the College of Engineering.

Signature:
Name: Asst. Prof.
Dr. Haroun A.K. Shahad
Date: / / 2005

CERTIFICATION

I certify that this thesis titled ***''DEVELOPING A MODEL FOR THERMODYNAMIC ANALYSIS OF A HYDROGEN-OXYGEN FUEL CELL''*** was prepared by **QUSAY RASHID** under my supervision at College of Engineering, **University of Babylon** in partial fulfillment of the requirements for the degree of Master of Science in Mechanical Engineering.

Signature:

Name: Asst. Prof.

Dr. Haroun A.K. Shahad

Date: / /2005

Acknowledgements

First of all, all thanks are due to **ALLAH** who gave me the ability and desire to complete this research work.

I would like to express my deepest appreciation to **Dr. Haroun A.K. Shahad** for his guidance and supervision throughout the duration of this project. I would also like to express my appreciation to the staff of the Department of Mechanical Engineering in the college of Engineering at Babylon University.

Furthermore, deepest thanks to my friends for their help to accomplish this study, especially Nawras, Mraoui and Maher.

Last but not least, I would like to thank **my parents** for making my education is possible. They have supported me in everything that I have done and I am grateful for that.

Qusay

2005

CHAPTER 1

INTRODUCTION

1.1 General :

The hope of technology is to provide utility and comfort with no damage to the user or to the surroundings. For many years now, petroleum products and other fossil fuels have given us utility and comfort in a variety of areas, but are blamed for such disasters as lung disease and global warming. Also, the fears of depleting the petroleum supply demand that new energy sources be developed to take its place. With the advent of fuel cell technology, a large step is being made to reduce emission and to improve the efficiency of power production, while using alternative energy sources. With recent improvement in power density - especially in Polymer Electrolyte Membrane Fuel Cell, it is becoming possible to use this technology in automobiles.

Fuel cells are electrochemical devices that convert chemical energy of the reactants directly into electricity and heat with high efficiency. Electrochemical processes in fuel cells are not governed by ***carnot's law*** and therefore high operating temperature is not necessary for achieving high efficiency. Furthermore, contrary to

internal combustion engines, the efficiency of fuel cell is not strongly dependent on operation power.

The fuel cell uses hydrogen (or hydrocarbon) as a fuel and oxygen (or air) as an oxidizer. Each gas is introduced at a high pressure into a channel; the two channels are separated from each other by membrane electrode assumbly. The membrane electrode assumbly has a gas diffusion backing on either side of the membrane (electrolyte); which may be solid or liquid. Solid polymer (eg.Nafion), porous ceramic (Zirconia oxide), and alkaline solutions (potassium hydroxide) have been successfully used as electrolytes. When a solid electrolyte is used, its surface is first provided with a catalyst to facilitate the ion migration process. When a liquid electrolyte is used, separate electrodes are necessary. The electrical load is connected between the anode (hydrogen side) and the cathode (oxygen side) [1].

Fuel cells have several highly attractive characteristics. The efficiency of a fuel cell can be higher than efficiency of conventional energy conversion processes and the performance remains good even at partial loads. The only waste product is oxidized fuel. Normally, the fuel is hydrogen and consequently, the product is water. Carbon dioxide may be present as well, if a hydrocarbon fuel is used. Furthermore, the lack of moving parts (silence) in the energy converter and modular design make the maintenance easier. Due to modular design and rapid respond to load changes, fuel cell technology can be used in a wide range of applications: stationary such as (Power plants, Home use, Hospitals and Hotels), enclosed environments such as (space station, space vehicles), and motive transportation such as (personal vehicles (zero-emission vehicle (ZEV)), military vehicles) [2]. Finally, fuel cells can use many different types of fuel such as natural gas, propane, landfill gas, diesel, methanol, and hydrogen. This versatility ensures that the use fuel cells will not be affected due to the unavailability of certain fuel.

There are five main classes of fuel cell. The properties of these five types are summarized below in table 1, with each taking the name of electrolyte used in its fabrication.

Table 1.Characteristics of the Primary Fuel Cell Classes, Ref. [3] .

	PEMFC	AFC	PAFC	MCFC	SOFC
Electrolyte	Solid polymer ionic membrane (Nafion)	Potassium Hydroxide (KOH)	Concentrate Phosphoric Acid (H_3PO_4)	Molten Sodium, Potassium and Carbonates $(Na,K)_2CO_3$	Zirconium Dioxide ceramic $(Zr,Y)O_{2-}$
Temperature(^0C)	50 – 100	50 – 200	180 – 220	600 – 700	850 – 1000
Charge Carrier	H^+	OH^-	H^+	CO_3^-	O^{2-}
Catalyst	Platinum	Platinum	Platinum	Nickel	Nickel zirconia
Cell Hardware	Carbon- Based	Carbon- Based	Graphite – Based	Stainless Steel	Ceramic
Main Advantages	Fast starting High power density Solid electrolyte Reduce corrosion problems	Cheap materials High performance	Relatively tolerant to fuel impurities High efficiency	High efficiency Fuel flexibility, can use co & natural gas Cheap catalysts	High efficiency Fuel flexibility Cheap catalysts Solid electrolyte advantage
Main Disadvantages	Sensitive to fuel impurities Expensive materials	Expensive catalysts Very sensitive to Fuel impurities Corrosive electrolyte	Expensive materials Corrosion problems Low operation life Low power density	High temperature Enhances corrosion And component breakdown	Fragile materials High temperature Enhances component breakdown
Power density (kW/m^2)	3.5 – 6.5	0.7 – 8.1	0.8 – 1.9	0.1 – 1.5	1.5 – 2.6
Reforming	External	External	External	External or internal	External or internal

These five classes of fuel cell can essentially be further grouped into one of two classes, distinguished as either low temperature fuel cells(AFC, PEMFC, PAFC), or high temperature fuel cells(MCFC, SOFC), Ref. [3].

1. 2 Polymer Electrolyte Membrane Fuel Cells.

A polymer Electrolyte Membrane Fuel Cells (PEMFC) or an equivalent term (Proton Exchange Membrane Fuel Cell, Polymer Electrolyte Fuel Cell, Solid Polymer Fuel Cell and Solid Polymer Electrolyte Fuel Cell) is a fuel cell that uses a thin ion conducting solid electrolyte. A solid electrolyte (polymer electrolyte membrane) has its advantages over liquid electrolytes in that it has a high power density, less corrosion and separation of electrodes are required [4]. The low temperature of these

cells ensure a quick start up time and its wide application range includes the transport industry. One of the drawbacks to PEMFC's in the past was the fact that they required expensive platinum metal catalysts. Development in recent years mean that only minute amounts of platinum are now used and therefore the cost of platinum is now a small part of the total price of a PEMFC. The large number of application for PEMFC is mainly due to enormous power range and versatility of the fuel cell. The power range is from a few watts to several hundred kilowatts, with temperature only ranging from 25 ^{0}C to 100 ^{0}C. PEMFC's are particularly suited to the transport industry because they can start quickly due to a low operating temperature, no corrosive fluid hazards, and small in size[5] and the cell can work in any orientation. These factors and the potential for PEMFC's to produce zero emission's create a great prospect for clean energy in the transport industry.

A normal PEM fuel cell will produce (0.7-1) volt. To create a large system the area of each cell (A) can be increased and several cell units can be connected in series to create a stack. The output voltage depends on the voltage of each cell and the number of cells in the stack. A typical PEMFC stack structure is shown in Figure (1 – 1).

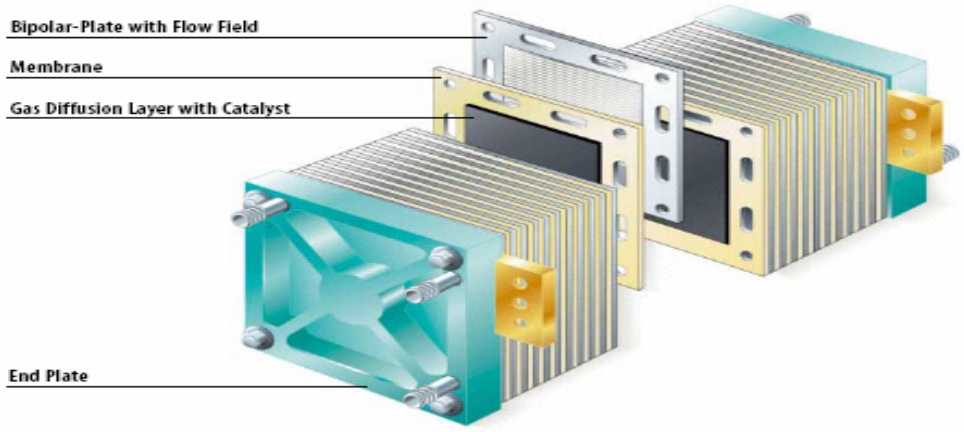

Figure(1 – 1):Typical Fuel Cell Stack, Ref.[5]

A fuel cell system includes a fuel cell stack and auxiliary component: air blower control system, inverter, heat exchanger and sometimes a compressor as seen in appendix B[6].

1.2.1 Basic Principles of Operation.

PEM fuel cells use hydrogen and oxygen to produce electricity, heat and water. The physics of the PEM fuel cell can be considered as the opposite of electrolysis. In electrolysis an electric current is passed through water to produce hydrogen and oxygen. In a fuel cell, hydrogen and oxygen gases are passed either side of the polymer electrolyte membrane which produces an electric current, heat and water. The electrochemical reactions for the PEM fuel cell are shown below[7].

$$anode \quad reaction \quad H_2 \rightarrow 2H^+ + 2e^- \qquad V^0_{anode} = 0.000volt \qquad .....(1.1)$$

$$cathode \quad reaction \quad O_2 + 4H^+ + 4e^- \rightarrow 2H_2O \qquad V^0_{cathode} = 1.229volt \qquad .....(1.2)$$

$$overall \quad reaction \quad \frac{1}{2}O_2(g) + H_2(g) \rightarrow H_2O(l) + Electricity(DC) + Heat \qquad .....(1.3)$$

A PEMFC primarily consist of three components: a negatively charged electrode (cathode), a positively charged electrode(anode), and a polymer electrolyte membrane. The simple chemistry of the fuel cell involves hydrogen being ionized on the anode and oxygen reduced on the cathode. Protons (H^+) are transported from the anode to the cathode through the polymer electrolyte membrane and electrons are carried to the cathode through an external circuit. On the cathode, oxygen react with protons and electrons forming water and producing heat. Both the anode and cathode contain a catalyst layer, usually platinum (Pt), to speed up the electro-chemical process. The basic PEM fuel cell operation is seen from Fig.(1-2) [6].

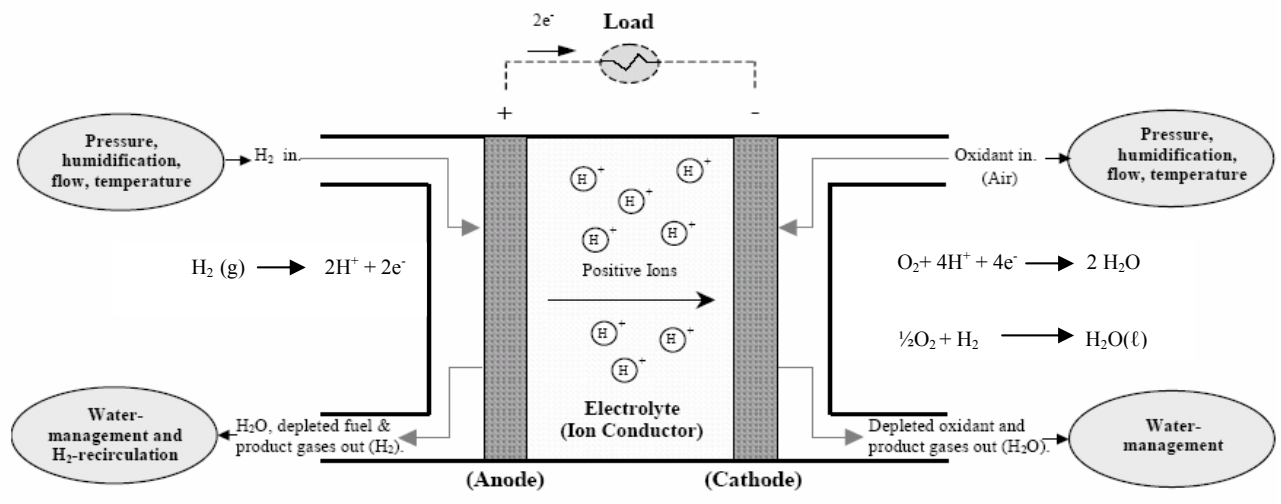

Figure (1 - 2): Schematic principle of single PEM fuel cell, Ref.[6]

If the platinum catalyst is taken into account, the oxidation process and reduction process which take place at the anode and cathode respectively, as follow[8].

at anode $H_2 + Pt \longrightarrow Pt\cdots H_{2,ads}$ .....(1.1)

$Pt\cdots H_{2,ads} + H_2O \longrightarrow Pt + 2e^- + 2H_2O\cdots H^+$ ..... (1.2)

at cathode $H_2O\cdots H^+ + Pt + 2e^- \longrightarrow Pt\cdots H^+ + H_2O$ .....(1.3)

$1/2O_2 + Pt \longrightarrow Pt = O$ .....(1.4)

$2Pt\cdots H^+ + Pt = O \longrightarrow 3Pt + H_2O$ .....(1.5)

Where Pt is solid platinum catalyst and $H_{2,ads}$ is adsorbed hydrogen. As can be seen by above expression, the hetrogeneous conversion take place in two steps. First, the hydrogen molecule bonds with the catalyst in a surface (or chemical adsorption) reaction Eq.(1.4) that increases the rate of the overall process. Second, each hydrogen atom is adesorbed from the catalyst and separated into proton and an electron Eq.(1.5). At the cathode side oxygen is reduced to water in presence of protons, electrons on platinum catalyst surface. This reaction mechanism is more complicated and less understood. This is a multi-step, multi-species reaction, which is very difficult to characterize in terms of electrochemistry[9]. The Pt catalyst strongly affects the oxidation taking place at the anode electrode. It has less influence on the rate of the reduction reaction, taking place at the cathode electrode. Therefore, the loading of the Pt is typically higher on the cathode side than the anode. Current, platinum use is about 0.1 mg /cm^2 in the anode and 0.5 mg /cm^2 in the cathode [10]. However, even with the higher loading, it turns out that the reduction reaction at the cathode is a limiting reaction for fuel cell stack operation.

1.2.2 Fuel Cell Components.

1.2.2.1 Polymer Electrolyte Membrane.

The electrolyte membrane allows proton conduction to complete the electric circuit in fuel cell. It also has several other key functions. The membrane prevent electron conduction so the electricity flows through the external circuit that is through

the load. Ideally, the membrane prevents any hydrogen or oxygen molecules from being transported through it. The most common used material in PEMFC prototypes is ***Nafion*** (a polytetrafluoroethylene (PTFE) chain with side chains terminating in an SO_3H group or is a perfluorosulfonic acid (PFSA)). It is made with various thickness which are shown in appendix A (table1). The chemical structure of the Nafion membrane material is shown in Figure(1–3).

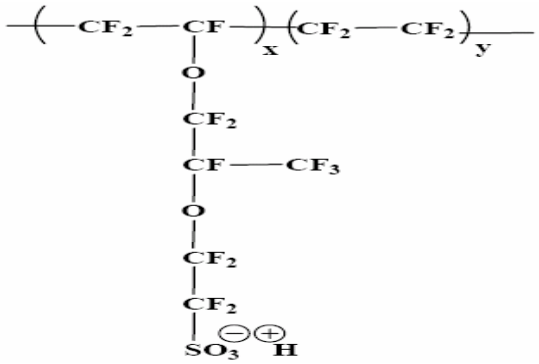

Figure (1 – 3): Chemical structure of Nafion, Ref.[10]

Nafion consists of three regions

A-The Teflon – like flourocarbon backbone, hundreds of repeating ─CF_2─CF─CF_2─ units in length (hydrophobic),

B -The side chains, ─ O ─ CF_2─ CF─ O ─ CF_2 ─ CF_2 ─ which connect the molecules backbone to the third region,

C-The ion groups(clusters)consisting of sulfonic acid ions, $SO_3^-H^+$ (hydrophilic)[10]. These regions are depicted in Figure (1 - 4).

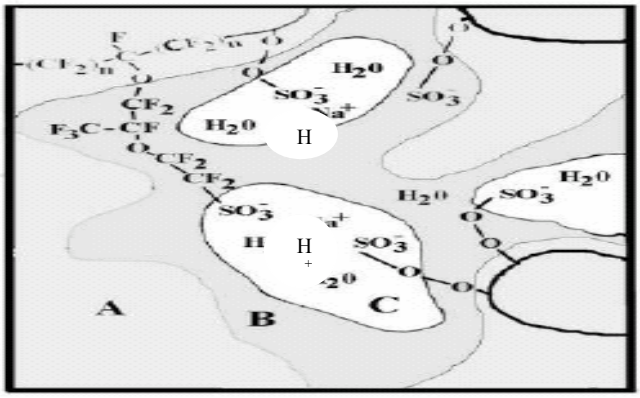

Figure(1 - 4): Three phase model of Nafion; a flurocarbon on region A, interfacial zone B, and an ionic cluster region C, Ref.[10]

The essential features of Nafion are [8]:

• They are highly chemical resistant.

• They are mechanically strong and can be constructed into thin films.

• They can absorb large quantities of water (up to 50% by weight).

• They allow good transport of H^+ ions when well hydrated .

• They are acidic.

The ion selectivity of a PEM is the result of it's unique structure, mainly the presence of SO_3^-H side groups when the membrane is fully hydrated, the negatvely charged SO^-_3 groups serve as fixed charge sites that attract positive hydrogen ions Fig. (1-5). It is believed that the protons jump from one negative site to another while moving along the membrane pore. The flow of ions across the electrolyte membrane is assumed to be one dimensional [12].

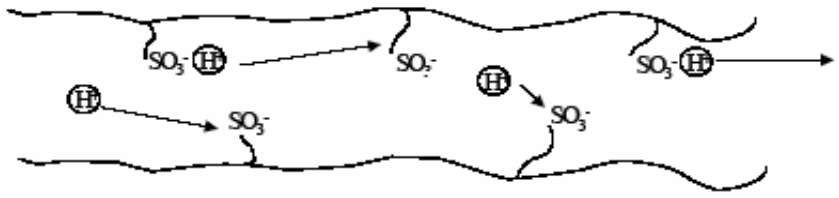

Figure(1 - 5): Hydrated PEM, Ref.[12]

Polymer electrolyte membrane must be hydrated to be conductive. This limits the operating temperature of PEM fuel cells to the boiling point of water and makes water management a key issue in PEM fuel cell development.

1.2.2.2 Electrodes.

All electrochemical reactions take place on the electrode surfaces. To speed up cell reactions, electrodes contain catalyst particles, virtually always platinum or an alloy of platinum and other nobel metals. Low operating temperature makes the use of catalysts necessary [7], especially for the cathode reaction which is very slow if catalyst is not present.

The electrodes are usually made of porous mixture of carbon supported platinum and ionomer. In order to be able to catalyze reactions, catalyst particles must have contact to both protonic and electronic conductors. Furthermore, there must be passages for reactants to reach the catalyst sites and for reaction products to exit. The conducting point of the reactants, catalyst and electrolyte is conventionally referred to as the three phase interface (Fig.(1-6 a)). In order to achieve acceptable reaction rates, the ***effective area*** of the active catalyst sites must be several times higher than the ***geometrical area*** of the electrode. Therefore, the electrode must be a three dimensional porous network of catalyst particles, electronic and protonic conductors and passages open for gas transport. Nowaday, most PEMFC developers have chosen the thin-film approach, in which the electrodes are manufactured directly on the membrane surface, for their product prototypes. The benefits of thin – film electrode include lower price, better utilization of catalyst and improved mass transport [13]. The thickness of a thin-film electrode is typically 5–15 μm and the catalyst loading is between (0.1 – 0.3) mg /cm^2. The shape of electrode is shown in Figs.(1 – 6 b&c).

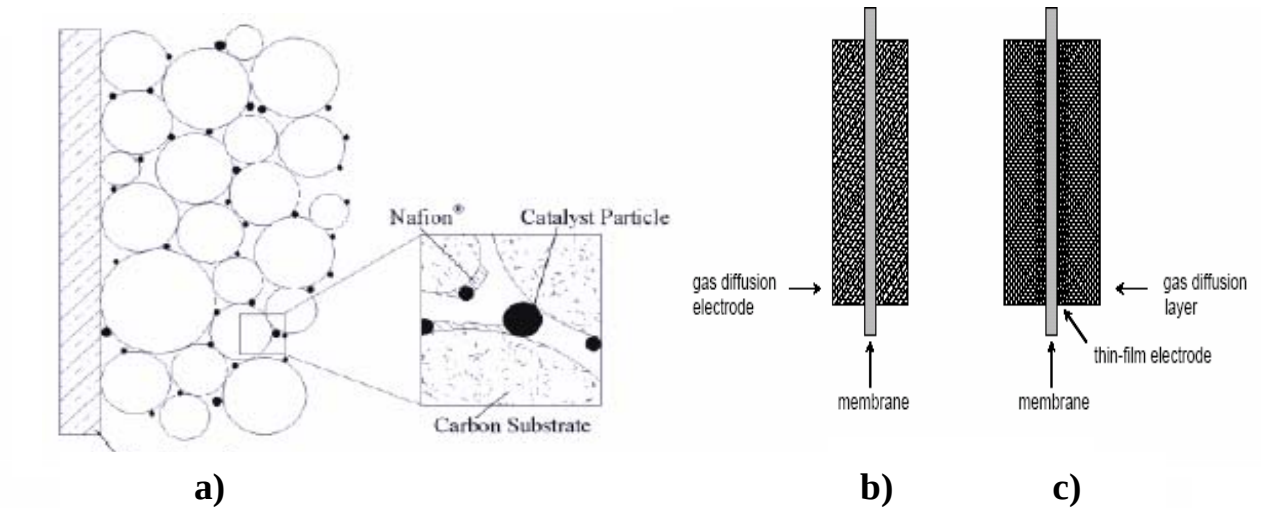

Figure(1 - 6): a)The three phase boundary formed by the catalyst particles, the ionomer and the gas phase in a porous structure, ensuring both electronic and ionic contact. Different MEA structure: b) gas diffusion electrodes c) thin-film electrodes, Ref. [11]

1.2.2.3 Gas Diffusion Backings.

The gas diffusion backing (also gas diffusion media; electrode backing; diffuser and uncatalyzed gas diffusion electrode) is made of a sufficiently porous and

electrically conductive material. The most common materials are carbon cloths and carbon papers. The gas diffusion backings are characterized by their thickness (the typical thickness of commerical products is 300–400μm), and the presence of hydrophobic and hydrophilic regions[13]. In a PEM fuel cell, the membrane electrode assembly (MEA) has a gas diffusion backing on either side of the membrane. This provides three main functions, firstly, it makes an electrical contact between the bipolar plates; secondly, the diffusion backing also distributes the hydrogen and air (oxygen) to the electrodes; and lastly, allows the product water to flow between the electrode and the flow channels.

1.2.2.4 Bipolar Plate.

Most fuel cells, also other types than PEMFC, consist of a stack structure with bipolar plates, also called separator plates or flow field plates, separating the reactants of adjacent unit cells. They also serve as current collectors and from supporting structure of the stack. One face of bipolar forms the anode compartment of one unit cell and the other side is the cathode compartment of the adjacent unit cell. In a unit cell, separator plats have flow channels only on one side and are sometimes called monopolar plates. The total voltage of a stack is determined by the number of unit cells and the current by the active area of the unit cells as in Figure (1 – 7).

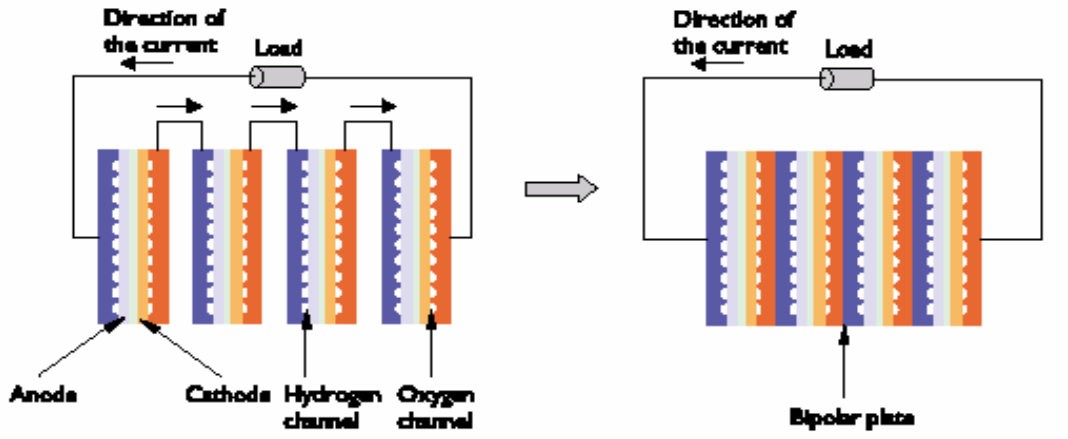

Figure (1 – 7):Sketch of a bipolar fuel cell stack, Ref. [8]

The requirement for a bipolar plate material are high conductivity, and be impermeable to gases. Due to the presence of reactant gases and catalyst, the material

should be corrosion resistant and chemically inert [7]. It should also be cheap and suitable for high volume manufacturing methods.

Most PEMFC bipolar plates are made of hydrophilic resin* impregnated graphite, but also stainless steel has been used [5]. Solid graphite is highly conductive , chemically inert and resistant to corrosion, but expensive and costly to manufacture. Stainless steel is very available, but expensive to machine. In addition, stainless steel must often be coated to prevent corrosion. The bipolar plates are typically have flow channels on their surfaces. The channel geometry may be different on the anode and on the cathode. Flow directions on the electrodes may also be different in relation to each other. In addition to co-flow, also counter flow and cross flow patterns are possible. The choice and optimization of the flow field geometry of the bipolar plates affects strongly the performance of the PEMFC, especially through water management and the distribution of gases to the electrodes [13]. The basic channel types are shown in Figure (1 – 8).

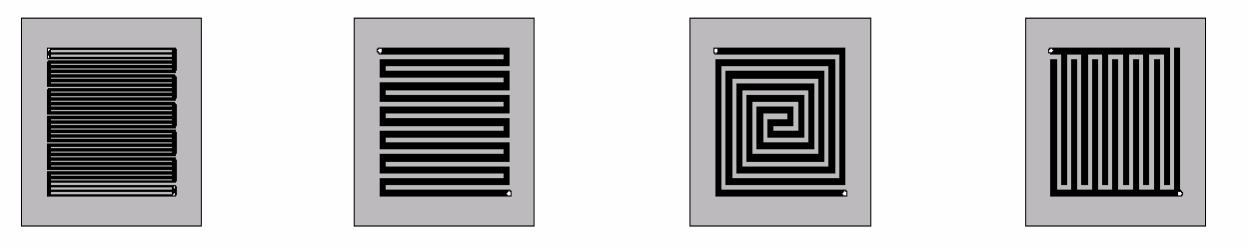

Figure(1 - 8):The channel geometries evaluated in the measurements: the original Globe Tech geometry, the serpentine geometry, the spiral geometry and the discontinuous channels geometry, respectively, Ref. [13]

1.2.3 The Polarization Curve

The reversible open circuit voltage of a H_2/O_2 fuel cell at a temperature of 25 °C and pressure of 1 atm is 1.229 V, assuming that the produced water is remains in liquid state. Practical open circuit voltages are lower because of mixed potentials, which may be due to, for example, impurities in the anode gas or molecular hydrogen diffusing to the cathode. The effect of the latter phenomenon increases

* Hydrophilic resin is used to enhance liquid water transfer.

when extremely thin membranes are used, as it is usually the case in small fuel cells. The open circuit potential depends on the activities of the reactants, and therefore, it is lower when air is used on the cathode instead of pure oxygen. When current is drawn from the cell, various losses begin to arise. These losses are commonly classified to three types:

I- Activation losses which are caused by limited reaction rates at the surface of the electrodes, and is dominant at low current density and increases *marginally* with an increase in current density. It is called an activation loss because it relates to the activation energy required at both the anode and cathode of the fuel cell.

II- Ohmic losses which are caused by the resistance to the flow of ions(protons) in the electrolyte and to the transfer of electrons through the electrode materials. This loss is directly proportional to the current density. It is dominant in the middle section of the polarization curve.

III- Concentration (mass transport) losses is caused by a loss of concentration of the fuel or oxidant at the surface of the electrodes. This loss becomes important at the higher currents when the fuel and oxidant are used at higher rates and the concentration in the gas channel is at a minimum. This is sometimes called the diffusion loss . The polarization curve of a PEMFC usually consists of three distinct regions, which result from the three types of losses. The typical shape of the polarization curve is shown in Figure (1 - 9).

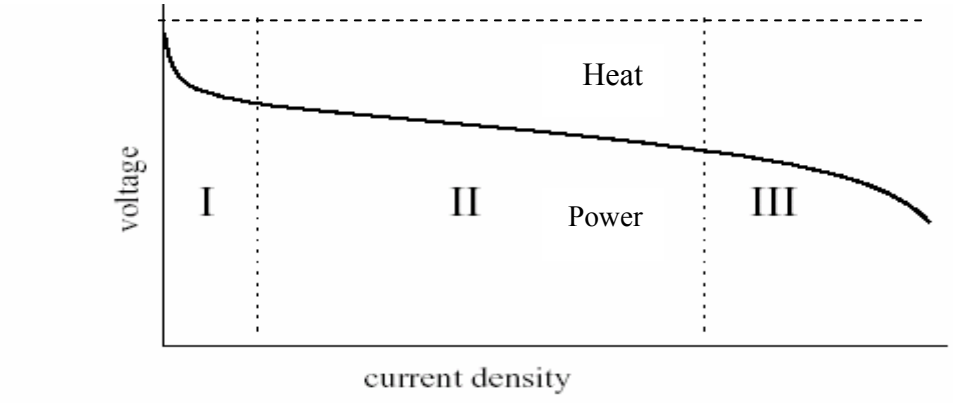

Figure(1–9): The typical polarization curve of a PEMFC. The regions dominated by different Losses are indicated: I- activation losses; II- ohmic (IR) losses; III- mass transport losses.

1.3 Objective and Scope of the Present Work

The objective of this work is divided into two parts. The first part is to analyze thermodynamically a PEM fuel cell and to examine factors which affect fuel cell performance such as :

• type and thickness of the polymer membrane.

• operation conditions (temperature, pressure and humidification of the reactant gases).

• electrode kinetics, i.e, electrode structure and catalyst loading .

The second part is to solve the equations governing the heat, mass and charge transfer in a PEMFC to study the membrane performance for different operating conditions.

1.4 Layout of the Thesis.

This thesis consists of six chapters. After this introductory chapter, **C**hapter **T**wo is concerned with a brief literature review and background of losses of PEM fuel cell. The basic reactions and the essential characteristics of this fuel cell type are explained in this chapter. The analytical part of the work is described in **C**hapter **T**hree which includes discussions on different losses and factors affecting the performance of the cell. **C**hapter **F**our is concerned with a computer program, which is constructed to perform all calculations based on the theoretical analysis. The results of the work are summarized in **C**hapter **F**ive. Finally, in **C**hapter **S**ix, conclusions are drawn and an outline for future work is presented.

CHAPTER 2

LITERATURE REVIEW

2.1 Introduction.

The invention of the fuel cell is widely attributed to ***Sir William Grove.*** In 1837, he discovered that mixing hydrogen and oxygen in the presence of an electrolyte produces electricity and water. The same phenomenon had been observed already in 1802 by ***N. Gutherot*** [14], but somewhat unfairly, he was not been credited for his discovery. The term "Fuel Cell" was coined in 1889 by ***L.Mond*** and ***C.Langer***, who attempted to develop a fuel cell that uses industrial coal gas and air. Researchers has since attempted to model the performance of the fuel cell for an insight into the improved design and application of the fuel cell. Much of the modeling centers on the fuel cell's polarisation curve, that is, the relationship between the voltage output to load currents.

2.2 Model Review.

The steady state performance of the fuel cell stack is expressed by the polarisation curve, which is a graph of the voltage versus the load current for a given set of operating conditions. A steady state model can be used to predict the polarisation curve. The present PEM fuel cell models can be divided into two categories, ***analytical and empirical***. Analytical models are based on theory while

empirical models are based on experimentation. Unfortunately, the performance of a PEM fuel cell is extremely difficult to be completely modelled analytically. Its performance depends on many variables. These include temperature, pressure, current, water content of the membrane, stoichiometry of the inlet gases, etc. Additionally, many of the variables that influence performance are inter-related. For this reason, empirical models were introduced. In general, these models are only accurate over small ranges of operating conditions. Both analytical and empirical models require experimental data. The empirical model uses the measured data to fit the fuel cell's performance to a described equation form, and the analytical model depends on experimental data to investigate the model's accuracy.

Proton exchange membrane fuel cells are highly complicated systems. The measure of performance is most often associated with PEMFC polarization curve, which describes the output voltage over a range of current densities for a specific set of operating conditions. The operating voltage is governed by the thermodynamic equilibrium potential and the losses in the system.

2.2.1 Analytical Model Review.

The analytical model can be classified as either simple or complex. Simple models examine the operation of fuel cell stack voltage in respect to the maximum theoretical voltage and the major voltage losses. Complex models use more detailed techniques and require detailed information on the materials and makeup of the fuel cell stack. Generally, the analytical models attempt to model the operation of the fuel cell by short equations that predict the reversible voltage and any losses. These models are based around the reversible voltage and major losses. Some earlier work by groups in 1968 (eg. Berger) set the groundwork for the major losses and the theoretical background.

Berger [15], summarized the understanding of the fuel cell theory and experimentation up to the date of publication. A number of terms and analysis were given that are still relevent today. The basic structure of fuel cell modeling was

outlined. The reversible voltage and the activation, ohmic and concentration losses were described. The reversible voltage was given in the same form that is used today for low temperature PEM fuel cell models. The book relates the theoretical maximum voltage to the temperature of the fuel cell and partial pressure of the reactants. The reversible voltage also required the knowledge of values of constants consisting of the universal gas constant, Faraday's constant; the change in Gibbs free energy at STP and the molar entropy of fuel cell reaction equation (2.1). This equation describes the reversible voltage of each cell and is still used in existing fuel cell modeling [15].

$$V_{rev} = 1.229 + (4.308 * 10^{-5})\, T \ln\{ P_{H2}(P_{O2})^{0.5} \} - (8.453 * 10^{-4})(T - 298.15) \quad \ldots\ldots\ldots (2.1)$$

The ***Tafel*** equation was also used to model the activation loss. One of the forms of the Tafel loss is:

$$V_{act} = A_T \ln\left[\frac{I}{I_0}\right] \quad \ldots\ldots\ldots (2.2)$$

Where A_T was initially described as an empirical constant, I, is the cell current and I_0 is the exchange current (the current that flows back and forth for the reversible reactions at each electrode).

Gregor Hoogers.[16], outlined the operation of fuel cells with respect to the reversible voltage and four losses, namely the activation, ohmic, concentration and fuel crossover losses. The fuel crossover loss described here as a loss relating to the wasted fuel that passes through the electrolyte without producing an external current. It is also used to model electron transfer through the electrolyte. A lot of time is devoted to give a theoretical background to the reversible voltage and the losses.

Maggio et al.[17], gave a different approach to the concentration loss. They called it the diffusional loss and added the convection loss that is usually assumed to be zero. They found that the convection loss is around 1% of the total losses

in the PEM fuel cell when the fuel cell had a high and low load. Most researchers disregard this loss as well. Mass transport loss mostly comprises of a concentration loss so these terms are often interchangeable in fuel cell modeling. Concentration loss is usually derived from ***Nernst*** diffusion layer thickness called ***Fick first law*** :

$$V_{con} = -B\ln\left[1 - \frac{I}{I_L}\right] \qquad \text{.....(2.3)}$$

Where B is empirical constant, I is the cell current and I_L a limiting current which is the current at the a point when the gas is used at a rate equal to the maximum supply speed (see section 3.3.4). This loss is used in many models althrough the strict dependence on the important operating conditions (stoichiometry, pressure, humidity and temperature) is unclear. The theoretical value of B is (RT / 2F) for the hydrogen gas and (RT / 4F) for oxygen.

2.2.2 Empirical Model Review.

Because of the complexity and interdependence of variables on the performance of the fuel cell an empirical equation is required to predict the polarisation curve of the fuel cell stack for a given set of operating conditions. It's disadvantage is that the polarisation curve must be recalculated for any change in an operating condition (eg. Humidity). This reliance on experimental data is the major disadvantage for empirical models. For example, an empirical model has omitted the temperature from the modelled activation loss, but if the temperature of fuel cell was changed from 45^0C to 55^0C then an entire set of experimental measurements would have to be made to develop a new empirical model for the prediction of the polarisation curve. A comprehensive empirical model will be needed to identify the correct dependence of the most important performance factors that is the temperature, pressure, stoich-iometry, relative humidity and current of the fuel cell[5].

Kim et al.[18], presented an empirical equation that gave an accurate prediction of the polarisation curve. This equation is given below,

$$V_{cell} = V_{o,k} - R_{cell,k}\, I - b_k \ln(I) - m_k \exp(n_k I) \qquad \text{.....(2.4)}$$

Where: V_{cell} is cell voltage (mV), I is current density(A/cm^2), $R_{cell,k}$ is ohmic resistance (Ω.cm^2), b_k is Tafel slope (mV/decade), m_k is concentration loss coefficient (mV), $V_{o,k}$ is open circuit potential of the cell (mV), and n_k is concentration loss coefficient (cm^2/mA).

Although initially the empirical equation mentioned did not give a detailed consideration of the physical relevance of the model terms, the terms in the equation can be seen to represent all the possible losses in the fuel cell. This gave a fit of the polarisation curve (see Fig.(2-1)) but must be recalculated for difference operating conditions (eg: hydrogen stoichiometry).

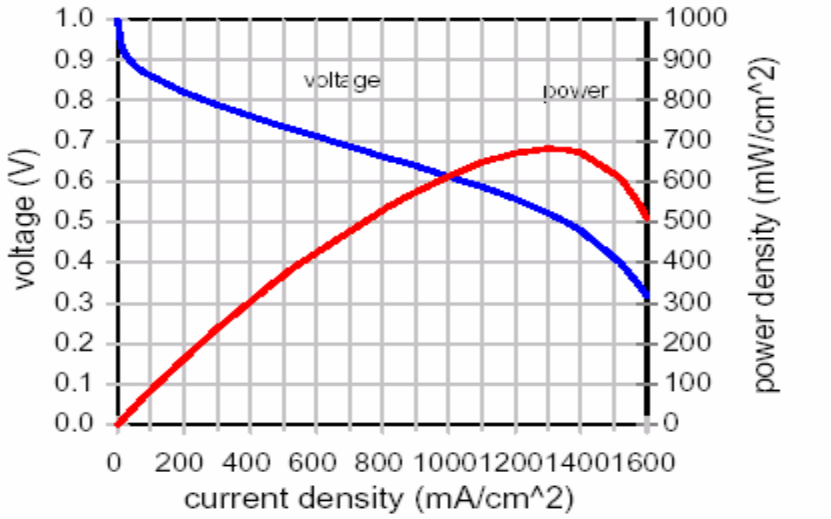

Figure(2 – 1): Empirical Fit of Polarisation Curve, Ref. [18]

Shapiro [19], presented in his book an empirical equation of polarisation curve.

$$V = 1.03 - 0.06 * \ln(1000I) - (1.12 - 2.49T)I + 0.14 * \ln(PO_2) + (T - 333)0.00041 * \ln(1000I) \quad ....(2.5)$$

wherePO_2: average partial pressure of oxygen (atm).

This equation gives the voltage of each fuel cell based on the current, temperature, and oxygen levels available. Note that higher voltages result from low current densities, high temperatures, and high oxygen partial pressure. The first term in equation (2.5) stands for the open circuit voltage 1.03 volts. The second term is the result of the Tafel equation, which is a measure of the overpotential (loss) of the fuel cell due to the activation energy, the third is the ohmic loss term, the fourth term accounts for the

effect of the changes in oxygen partial pressure and finally, the last term is an additional temperature effect.

Amphlett et al. [20], related the open circuit voltage to the operating temperature and the reactant partial pressure. They used the Butler Volmer equation and an expression for the exchange current to derive expressions for the anodic and cathodic activation overvoltages that depend on the temperature, oxygen concentration , and current. They define the ohmic resistance losses as a sum of the losses from electron transfer through the electrode and proton transfer across the membrane. They take great care to derive the ohmic resistance of the membrane with respect to the proton concentration, temperature, and current. The final expression for the ohmic losses is so complicated that the authors propose using the analytical model only to gain an insight into the important variables required to create an effective empirical model. They found an empirical equation for each parameter and for the entire IR_{Loss}. This technique is used as a supplement to analytical models. Following this the empirical form of the ohmic loss is,

$$V_{ohm} = I (\varepsilon_1 + \varepsilon_2 I + \varepsilon_3 T) \quad \text{.....(2.6)}$$

where: ε_1, ε_2 and ε_3 are empirical coefficients for V_{ohm} .

Empirical modeling techniques are also used for developing an equivalent circuit that can model the dynamic performance of the fuel cell stack. This technique uses the experimental procedures of current interruption and Electro-chemical Impedance Spectroscopy (EIS). Current interruption method is more straightforward than the AC impedance method , since the magnitude of ohmic loss can be obtained directly from the data. The AC impedance method reveals more information about the cell, but the analysis of the data is more complicated, because resistance is not measured directly, i.e. the resistance is not a function of terminal voltage[5].

2.2.2.1 **Experimental Techniques:** Current Interruption method.

The principle of the current interruption method is to interrupt the current flow and observe the voltage transient. When the current is interrupted, the potential drop caused by ohmic resistance vanishes almost immediately. The relaxation rate of electrochemical and diffusion loss is considerably slower [21]. Therefore, the **free voltage** can be ideally obtained by measuring the voltage with an appropriate delay after the current interruption. The ideal transient is depicted in Figure(2 – 2). The ohmic loss is the difference between the **free voltage** and the operating voltage. The resistance can be calculated from the ohmic loss using **ohm law**.

$$R_R = \frac{\Delta E}{I} = \frac{(free \quad voltage) - (operation \quad voltage)}{current \quad density} \qquad \text{.....(2.7)}$$

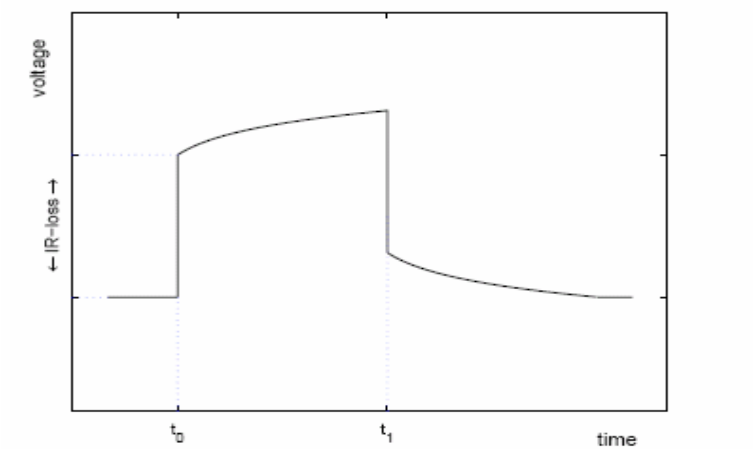

Figure(2 – 2): Voltage transient after the current interruption in an ideal fuel cell, Ref.[21]

In figure (2 – 2), the cell is first operated at a fixed current. At $t = t_0$, the current flow is interruption and the ohmic losses vanish almost immediately. After the current flow is interrupted, electrochemical losses start to relax and the voltage rises logarthmically toward the open circuit voltage. At $t = t_1$, the current is switched back on and the losses are observed to reappear. Using current interruption method at very low current densities is difficult, since the amplitude of the noise will be comparable to the difference between the operating current and open circuit current. Furthermore, constructing an interruptier that produces clean current decays on the required

nanosecond scale at high currents is difficult. The current interrupt method can be applied by using a ***Digital Storage Oscilloscope*** (DSO) as shown in figure(2–3).

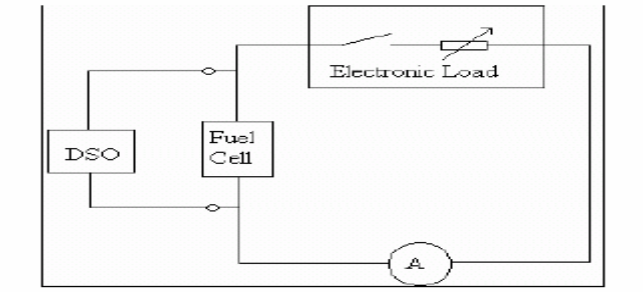

Figure(2 – 3): Current Interruption Test set- up, Ref. [21]

$$V_{act} = V_{open\ circuit} - IR_{free\ voltage} \quad \text{.....(2.8)}$$

2.2.3 Miscellaneous Models Review.

Most current fuel cell models have been developed to only individually address the PEMFC performance issues. The experimental data and mathematical models found in the literature are valid only under specific assumptions and idealized conditions that often times are unrealistic. Nevertheless, the mathematical modeling of a PEMFC are summarized below.

Springer, Zawodzinski and Gottesfeld [22], showed that the cell voltage could also be reduced when membrane water content is low due to anode dehydration. They concluded that maintaining a high water flux from the cathode to the anode lowered the membrane resistance, which increased the cell voltage. Also, they argued that the convective transport for water is limited to the drag force on water molecules due to proton flux. The ***Springer et al.*** model of PEM is summarized in appendixA, table(4).

Bernardi and Verbrugge [23], developed a comprehensive steady state, isotherm-al, one dimensional model of the physical and electrochemical processes in a PEMFC and applied it to investigating factors that limit cell performance, such as the porosity and volume fraction of the electrode available for gas transport. They claim that due to capillary forces, the liquid and gas pressure evolve separately within the backing

layer. This important assumption implies that the gas and liquid phases are not in equilibrium within the cathode backing layer. Their model is valid for fully hydrated membranes only, and they do not take into account the drag force on water molecules due to proton flux. In addition, their model is unable to predict the flooding due to liquid water in the cathode backing layer and the polarization curve diverges from experimental data for high current densities. AppendixA, table(5) presents a summary of this model.

Parthasarathy et al. [24], presented experimental results for many of the kinetic and mass transport parameters required for modeling the oxygen reduction reaction at the fuel cell cathode (Appendix A,Table 6). They used a microelectrode, consisting of a thin platinum wire encased in Nafion, to simulate the catalyst layer of a proton exchange membrane fuel cell. They present results for the Tafel slope, exchange current density, circuit voltage, and solubility and diffusivity of oxygen in Nafion for temperatures ranging from 30 ^{0}C to 80 ^{0}C. The tests were conducted with an applied oxygen pressure of 5 atm. The results for exchange current density show an increase in magnitude with temperature as well as with operating current. At low currents, there is an oxide layer present on the catalyst that reduces the exchange current density, this oxide layer is not present at high currents. The transfer coefficient also increases with temperature as does the open circuit voltage. The solubility of oxygen in Nafion decreases with temperature while the diffusion coefficient increases.

Genevey et al. [25], presented a comprehensive model of the cathode catalyst layer. The model is based on an agglomerate catalyst layer structure and includes the transport of thermal energy, gas species, liquid water, and charge. In addition, the model is transient and can be used to illustrate how the various transport processes occurring within the catalyst layer behave over time. The authors presented results showing how catalyst layer structural properties, porosity and reaction surface area in particular, affect performance. The model requires careful specification of boundary conditions on both the membrane and gas diffusion layer (GDL) boundaries. In

addition, it is necessary to specify a limiting cell current density. The ***Genevey et al.*** model of PEM is summarized in appendixA, table(7).

Siegel et al. [26], used a two-dimensional along-the-channel-model to evaluate fuel cell performance at 80^0C, but at a pressure higher than atmospheric pressure with an assumption of fully humidified reactant gases. Siegel et al. focused on modeling operating regimes where mass transport phenomena was dominant, and included mass transport between vapor and liquid. The model was then solved numerically with a CFD program and the results were evaluated against experimental results. Siegel observed that with fully saturated inlet gases, the loss of performance observed at higher current densities was due to mass transfer limitations associated with the accumulation of water in the cathode gas diffusion layer. Furthermore, the electro-osmotic drag can decrease water content and conductivity at the anode, as well as increase the water saturation of the cathode gas diffusion layer, restricting reactant gas permeability through cathode. This model is summarized in appendix A, table (8).

CHAPTER 3

MATHEMATICAL ANALYSIS

3.1 Introduction.

Analytical models focus on the theoretical voltage potential of the fuel cell and the major losses. These losses are the activation, ohmic and concentration losses. A model is developed to study the performance of PEMFC and the effect of several variable on this performance. In addition, the equations governing the heat, mass and charge transfer in a PEMFC are solved, to study the membrane performance for different operating conditions.

Many previous analytical models are developed [27] but did not deal with water content in the membrane. It is assumed in this model, that the gas flow rate and the design of the gas flow fields are sufficient to guarantee removal of excess liquid water. The membrane is assumed to be well hydrated without being flooded. The option for humidification of the hydrogen gas is a precautionary measure. These facts which are combined with the practical values of the hydrogen relative humidity should ensure that the stack has a well hydrated membrane as required. If the membrane is too dry the operation of the fuel cell should be stopped as this can damage the membrane. One checking technique for determining this problem is to perform a ***current interrupt*** test when the load current is set to a new level.

The water content in the membrane primarily depends on the relative humidity and mass flows of the air and hydrogen. The relative humidity of the air is the least

significant of these. If the temperature of the stack is beyond the recommended limit of 80^0C, the stack may have water management problems because the water in the membrane would be in a vapor phase.

3 . 2 Analysis of Performance of Reversible PEMFC.

3.2.1 Assumptions

The model presented here is based on the following assumptions:

1- The fuel cell operates under steady state conditions.

2- The gases are ideal for the pressure variation.

3- The temperature of the fuel cell is constant at all points in the fuel cell stack.

4- The product consists of pure liquid water and no steam content.

5- The membrane is considered impermeable to gases and crossover of reactant gases is neglected (no internal current).

6- Assuming that P_{H_2O} for water is 1 atm.

7- $\Delta\bar{g}_T \cong \Delta\bar{h}_{298.15K} - T\Delta\bar{s}_{298.15K}$, i.e. the fuel cell variations are isothermal plus the change in the molar enthalpy and the change in molar entropy at varying temperature are equal to their value at the standard temperature.

3.2.2 Modeling Equations

The reversible cell voltage (V_{rev}) is the maximum theoretical voltage of the cell. The maximum cell voltage is derived from the maximum amount of energy that is available to do useful work, that is the change in Gibbs free energy per mole. This is independent of the load on the fuel cell. The ***Nernst*** voltage (V_{Nernst}) is the theoretical voltage when the fuel cell is operating at the standard temperature 298 K. The reactants pressure variations are included in V_{Nernst} . The temperature variation will be described later.

$$V_{rev} = V_{Nernst} + V_{Temp} \qquad \text{.....(3.1)}$$

Larminie and Dicks [28], gave a detailed description of the reversible voltage. The reversible voltage for a reaction is defined as the maximum chemical energy

available for electrical work divided by the electrical charge transferred in the process as follows:

$$V_{rev} = \frac{-\Delta \bar{g}_f}{2F} \qquad \text{.....(3.2)}$$

where: $\Delta \bar{g}_f$ is the change in Gibbs free energy of formation per mole, F is Faraday's constant(96485.3 C/mol). The Gibbs free energy is the energy available to do external work, neglecting any work done by changes in pressure and /or volume[28]. Free energy earns its name because it is the energy that is available or free for conversion into usable energy [3].

Michael Mozurkewich [29], stated that the change in Gibbs free energy Δg is one of the most important concepts in thermodynamics. Δg is the criterion for deciding whether or not a change of any kind will tend to occur in reaction. Chemical reactions that have a negative value of Δg under the accommodating conditions are spontaneous, a positive value tells us that the reverse reaction tends to occur, whereas a zero value implies equilibrium. The overall fuel cell reaction, for example:

$$H_2(g) + \frac{1}{2} O_2(g) \rightarrow H_2O(l)$$

is likely to occur in the presence of a catalyst, and Δg always has a negative value. $\Delta \bar{g}_f$ changes for different molecular states of the materials in the fuel cell and at different fuel cell temperature as shown in table (2), appendix A[30].

The reversible voltage is more complex than it seems at first inspection. As stated the change in Gibbs free energy varies when the pressure of the reactants (H_2 and O_2) changes and when the fuel cell is operating at different temperatures. When looking at the reversible voltage Eq.(3.2), the complexity of it resides in Gibbs free energy of formation per mole. In the operation of the hydrogen fuel cell two moles, $2N_A$ electrons are conducted in the external circuit for each mole of H_2 and half mole of O_2 is used. One mole of H_2 and half mole of O_2 are used to produce a mole of H_2O and two mole of electrons. Therefore the charge that will flow in the external circuit in this case is:

$$\text{Total Charge} = \text{Number of electrons} * \text{charge of electron}$$
$$= 2N_A * -e = -2\,N_A * e$$
$$= -2F \quad [C/mol] \qquad \ldots\ldots\ldots\ldots(3.3)$$

where N_A is Avagadro's number.

Remembering that the Faraday's constant is the charge of one mole of electrons.

In theory, the power generated by a single fuel cell is simply the reversible potential times the number of electrons generated per second (i.e, the current) [31]. In the other word, the electrical energy is the electrical work done in moving the charge - 2F.

$$\text{Electrical work} = \text{charge} * \text{voltage}$$
$$= -2F * V_{rev}$$
$$= \Delta\bar{g}_f \qquad \ldots\ldots\ldots\ldots(3.4)$$

3. 2. 2.1 Effect of Partial Pressure Variation.

The pressures of the products and reactants play a part in affecting the reversible voltage of the fuel cell. Basically increasing the pressure of the reactants increases the amount of reactants on the surface of the electrodes and so increases the chemical activity. The change in Gibbs free energy varies with partial pressures and temperatures of the fuel cell. This in turn changes the reversible voltage of each cell. The effect of variation of $\Delta\bar{g}_f$ from its standard value will be described.

The use of Nernst equation of a H_2 / O_2 fuel cell in terms of partial pressures of reactants and products is widely reported in literature [7].

$$V_{Nernst} = V^0 + \frac{RT}{2F}\ln\left[\frac{P_{H_2}\left(P_{O_2}\right)^{\frac{1}{2}}}{P_{H_2O}}\left(\frac{1}{P^0}\right)^{\frac{1}{2}}\right] \qquad \ldots\ldots\ldots\ldots(3.5)$$

A short derivation of Eq.(3.5) can be found in [30], as is summarised below. In the ideal gas case the thermodynamic term, activity is defined as:

$$a = \frac{P_i}{P^0} \qquad \ldots\ldots\ldots\ldots(3.6)$$

where: P_i = Partial pressure of the gas, P^0 =Standard pressure, 101.3 kPa

A physical interpretation of the Gibbs free energy is more accessible when ΔGs are expressed in terms of electrochemical activities. As described in [30], the change in Gibbs free energy of formation per mole can be described in term of activity.

$$\Delta\bar{g}_f = \Delta\bar{g}_f^{0} - RT\ln\left[\frac{a_{H_2}\left(a_{O_2}\right)^{\frac{1}{2}}}{a_{H_2O}}\right] \qquad \text{.....(3.7)}$$

where: $\Delta\bar{g}_f^{0}$ = Change in Gibbs free energy of formation per mole at STP($-237.2*10^3$) J/mol. Substituting Eq.(3.6) into Eq.(3.7) we get :

$$\Delta\bar{g}_f = \Delta\bar{g}_f^{0} - RT\ln\left[\frac{P_{H_2}\left(P_{O_2}\right)^{\frac{1}{2}}}{P_{H_2O}}\left(\frac{1}{P^0}\right)^{\frac{1}{2}}\right] \qquad \text{.....(3.8)}$$

By using $V^0 = \left(\frac{-\Delta\bar{g}_f^{0}}{2F}\right)$ and substituting Eq.(3.8), into Eq.(3.2) we get equation (3.5),

$$V_{Nernst} = V^0 + \frac{RT}{2F}\ln\left[\frac{P_{H_2}\left(P_{O_2}\right)^{\frac{1}{2}}}{P_{H_2O}}\left(\frac{1}{P^0}\right)^{\frac{1}{2}}\right]$$

This gives the reversible voltage at the standard temperature and varying pressure.

Most references[28,30] use the partial pressure of water in the fuel cell, P_{H_2O} as one atm. Because, liquid water is the main product H_2O can be assumed to be 1 atm. If this assumption is made, standard values are used and all partial pressure values are in atmospheres then the reversible voltage at the standard temperature reduces to:

$$V_{Nernst} = 1.229 + \frac{RT}{2F}\ln\left[P_{H_2}\left(P_{O_2}\right)^{\frac{1}{2}}\right] \qquad \text{.....(3.9)}$$

3. 2. 2.1 Effect of Temperature Variation.

Most literatures calculate the variation in V_{rev} due to a change in temperature (V_{Temp}) using an assumption that is applicable for low temperature PEM fuel cells (25^0C to 80^0C). More accurate method of calculating V_{Temp} in fuel cell has been included and the researcher explains how this method is simplified using the low temperature assumption already used by[28].

The Gibbs free energy can be defined as a function of enthalpy, entropy and the temperature :

$$\bar{g}_f = \bar{h}_f - T\bar{s}_f \qquad \text{.....(3.10)}$$

The change in $\bar{g}_f$ is :

$$\Delta\bar{g}_f = \Delta\bar{h}_f - T\Delta\bar{s}_f - \bar{s}\Delta T \qquad \text{..... (3.11)}$$

If the chemical reaction is at a constant temperature (isothermal), then the change in Gibbs free energy can be simplified. In a fuel cell, the chemical reaction can be considered to be at a constant temperature, then the last term in Eq.(3.11) will be neglected. Remember the value of $\Delta\bar{g}_f$ is still different for different temperatures as shown by the ($T\Delta\bar{s}$) term. The change in Gibbs free energy of formation in a reaction per mole is then:

$$\Delta\bar{g}_f = \Delta\bar{h}_f - T\Delta\bar{s}_f \qquad \text{.....(3.12)}$$

At the standard temperature 298.15K this equation becomes:

$$\Delta\bar{g}_{298.15k} = \Delta\bar{h}_{298.15k} - T\Delta\bar{s}_{298.15k} \qquad \text{.....(3.13)}$$

Substituting the standard values for $\Delta\bar{h}_{298.15k}$ and $\Delta\bar{s}_{298.15k}$ in the above equation gives:

$$\Delta\bar{g}_{298.15k} = -237.2 * 10^3 \quad J/mol$$

Another form of the Eq.(3.12) is as below:

$$\Delta\bar{g}_T = \Delta\bar{h}_T - T\Delta\bar{s}_T \qquad \text{.....(3.14)}$$

Although $\Delta\bar{h}_T$ and $\Delta\bar{s}_T$ are required to calculate $\Delta\bar{g}_T$. ***Brady and Holum*** [32] described how these are calculated " The magnitudes of $\Delta\bar{h}_T$ and $\Delta\bar{s}_T$ for a reaction are relatively insensitive to the temperature. This is because the enthalpies and entropies of *both* the reactants and products increase about equally with increasing temperature, so their difference, $\Delta\bar{h}_T$ and $\Delta\bar{s}_T$, remain nearly the same. As a result, it can use $\Delta\bar{h}_{298.15k}$ and $\Delta\bar{s}_{298.15k}$ as reasonable approximations of $\Delta\bar{h}_T$ and $\Delta\bar{s}_T$" This means that $\Delta\bar{g}_T$ can be written as:

$$\Delta\bar{g}_T \cong \Delta\bar{h}_{298.15K} - T\Delta\bar{s}_{298.15K} \qquad \text{.....(3.15)}$$

since $\Delta\bar{g}^{0}_{f} = \Delta\bar{h}_{298.15K} - 298.15 * \Delta\bar{s}_{298.15K}$, then the effect of temperature on $\Delta\bar{g}^{0}_{f}$ can be shown by[33]:

$$\begin{aligned}\Delta\bar{g}_{f}(T) &= \Delta\bar{g}_{T} - \Delta\bar{g}^{0}_{f} \\ &= \Delta\bar{h}_{298.15K} - T\Delta\bar{s}_{298.15K} - (\Delta\bar{h}_{298.15K} - 298.15 * \Delta\bar{s}_{298.15K}) \\ &= -(T - 298.15)\Delta\bar{s}_{298.15K} \end{aligned} \quad \ldots\ldots\ldots\ldots(3.16)$$

Using $V_{Temp} = \dfrac{-\Delta\bar{g}_{f}(T)}{2F}$, Ref.[28], the voltage difference of V_{rev} at different temperatures can be written as follows:

$$V_{Temp} = \frac{\Delta\bar{s}_{298.15k}}{2F}(T - 298.15) \quad \ldots\ldots\ldots\ldots(3.17)$$

Substituting Eq.(3.17) and Eq.(3.5) in Eq.(3.1), gives:

$$V_{rev} = \frac{-\Delta\bar{g}^{o}_{f}}{2F} + \frac{RT}{2F}\ln\left[\frac{P_{H_2}(P_{O_2})^{\frac{1}{2}}}{P_{H_2O}}\left(\frac{1}{P^{0}}\right)^{\frac{1}{2}}\right] + \frac{\Delta\bar{s}_{298.15k}}{2F}(T - 298.15) \quad \ldots\ldots\ldots\ldots(3.18)$$

Because the entropy change for the H_2/O_2 reaction is negative, the reversible voltage of the H_2/O_2 fuel cell decreases with an increase in temperature (assuming reaction product is liquid water)[3].

The equation above can be simplified using the following data,

- Using the standard values($\Delta\bar{g}^{0}_{f}$, *R, T,* $\Delta\bar{s}_{298.15k}$) given in table 3,appendix A.
- Using the pressure units of atm for all partial pressures.
- Assuming that P_{H_2O} for water is 1 atm.

$$V_{rev} = 1.229 + (4.308 * 10^{-5})T * \ln\left[P_{H_2}\left(P_{O_2}\right)^{1/2}\right] - (8.453 * 10^{-4})(T - 298.15) \quad \ldots\ldots..(3.19)$$

3 . 3 Actual Performance of the PEMFC.

3 . 3. 1 Open Circuit Voltage(Potential).

The open circuit voltage of a real PEMFC is always lower than the reversible cell voltage. This is mainly caused by three factors, which are activation loss of the cathode reactions, impurities on the catalyst surfaces, and side reactions.

Parathsarthy et al. [10], concluded that the low exchange current density of the oxygen reduction reaction, i.e the high activation energy required for reduction of oxygen, contributes to the decrease in potential. The exchange current density at the anode side is **five** orders of magnitude higher than the cathode side [8]. The open circuit voltage which was illustrated by Ref. [14] can be expressed as:

$$V_{OC} = V_{rev} + \frac{RT}{4\alpha F}\log I_{0,C} \qquad \text{.....(3.20)}$$

Bockris and Srinivasan [34], concluded that the main cause of lowered open circuit voltage is impurities that cause reduction reactions at the cathode. Possible impurities include all species that react electrochemically on platinum surfaces at the operating conditions of PEMFC, even including hydrogen that has diffused from the anode.

3. 3. 2 Activation Loss.

The activation loss occurs since the chemical process initially needs activation energy to insure that the reaction tends toward the formation of water and electricity, as opposed to the reverse reaction. This loss only occurs at low current densities in low temperature fuel cell [3]. These losses are basically representative of a loss of overall voltage at the expense of forcing the reaction to completion, i.e, forcing the hydrogen to split into electrons and protons, and the protons to travel through the electrolyte membrane, and then combine with the oxygen and returning electrons. This loss is often termed overpotential (also known as overvoltage and polarization.), and is essentially the voltage difference between the two terminals. Through

experimentation ***Tafel*** was able to describe mathematically these losses. In 1905 Tafel observed that this voltage loss is proportional to the logarithmic of current. The activation voltage loss of one cell is described as:

$$V_{act} = A_T \ln\left(\frac{I}{I_0}\right) = A_T \ln\left(\frac{i}{i_0}\right) \qquad \text{.....(3.21)}$$

where :A_T= Tafel slope,

The units for the current density and exchange current density are often quoted in mA/cm^2 or A/cm^2. The cell current depends on the area (the size) of the cell. In the tafel equation these terms are combined to form a ratio and same units are used for both, this is not important. Because of this fact it does not matter if current or current density is used in equation (3.21). Note that this equation only holds for $i \rangle i_0$. If i was smaller than i_0 then the activation losses term would be negative, indicating again in voltage instead of a loss.

Consider the reaction at the cathode, shown in Eq.(2.2). At zero current there is really an equilibrium between the products and the reactants, so the forward and backward reaction occur as shown in the following equation:

Cathode reaction $O_2 + 4H^+ + 4e^- \longleftrightarrow 2H_2O$

The current that occurs in this equilibrium reaction is called the exchange current. It is the current that continually ***transpires*** between the products and reactants. When the cathode reaction in equation(1.2)moves in one particular direction (i.e. to the right) then the reaction is shifting. If the reaction is quite active there will be a higher value of (i_0) and the losses involved in changing an existing reaction will be less than starting a slow reaction. It can be seen from this that a high exchange current density is ***desired***. The exchange current is the dominant factor in the activation loss. The value of A_T plays a secondary role. In the case of the anode reaction the exchange current is much larger and thus produces a small loss compared to the cathode reaction. For a typical low pressure PEMFC operating at ambient pressure I_0 for the hydrogen anode would be between (0.1 – 100) mA/cm^2.

The cathode exchange current is about 10^{-5} times smaller [8]. As stated the anode reaction is more active and has smaller losses compared to the cathode. That is why the activation loss of the anode is often neglected.

As discussed previously, the constant A_T has been given theoretical justification and it can be given as [30].

$$A_T = \frac{RT}{2\alpha F} \qquad \text{……..(3.22)}$$

The charge transfer coefficient (α) will be related to the shape of the free energy barrier [35]. However, it is just an experimental factor. Its value is between 0 and 1 depending on the type reaction and electrode material. When the current is low for example, the electrochemical reaction at the electrode is at a set rate, when the load current increases, the rate at which the electrochemical reaction takes place must also increase. Increasing the temperature of the fuel cell will increase the constant A_T as shown in Eq.(3.22). *The minimising effect of increasing the temperature of the cell on i_0 will be dominated.* Therefore, the effect of raising the temperature will increase the activation loss as seen with PEM fuel cell operated at a higher temperature.

Ideally the exchange current i_0 can be experimentally found for a range of operating conditions such as fuel partial pressure, stoichiometry and fuel cell temperature. The electrochemical reactions occur at each electrode, so there will be an activation loss at each electrode, the kinetics of the electrochemical reaction are expressed by the ***Butler- volmer equation*** as follows [16 and 36]:

$$i = i_0\left[\exp\left(\frac{-n.\alpha.F.V_{act}}{RT}\right) - \exp\left(\frac{n(1-\alpha).F.V_{act}}{RT}\right)\right] \qquad \text{…….(3.23)}$$

where n = 2 for hydrogen at the anode, and n = 4 for oxygen at the cathode. The parameter α and I_0 are evaluated from experimental Electrochemical Impedance Spectroscopy (EIS). The details of the derivation of Eq.(3.23)is given in Appendex C.

The activation loss for the oxygen cathode of PEMFC is the dominant part of the total activation losses. It is calculated by using the following equation[8 and 36].

$$V_{act,c} = \left(\frac{RT}{4(1-\alpha)F}\right)\ln\left[\frac{I}{I_{0.C}}\right] \qquad \text{……...(3.24)}$$

The anode activation loss has less effect on total activation losses and is calculated from the following equation [36 and 37].

$$V_{act,a} = \left(\frac{RT}{2\alpha F}\right)\ln\left[\frac{I}{I_{0.a}}\right] \qquad \text{.....(3.25)}$$

Sometimes, this equation has another form as [8].

$$V_{act,a} = \frac{RT}{F}\frac{I}{I_{0.a}} \qquad \text{.....(3.26)}$$

Appleby and foulkes [37] used Eqs.(3.24) and (3.25) to give the Relationship as follows:

$$V_{act} = \left(\frac{RT}{4(1-\alpha)F}\right)\ln\left[\frac{I}{I_{0.c}}\right] + \left(\frac{RT}{2\alpha F}\right)\ln\left[\frac{I}{I_{0.a}}\right] \qquad \text{.....(3.27)}$$

$\alpha = 0.5$,then

$$V_{act} = \left(\frac{RT}{2F}\right)\ln\left[\frac{I}{I_{0.c}}\right] + \left(\frac{RT}{F}\right)\ln\left[\frac{I}{I_{0.a}}\right] \qquad \text{.....(3.28)}$$

Berger [15] proposed an analytical relationship of exchange current of the anode ($I_{0,a}$) and cathode ($I_{0,c}$). He gave the exchange currents in terms of temperature and the concentration of hydrogen and oxygen as follows:

$$I_{0,c} = n_c.F.B_c\left(C_{proton}\right)^{1-\alpha_c}\left(C_{O_2}\right)^{1-\alpha_c}\left(C_{H_2O}\right)^{\alpha_c}\exp\left(\frac{-\Delta G^{\#}_{0,C}}{RT}\right) \qquad \text{.....(3.29)}$$

$$I_{0,a} = n_a.F.B_a\left(C_{H_2}\right)\exp\left(\frac{-\Delta G^{\#}_{0,a}}{RT}\right) \qquad \text{.....(3.30)}$$

the derivation of Eq(3.29)and Eq(3.30) is summarised in Appendix C[38].

3.3.3 Ohmic Loss.

The ohmic loss of the fuel cell is related to the current, temperature of fuel cell and water content in the membrane. Water content in the membrane depends on to the humidity, pressure and stoichiometry of the inlet gases. The relative humidity of hydrogen is particular importance to water content. The membrane is prefered to be saturated during fuel cell operation.

The resistance of the membrane is expected to increase with current. This is because the water flow in the membrane increases as the current increases. The current is proportional to the electro - osmotic drag. This phenomenon dehydrates the anode side of the membrane and decreases its performance. The ohmic loss of the fuel cell is given as,

$$V_{ohm} = i(R_{electrode} + R_{membrane} + R_{plate}) \qquad \text{.....(3.31)}$$

where : $R_{Electrode}$ and R_{Plate} are the resistance of the electrodes, and bipolar plates. Sometimes are neglected, because their value are small in comparison with the resistance of membrane; therefore, the above equation becomes[36].

$$V_{ohm} = i.R_{membrane} = I.A.R_{membrane} \qquad \text{.....(3.32)}$$

where A is the active area of the membrane, I is current density (defined as current density per unit active area of the membrane), and the resistance, $R_{membrane}$, is given:

$$R_{membrane} = \frac{L.\delta}{A} \qquad \text{.....(3.33)}$$

In which δ and L are the resistivity and thickness of the membrane respectively. It can also be noted that $\delta = 1 / \sigma_m$ **,** and the proton conductivity $\sigma_{\mathbf{m}}$ $(T,\lambda_{H2O/SO3})$ in the membrane is modelled by ***Springer et al.***[22] as:

$$\sigma_m = 100\exp\left[2416\left(\frac{1}{303} - \frac{1}{T}\right)\right](0.005139\lambda_{H_2O/SO_3} - 0.00326) \qquad \text{.....(3.34)}$$

where: $\lambda_{H2O/SO3}$ is the water content in the membrane defined as the number of water molecules per mole SO_3^- groups (*mol* H_2O*/mol* SO_3^-) and water content on the membrane depends on the water activity (a) according to the following empirical equation [39].

$$\lambda_{H2O/SO3} = 14.9a - 44.7a^2 + 70a^3 - 26.5a^4 - 0.446a^5 \qquad 0 < a < 1 \quad \text{.....(3.35)}$$

The water activity is in turn calculated by [39].

$$a = \frac{P_{H_2O}}{P_{sat}(T)} \qquad \text{.....(3.36)}$$

According to Dalton's law the partial pressure of a species *i* is equal to its molar fraction X_i multiplied with the total pressure of the gas phase P , which gives:

$$a = \frac{X_{H_2O}.P}{P_{sat}(T)} \qquad \text{.....(3.37)}$$

The saturation pressure of water vapor can be computed from ***Springer et al .***

$$\text{Log } P_{sat}(T) = -2.1794 + 0.02953(\text{T-}273.15) - 9.1837*10^{-5}(\text{T-}273.15)^2 + 1.445*10^{-7}(\text{T-}273.15)^3 \qquad \text{.....(3.38)}$$

The calculated saturation pressure is in atm. Apparently the water mole fraction, water activity, and water content all vary spatially in the membrane layer, and thus the membrane conductivity (σ_m**)** varies also **[**22**]**. The activity is between (0,1). Lastly, the ohmic loss voltage may also be written as:

$$V_{ohm} = \frac{I.L}{\sigma_m} \qquad \text{.....(3.39)}$$

Thus, resistance of the membrane is dependent on the membrane thickness and conductivity, which is a function of temperature and membrane hydration state. Two general methods are available for measuring the combined resistance of ionic and electronic conductors of an operating fuel cell, which are the AC impedance method and the current interruption method (Chapter 2, section 2.2.2.1).

On the other hand, the mole fraction of water vapour in the incoming gas stream is simply the ratio of the saturation pressure and the total pressure[40]:

$$X_{H2O,in} = \frac{P_{sat}(T)}{P_{in}} \qquad \text{.....(3.40)}$$

Since the sum of all molar fractions is unity, the mole fraction of oxygen can be obtained:

$$X_{O_2,in} = 1 - X_{H_2O,in} \qquad \text{.....(3.41)}$$

3.3.4 Concentration Loss.

Model for concentration loss of the electrodes have been based on **Fick 's** first law of diffusion.

$$J_m = D\frac{\partial c}{\partial x} \qquad \text{.....(3.42)}$$

Where J_m is the molar flux density, D is the diffusion coefficient, and $\partial c/\partial x$ is the molar concentration gradient. For an ideal gas flowing through an electrode in which the morphology is characterized by a porosity, ϵ ,and a tortuosity, τ , the molar flux is given by [36].

$$J_m = \frac{D}{RT}\frac{\partial P}{\partial x}\left(\frac{\varepsilon}{\tau}\right) \qquad \text{.....(3.43)}$$

where: R is the gas constant, T is the temperature, and $\partial P/\partial x$ is the partial pressure gradient of the reactant gas across the thickness of the electrode and $\frac{\varepsilon}{\tau} = 0.1$ [36].

The electrical current density is given by:

$$I = n\,F\,J_m \qquad \text{.....(3.44)}$$

So that from Eq.(3.43)

$$I = nF\left(\frac{D}{RT}\right)\left(\frac{P_1 - P_2}{\vartheta}\right)\left(\frac{\varepsilon}{\tau}\right) \qquad \text{.....(3.45)}$$

Where P_1 & P_2 are the reactant species partial pressures at the outer surface of the electrode and the electrode – electrolyte interface ; the term ϑ is the electrode thickness. When the pressure at the electrochemical reaction site located near this interface is negligibly small then the limiting current density* is:

$$I_L = nF\left(\frac{D}{RT}\right)\left(\frac{P_1}{\vartheta_L}\right)\left(\frac{\varepsilon}{\tau}\right) \qquad \text{.....(3.46)}$$

---

* The limiting current density (I_L) is a measure of the maximum rate at which a reactant can be supplied to an electrode, and occurs when the reactant concentration at the electrode surface is **zero**, as follows:

$$I = n\,F\,D\,(C_B - C_S)\,/\,\vartheta$$

where C_B is the bulk concentration, C_S is surface concentration .

when $C_S = 0$: $\quad I_L = n\,F\,D\,C_B\,/\,\vartheta_L$

Where ϑ_L is electrode thickness corresponding to the limiting current density. The ratio of Eqs.(3.45) and (3.46) gives:

$$\frac{I}{I_L}=\left(\frac{P_1-P_2}{P_1}\right)\left(\frac{\vartheta_L}{\vartheta}\right) \qquad \text{.....(3.47)}$$

assuming that the diffusion length is independent of partial pressure, i.e., $\vartheta_L=\vartheta$, so:

$$I=\left(1-\frac{P_2}{P_1}\right)I_L \qquad \text{.....(3.48)}$$

When the fuel cell is operating under the closed circuit condition and producing a current, the system is not at equilibrium. However, the *Nernst equation* may be applied to the steady state condition in the form:

$$V_{con}=\frac{RT}{nF}\ln\left[\frac{p_1}{p_2}\right] \qquad \text{.....(3.49)}$$

Using the Eq.(3.48), equation (3.49) can be written as [36].

$$V_{con}=\frac{RT}{nF}\ln\left[\frac{I_L}{I_L-I}\right] \qquad \text{.....(3.50)}$$

where $n=2$ for the hydrogen at the anode, and $n=4$ for oxygen at the cathode, this equation becomes[8].

$$V_{con}=\frac{RT}{2F}\ln\left[\frac{I_{L,a}}{I_{L,a}-I}\right]+\frac{RT}{4F}\ln\left[\frac{I_{L,c}}{I_{L,c}-I}\right] \qquad \text{.....(3.51)}$$

where $I_{L,a}$ & $I_{L,c}$ are the anode and cathode limiting current densities, respectively. This loss occurs in both low and high temperature fuel cells, but is only *prevalent at high current densities***.** It is the result of loosing a high concentration of either fuel or oxygen at the anode and cathode, respectively. It essentially occurs because the fuel cell is using fuel or oxygen *faster* than it can be supplied[25].

3.4 Summing of Electrode Losses.

Activation and concentration losses can exist at both the positive (cathode) and negative (anode) electrodes in fuel cells. The total losses at these electrodes is the sum of V_{act} and V_{conc} , or

$$V_{LOSS\ at\ anode} = V_{act\ at\ anode} + V_{conc\ at\ anode} \qquad \text{.....(3.52a)}$$

and

$$V_{LOSS\ at\ cathode} = V_{act\ at\ cathode} + V_{conc\ at\ cathode} \qquad \text{.....(3.52b)}$$

The effect of the losses is to shift the standard voltage (potential) of electrode ($V^0_{electrode}$) to a new value ($V_{electrode}$)[3] .

$$V_{electrode} = V^0_{electrode} \pm | V_{LOSS\ at\ electodde} | \qquad \text{.....(3.53)}$$

• *For the anode.*

$$V_{anode} = V^0_{anode} + | V_{LOSS\ at\ anode} | \qquad \text{.....(3.54)}$$

Sub.Eq.(3.25) and Eq.(3.50)in Eq.(3.52a) and all in Eq.(3.54) to give :

$$V_{anode} = V^0_{anode} + \frac{RT}{n_a \alpha F} \ln\left(\frac{I}{I_{0,a}}\right) + \frac{RT}{n_a F} \ln\left(\frac{I_{L,a}}{I_{L,a} - I}\right) \qquad \text{.....(3.55)}$$

$\alpha = 0.5$, $n_a = 2$ and the standard potential for the anode reaction is 0.000 volt. So:

$$V_{anode} = \frac{RT}{F} \ln\left(\frac{I}{I_{0,a}}\right) + \frac{RT}{2F} \ln\left(\frac{I_{L,a}}{I_{L,a} - I}\right) \qquad \text{.....(3.56)}$$

•*And for the cathode.*

$$V_{cathode} = V^0_{cathode} - |V_{LOSS\ at\ cathode}| \qquad \text{.....(3.57)}$$

Sub. Eq.(3.24) and Eq.(3.50) in Eq.(3.52b)and all in Eq.(3.57) to give:

$$V_{cathode} = V^0_{cathode} - \frac{RT}{n_c \alpha F} \ln\left(\frac{I}{I_{0,c}}\right) - \frac{RT}{n_c F} \ln\left(\frac{I_{L,c}}{I_{L,c} - I}\right) \qquad \text{.....(3.58)}$$

$\alpha_c = 0.5$, $n_c = 4$ and the standard potential for cathode reaction is 1.229 volt. So:

$$V_{cathode} = 1.229 - \frac{RT}{2F} \ln\left(\frac{I}{I_{0,c}}\right) - \frac{RT}{4F} \ln\left(\frac{I_{L,c}}{I_{L,c} - I}\right) \qquad \text{.....(3.59)}$$

The net result of current flow in a fuel cell is to increase the anode potential (V_{anode}) and to decrease the cathode potential ($V_{cathode}$) thereby reducing the cell voltage. The cell voltage includes the contribution of the anode and cathode potentials and ohmic loss:

$$V_{cell} = V_{cathode} - V_{anode} - IR \qquad \text{.....(3.60)}$$

3. 5 Efficiency of a Hydrogen Fuel Cell.

Electrical and heat energies are produced by the overall reaction, Eq.(2.3). Theoretically, the Gibbs free energy of the reaction is available as electrical energy and the rest of the reaction enthalpy is released as heat. In practice, a part of the Gibbs free energy is also converted into heat by the loss mechanisms[8]. The thermal efficiency of an energy conversion device is defined as the amount of useful energy produced relative to change in stored chemical energy that is released when the fuel is reacted with an oxidant [3]. The amount of useful electrical energy in the system is the Gibbs free energy of the reaction. Some energy in the system is not available to do useful work and is always output as heat. Writing the first law for the fuel cell which assumed as a steady flow system,

$$(h\,dv)_{H2O} - (h\,dv)_{O2} - (h\,dv)_{H2} + \delta Q + \delta W_e = 0 \qquad \text{.....(3.61)}$$

Where: h = specific enthalpy (*J/mol*), dv = stoichiometric coefficient (*mol*), Q = heat transfer from cell (*J*) and *We* = electrical work done by cell (*J*). The second law requires the entropy generation to be positive,

$$(S\,dv)_{H2O} - (S\,dv)_{O2} - (S\,dv)_{H2} + \delta Q/T \geq 0$$

or,
$$T(S\,dv)_{H2O} - T(S\,dv)_{O2} - T(S\,dv)_{H2} + \delta Q \geq 0 \qquad \text{.....(3.62)}$$

substituting Eq.(3.61) into Eq.(3.62), we get

$$(h - TS)dv_{H2} + (h - TS)dv_{O2} - (h - TS)dv_{H2O} \geq \delta W_e \qquad \text{.....(3.63)}$$

Which may be written in terms of the Gibbs function, $g = h - TS$, as:

$$(g\,dv)_{H2} + (g\,dv)_{O2} - (g\,dv)_{H2O} \geq \delta W_e$$

integration:
$$-\Delta g_f \geq W_e \qquad \text{.....(3.64)}$$

The maximum work generated by the fuel cell occurs when the equality in equation (3.64) is satisfied. From above, the maximum efficiency of fuel cell reaction is [30]:

$$MAXIMUM\ EFFICIENCY = \frac{Maximum\ Electrical\ Energy}{Thermal\ Energy} = \frac{\Delta \bar{g}_f}{\Delta \bar{h}_f} = \frac{n_{electron}.F.V^0}{\Delta \bar{h}_f} \quad .....(3.65)$$

Under standard conditions($V^0=1.229\ volt$), the maximum thermodynamic efficiency is limited to *83%*, if the assumption that water stays in the liquid form is incorrect, the waste heat that must be rejected decreases because the vaporization of water cools the stack [7]. By convension the value of the change in Gibbs free energy for the fuel cell reaction $\Delta \bar{g}_f$ and the value of the thermal energy, commonly called the calorific value or change in enthalpy of formation $\Delta \bar{h}_f$, are always negative.

There is a discrepancy to the amount of the thermal energy in the fuel cell reaction. It is related to the product of the reaction for hydrogen and oxygen. When the product is steam the value of $\Delta \bar{h}_f$ is referred to as the lower heating value (LHV).

$$H_2 + \tfrac{1}{2}O_2 \longrightarrow H_2O\ (\text{steam}) \qquad \Delta \bar{h}_f = -241.83\ \text{KJ/mol}$$

The negative sign denotes that the energy is *released* during the reaction and not absorbed. The efficiency of an actual fuel cell can be expressed in terms of the higher heating value (HHV)*. If all the energy from the enthalpy of formation (using the HHV) were transferred into electrical energy, the maximum theoretical voltage of the cell would be 1.48 *volt* , so the cell efficiency can now be found:

$$Cell\ Efficiency = \frac{power\ output}{power\ input} = \frac{electrical\ energy}{higher\ heating\ value}$$

$$= \frac{n_{electron}.F.V_{cell}}{\Delta \bar{h}_f} = \frac{V_{cell}}{1.48} \qquad .....(3.66)$$

Heat generation in a PEM fuel cell includes entropic heat of reactions and the irreversible heat of the electrochemical reactions. The entropic heat, also called reversible heat is the difference between the total chemical energy of reactants and the maximum usable work according to the second law of thermodynamics. The reversible heat release,Q_{rev} , can be written as[41]:

* HHV is used in the calculations since most fuel cells operate below the boiling point of water.

$$Q_{rev} = (-T.\Delta s).n'_{H_2} = (-T.\Delta s).\left(\frac{I}{2F}\right) \qquad \text{.....(3.67)}$$

Where n'_{H_2} is the hydrogen flux consumed in the fuel cell reaction ($mol/s.cm^2$).

The irreversible heat results from the irreversibility of the electrochemical reactions. This irreversible heat is attributed to ohmic and activation losses in PEMFC[41and42]

$$Q_{irrev} = (V_{rev} - V_{cell}).I \qquad \text{.....(3.68)}$$

The total heat generation, Q_{total} , is given by:

$$Q_{total} = Q_{rev} + Q_{irrev}$$

$$Q_{total} = (-T.\Delta s).\left(\frac{I}{2F}\right) + (V_{rev} - V_{cell}).I \qquad \text{.....(3.69)}$$

3.6 Consumption of Fuel and Air.

From the basic fuel cell reaction on the anode side (Eq.(2.1)) it is seen that 1 mole of hydrogen and 2 moles of electrons are passed to the cathode side. By using Avogadro's number the charge is calculated,

The charge produced from 1 mole of hydrogen $= -2N_A.e^- = -2F$ [C/mol] .....(3.70)

Dividing by time, rearranging and using conventional current (which is opposite to the actual charge flow) for each cell getting,

$$\text{H}_2 \text{ used per cell} = \frac{i}{2F} \qquad \text{[mol/s]} \qquad \text{.....(3.71a)}$$

For the entire stack this is ,

$$\text{Total H}_2 \text{ used} = \frac{i.N_{Cell}}{2F} \qquad \text{[mol /s]} \qquad \text{.....(3.71b)}$$

Which expressed in terms of mass flow yields[43]:

$$\text{H}_2 \text{ usage} = \dot{m}_{H_2} = \frac{M_{H_2}.i.N_{Cell}}{2F} = 1.05*10^{-8}*i*N_{Cell} \qquad \text{[kg /s]} \qquad \text{.....(3.72)}$$

Where the molar mass of hydrogen: $M_{H_2} = 2.02*10^{-3}[kg/mol]$, and F= 96485.3 $[C/mol]$.

The stoichiometric ratio* for H_2 ($S.R_{H_2}$)is then,

$$S.R_{H_2} = \frac{(\dot{m}_{H_2})_a}{1.05*10^{-8}*i*N_{Cell}} \qquad \text{.....(3.73)}$$

* Ratio of the input gases(hydrogen or air) compared to the amount of the gases used.

where: $(\dot{m}_{H_2})_a$ is the mass flow of hydrogen supply (kg /s)

On the other hand, the mass flow of oxygen is calculated in the same manner as for the anode side. On the cathode side (Eq.(2.2)) two oxygen ions and 4 electrons from one mole of oxygen hence:

The charge consumed from 1 mole of oxygen $= -4N_A.e^- = -4F$ [*C/mol*] ……(3.74a)

For entire stack getting,

$$O_2 \text{ used per cell} = \frac{i.N_{Cell}}{4F} \quad [\text{mol / s}] \qquad \ldots\ldots(3.74b)$$

The units for this flow rate is not in a conventional form so it is often expressed in Kg/s or another unit. Also the expression must be in terms of air not oxygen since air is the inlet gas. Using the molar proportion of oxygen to air of 0.21 and the molar mass of air as $28.97*10^{-3}$ (kg/mol) [1], the amount of air required is;

$$\text{Air usage} = \dot{m}_{air} = \frac{M_{air}.i.N_{Cell}}{X_{O_2}.4F} = 3.57*10^{-7}*i*N_{Cell} \quad [\text{kg /s}] \qquad \ldots\ldots(3.75)$$

The stoichiometric ratio for air ($S.R_{air}$)is then,

$$S.R_{air} = \frac{(\dot{m}_{air})_a}{3.57*10^{-7}*i*N_{Cell}} \qquad \ldots\ldots.(3.76)$$

where: $(\dot{m}_{air})_a$ is the mass flow of air supply,(kg /s)

By dividing Eq.(3.72) on Eq.(3.75), it can be get,

$$\left(\frac{\dot{m}_{H_2}}{\dot{m}_{air}}\right)_s = 0.0294 \qquad \ldots\ldots\ldots(3.77)$$

and the equivalent ratio is equal to,

$$\phi = \frac{\left(\frac{\dot{m}_{H_2}}{\dot{m}_{air}}\right)_a}{\left(\frac{\dot{m}_{H_2}}{\dot{m}_{air}}\right)_s} = \frac{1}{0.0294}\left(\frac{\dot{m}_{H_2}}{\dot{m}_{air}}\right)_a \qquad \ldots\ldots\ldots(3.78)$$

3.7 Water Management .

Water management in a PEMFC is one of the most essential issues for obtaining good performance. The commonly used perfluorosulfonate membranes (Nafion) need to be hydrated in order to be proton conductive, and because of the proton conducting phase present in the electrodes, they also need to be humidified in order to function. In other parts of the cell, the amount of liquid water should be kept to the minimum. Liquid water must be prevented from accumulating on the electrode surfaces, in the pores of the gas diffusion layers, and in the gas channels. Liquid water in these regions blocks the transport of reactants to the active catalyst sites, thus reducing performance. The objective of effective water management is thus to regulate the transport of water in such way that a sufficient amount of water is retained in the proton conductive phases, but excess liquid water is removed from the cell at the same rate as it is produced, with minimum blocking of the gas transport paths [40].

Figure (3-1) shows the flows of water in a PEMFC. Water is produced on the cathode, and additional water may be supplied to the cell along the inlet gas streams if the product water is not sufficient to maintain the proton conductive phases humidified. When ambient air is used as a source of oxidant, the cathode conditions are affected by ambient temperature and relative humidity. Water transport between the anode and the cathode takes place by three different processes. Protons migrating through the membrane drag water molecules along with them. This phenomenon is referred to as electro-osmotic drag. The formation of a water concentration gradient inside the membrane gives rise to diffusion, which usually counters the **electro - osmotic drag** and is often referred to as **back diffusion**. Furthermore, if there is a pressure difference across the membrane, **hydraulic permeation** contributes to the water transport. The net water transport through the membrane is the resultant of these three processes.

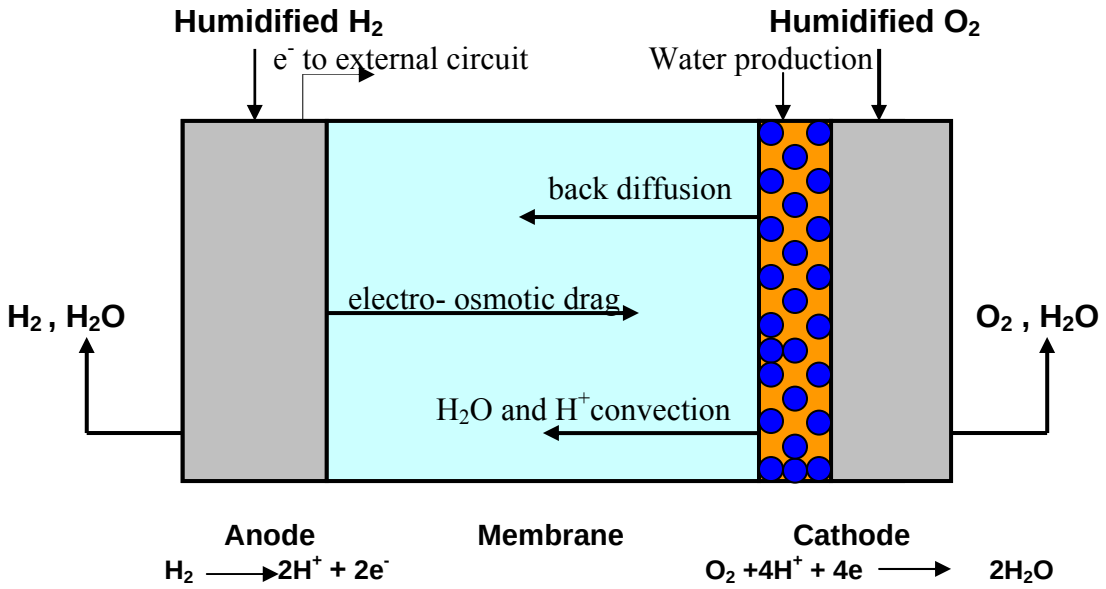

Figure (3 -1): The flows of water in a PEMFC.

The direction and magnitude of net water transport is a function of several factors, such as current density, temperature, gas flow rates, and the materials and geometry of the cell. It is likely that at high current densities, the electro-osmotic drag dominates, whereas at lower current densities, the back diffusion process is also significant, and the pattern of net water transport is more complicated and difficult to predict[8]. In this section, the equations governing the heat, mass and charge transfer in a PEMFC is solved, to study the membrane performance for different operating conditions. The membrane chosen for the present study is Nafion117. This Nafion is widely used for automotive applications, where the required operational range is from 80 ^{0}C to 100 ^{0}C. It has a high conductivity(conductance can be increased by increasing the water content, and increasing the ion exchange capacity) and is well known in industry. However, This model is based on the following assumptions:

1. **A transient, one-dimensional model of membrane of PEMFC.**
2. **Single phase.**
3. **Linear pressure gradient.**
4. **The water concentration is assumed to change linearly over the membrane thickness.**
5. **Capillary forces may be neglected because of the low velocity of mixture in the membrane.**
6. **Viscous force is also neglected in the energy equation.**
7. **No chemical or electrochemical reaction occurs in the membrane.**
8. **The proton concentration in the membrane is assumed to be constant(Electro-neutrality).**

3.7.1 Governing Equations.

The following is a list of the governing equations used to model the phenomena in the membrane as well as a brief description of the terms involved in each equation:

- **mass conservation equations**
- **momentum (Darcy) equation**
- **conservation of energy equation**
- **conservation of current**
- **potential equation in the polymer**
- **linear relation for the pressure of the mixture**
- **relation for the water activity at both the anode and cathode interface**
- **relation for water activity within the membrane**

3.7.1.1 Mass or Species Conservation Equations.

The conservation equation of the mass is (for proton and water) [44]:

$$\frac{\partial C_i}{\partial t} = -\frac{\partial}{\partial x} N_i \qquad \text{.....(3.79)}$$

C_i is the molar concentration (H_2O, H^+) and N_i is the molar flow due to the convection and the diffusion effect. In a diluted solution, N_i is given by the equation of Nernst- Planck [45]:

$$N_i = J_i + C_i u^m \qquad \text{.....(3.80)}$$

where u^m is the speed of the mixture and J_i is the diffusion flow. For water, flow is expressed by:

$$J_{H_2O} = -D_{C_{H_2O}} \frac{\partial C^m_{H_2O}}{\partial x} + n_{drag} \frac{i_x}{F} \qquad \text{.....(3.81)}$$

where $$n_{drag} = 2.5 \frac{\lambda_{H_2O/SO_3}}{22} \qquad \text{.....(3.82)}$$

and $$\lambda_{H2O/SO_3} = \frac{C^m_{H_2O}}{\frac{\rho^m_{dry}}{M^m} - bC^m_{H_2O}} \qquad \text{.....(3.83)}$$

with b=0.0126. n_{drag} is the measured drag coefficient (Springer et al.), i_x the protonic current in the x direction, F Faraday's constant, $\lambda_{H2O/SO3}$ is the water

content in the membrane (mol_{H2O}/mol_{SO3}), $\rho^m{}_{dry}$ is the dry membrane density (Kg/m^3) and M^m is the membrane molecular mass (kg_{dry}/mol_{so3}) [22].

In Eq. (3.81), $D_{C_{H_2O}}(m^2/s)$ is the diffusion coefficient including a correction for the temperature and for the water content. It is expressed in a fixed coordinate system with the dry membrane by (Springer et al.) such that :

$$Dc_{H_2O} = D^{'}\left\{\exp\left[2476\left(\frac{1}{303}-\frac{1}{T}\right)\right]\lambda_{H_2O/SO_3}\frac{1}{a}\frac{1}{17.81-78.9a+108a^2}\right\} \quad \text{.....(3.84)}$$

where a is the activity of water and $D^{'}$ (m^2/s) is the measured diffusion coefficient at constant temperature and in coordinates moving with the swelling of the membrane (Springer et al.) , it expressed by :

$$D' = 2.64227610^{-13}\lambda_{H2O/SO_3} \quad for \lambda_{H2O/SO_3} \le 1.23 \quad \text{.....(3.85a)}$$

$$D' = 7.7510^{-11}\lambda_{H2O/SO_3} - 9.510^{-11} \quad for 1.23 < \lambda_{H2O/SO_3} \le 6 \quad \text{.....(3.85b)}$$

$$D' = 2.562510^{-11}\lambda_{H2O/SO_3} + 2.162510^{-11} \quad for 6 < \lambda_{H2O/SO_3} \le 14 \quad \text{....(3.85c)}$$

The total molar flux for water can, thus, be written :

$$N_{H_2O} = J_{H_2O} + C^m_{H_2O}u^m \quad \text{.....(3.86)}$$

Where the mixture velocity u^m is given by the momentum (Darcy)equation :

$$u^m = -\frac{Kk^g_r}{\mu}\left(\frac{\partial p}{\partial x}\right) \quad \text{.....(3.87)}$$

K is the absolute permeability of the porous environments, K_r^g is the relative permeability, and μ is dynamic viscosity.

$$\mu = \frac{M_{H^+}C_{H^+}}{\rho}\mu_{H^+} + \frac{M_{H_2O}C_{H_2O}}{\rho}\mu_{H_2O} \quad \text{.....(3.88)}$$

The ***general equation*** of non stationary mass transfer is thus:

$$\frac{\partial C^m_{H_2O}}{\partial t} = -\frac{\partial}{\partial x}J_{H_2O} - \frac{\partial}{\partial x}\left(C^m_{H_2O}u^m\right) \quad \text{.....(3.89)}$$

By supposing the electro-neutrality of the membrane and a uniform distribution of charge sites, the transfer of proton(the mass conservation of protons) is simplified:

$$\frac{\partial C_{H^+}}{\partial x} = 0 \quad , \quad \frac{\partial C_{H^+}}{\partial t} = 0 \qquad \text{.....(3.90)}$$

The diffusive molar flux for the protons (J_{H^+}) can, therefore, be written as:

$$J_{H^+} = -\frac{F}{RT} D_{H^+} C_{H^+} \frac{\partial \phi_m}{\partial x} \qquad \text{……..(3.91)}$$

where Φ_m is the membrane proton potential and D_{H^+} the proton diffusivity(D_{H^+}=*4.5*10^{-5} (cm^2/s) for Nafion117*)[23]. Combining this diffusive flux with the convective flux results in the total molar flux for the hydrogen protons, i.e.

$$N_{H^+} = J_{H^+} + (C_{H^+} u^m)$$

$$N_{H^+} = -\frac{F}{RT} D_{H^+} C_{H^+} \frac{\partial \phi_m}{\partial x} + C_{H^+} u^m \qquad \text{…….(3.92)}$$

therefore, when a current crosses the membrane the concentration of proton remains constant (i.e, C_{H^+} = *1.2*10^{-3} (mol/cm^3) for Nafion117*)[23] .

3.7.1.2 Conservation of Energy.

Energy is transported by conduction and convection within the three phases of the membrane (polymer, liquid and gas). The effects of ohmic losses within the membrane are taken into account by an additional source term in the energy balance equation so that energy conservation is given by:

$$\overline{\rho c_p} \frac{\partial T}{\partial t} = \lambda_m \frac{\partial^2 T}{\partial x^2} - \overline{M c_p N} \frac{\partial T}{\partial x} + R_m \qquad \text{.....(3.93)}$$

where $$\overline{\rho c_p} = \rho_m^{dry} c_{p_m} + \rho_{H_2O}^m c_{p_{H_2O}} + \rho_{H^+} c_{p_{H^+}} \qquad \text{.....(3.94)}$$

with $$\rho_{H^+} = M_{H^+} c_{H^+} \qquad \text{.....(3.95)}$$

$$\rho_{H_2O}^m = M_{H_2O} c_{H_2O}^m \qquad \text{.....(3.96)}$$

$$\overline{M c_p N} = M_{H_2O} c_{p_{H_2O}}^m N_{H_2O} + M_{H^+} c_{p_{H^+}} N_{H^+} \qquad \text{.....(3.97)}$$

The transient energy effect associated with mass storage within the hydrated membrane is neglected due to the fact that the dry membrane mass does not change and is several orders of magnitude larger than that of the water which hydrates the

membrane. Substituting the expressions for N_{H2O} and N_{H^+} from Eqs.(3.86)and (3.92) , an expanded expression for $\overline{McpN}$ can be obtained, namely:

$$\overline{Mc_pN} = M_{H_2O}c^m_{p_{H_2O}}\left(C^m_{H_2O}u^m - D_{C_{H_2O}}\frac{\partial C^m_{H_2O}}{\partial x} + 2.5\frac{\lambda_{H_2O/SO_3}}{22}\frac{i_x}{F}\right) + M_{H^+}c_{p_{H^+}}\left(C_{H^+}u^m - \frac{F}{RT}D_{H^+}C_{H^+}\frac{\partial \Phi_m}{\partial x}\right) \quad \text{.....(3.98)}$$

In the equation of energy, λ_m is the thermal conductivity coefficient of the membrane and is supposed to be constant. The source term R_m is given by

$$R_m = \frac{i_x^2}{\sigma_m} \quad \text{.....(3.99)}$$

where σ_m is the conductivity of the membrane, it is a function of the temperature and water content as(Springer et al.)[22].

$$\sigma_m = \sigma_{m303}\exp\left[1268\left(\frac{1}{303} - \frac{1}{T}\right)\right] \quad \text{.....(3.100a)}$$

with σ_{m303} the conductivity of the membrane at 303 K :

$$\sigma_{m303} = 100(0.005139\lambda_{H_2O/SO_3} - 0.00326) \qquad for\lambda_{H_2O/SO_3} > 1 \quad \text{.....(3.100b)}$$

A theoretical value of the conductivity is defined by[23]:

$$\sigma_m = -\frac{F^2}{RT}D_{H^+}C_{H^+} \quad \text{.....(3.101)}$$

In this thesis, Eqs.(3.100a) and (3.100b) were used here.

3.7.1.3 Current Conservation.

The assumption of a uniform and fixed number of charge sites in the membrane and assuming an electro-neutrality gives the following equation for protonic current:

$$\frac{\partial i_x}{\partial x} = 0 \quad \text{.....(3.102)}$$

3.7.1.4 Ohm's Law.

The equation of the proton potential is derived from the Ohm's law. Both terms represent the proton flux divided by the membrane conductivity. The electro-

neutrality assumption allows the total molar proton flux given by Eq.(3.92) to be related directly to current density and results in the first term. The second term containing u_m represents the convective flux of protons. Combined they result in the following equation:

$$\frac{\partial \Phi_m}{\partial x} = -\frac{i_x}{\sigma_m} + \frac{F}{\sigma_m} C_{H^+} u^m \qquad \text{.....(3.103)}$$

3.7.1.5 Water Activity in the Interface.

The activity of the water vapor to the membrane interface is given by[39]:

$$a = \frac{RT}{P_{sat}(T)} C^g_{H_2O} \qquad \text{.....(3.104)}$$

where $C^g_{H_2O}$ is the water vapor concentration.

3.7.1.6 Mixture Pressure Relation.

As a rough approximation, the mixture pressure gradient is assumed to behave linearly between the anode and cathode interfaces so that.

$$p = p^g_{cax+} + \frac{\left\lfloor sp^l_{H_2O_{ccx-}} + (1-s)p_{ccx-} \right\rfloor - p^g_{cax+}}{x_{mx-} - x_{mx+}} (x - x_{mx+}) \qquad \text{.....(3.105)}$$

At the interface with the anode catalyst layer, the mixture pressure is assumed equal to that of the gas pressure ($\{p^g\}_{cax+}$) under the assumption that ***no liquid*** is present in the membrane pores. At the cathode catalyst interface, it is assumed that the mixture pressure can be approximated by a linear relation (see bracketed terms in Eq.(3.105)) between the gas pressure ($\{p^g\}_{ccx-}$), and the liquid pressure ($\{p^l_{H2O}\}_{ccx-}$), weighted by the saturation ratio s (the volume ratio of liquid water to gaseous water in the pores of the catalyst layer. For the results generated in Ch.5 saturation ratio was set to **zero**, therefore there was no effect of liquid pressure on the pressure gradient. The boundary coordinate at each interface is given by x_{mx+} and x_{mx-} .

3.7.1.7 Water Activity in the Membrane.

The relation for the water activity in the membrane (Nafion117) is given by[22]:

$$a = \frac{1}{2160}\left[c_1 + c_2\lambda_{H_2O/SO_3} + 216\left(c_3 - c_4\lambda_{H_2O/SO_3} + c_5\lambda^2_{H_2O/SO_3}\right)^{1/2}\right]^{1/3} - \frac{134183}{2160}\left[c_1 + c_2\lambda_{H_2O/SO_3} + 216\left(c_3 - c_4\lambda_{H_2O/SO_3} + c_5\lambda^2_{H_2O/SO_3}\right)^{1/2}\right]^{1/3} + \frac{797}{2160} \quad for \lambda_{H2O/SO3} \leq 14 \quad \text{.....(3.106a)}$$

where: $c_{1=}$ **-419561*10^4**, $c_{2=}$ **139968*10^3**, $c_{3=}$ **382482*10^6**, $c_{4=}$ **251739*10^3**, and $c_{5=}$ **419904*10^6**

$$a = 0.7143\left(\lambda_{H_2O/SO_3}\right) - 9.0021 \qquad for\ 14 \leq \lambda_{H2O/SO3} \leq 16.8 \qquad \text{…….(3.106b)}$$

$$a = 3 \qquad for\ \lambda_{H2O/SO3} > 16.8 \qquad \text{……..(3.106c)}$$

3.7.2 Initial and Boundary Conditions.

This section presents the initial and boundary conditions for the membrane mathematical model presented in Section (3.7.1). The following notations are used:

- The first letter symbolizes the domain:
  - c: catalyst layer
  - m: polymer membrane
- The second letter refers to the anode or the cathode:
  - a: anode
  - c: cathode
- The third letter indicates the normal to the interface:
  - x: perpendicular to the *t*- plane
- The fourth letter specifies the side of the interface:
  - +: catalyst layer-membrane interface anode side

In the membrane, the model presented in Section 3.7 is solved for the concentration of water ($C^m_{H_2O}$)and the temperature (T). Based on this solution and a voltage value at the anode catalyst boundary (*cax*+), a voltage drop across the membrane is determined. However, in order to solve for the transient temperature, concentration, and voltage profiles, initial and boundary conditions are needed. They are described in the following sections.

3.7.2.1 Water Concentration ($C^m_{H_2O}$).

The species equation for water requires two boundary conditions and one initial condition. The boundary conditions state that the water activity at the interface is in equilibrium with the water activity in the catalyst layers at (*cax*+ and *ccx*-), so that the equation for water activity takes the form:

$$\{a\}_{t,x=x_{mx-}} = \left\{ \frac{RT}{P_{sat}(T)} C^g_{H_2O} \right\}_{t,x=x_{ccx-}} \qquad \text{……..(3.107a)}$$

$$\{a\}_{t,x=x_{mx+}} = \left\{ \frac{RT}{P_{sat}(T)} C^g_{H_2O} \right\}_{t,x=x_{cax+}} \qquad \text{……(3.107b)}$$

The Clapeyron equation gives an expression for the saturation pressure as [13]:

$$P_{sat}(T) = P_0 \exp\left[\frac{\left(\frac{1}{T_0} - \frac{1}{T}\right) L_V M_{H_2O}}{R}\right] \qquad \text{.....(3.108)}$$

Given the water activity, the water concentration at the boundaries can be easily found using Eqs.(3.109) and (3.110)below. Eq.(3.109) formulates water concentration as a function of the water content and is used only with the boundary condition and initial conditions. Thus,

$$\left\{ C^m_{H_2O} = \lambda_{H_2O/SO_3^-} \frac{\rho^m_{dry}}{M^m} \frac{1}{1 + b\lambda_{H_2O/SO_3^-}} \right\}_{\substack{t,x=x_{mx-} \\ t,x=x_{mx+} \\ t=0,x}} \qquad \text{.....(3.109)}$$

where the water content, ($\lambda_{H2O/SO3}$ (t,x))is a function of the activity, i.e.

$$\left\{\lambda_{H_2O/SO_3^-} = 0.043 + 17.81(a) - 39.85(a)^2 + 36(a)^3\right\}_{\substack{t,x=x_{mx-} \\ t,x=x_{mx+} \\ t=0,x}} \quad for \quad a < 1 \qquad \text{.....(3.110}a\text{)}$$

$$\left\{\lambda_{H_2O/SO_3^-} = 14 + 1.4(a-1)\right\}_{\substack{t,x=x_{mx-} \\ t,x=x_{mx+} \\ t=0,x}} \quad for \quad 1 \le a \le 3 \quad 1 \le a < 3 \qquad 10b)$$

$$\left\{\lambda_{H_2O/SO_3^-} = 16.8\right\}_{\substack{t,x=x_{mx-} \\ t,x=x_{mx+} \\ t=0,x}} \quad for \quad 3 \le a \qquad \text{.....(3.110}c\text{)}$$

The initial condition for the concentration assumes a linear concentration profile across the membrane:

$$\left\{C^m_{H_2O}\right\}_{t=0,x} = \left\{C^m_{H_2O}\right\}_{t=0,x=x_{mx-}} + \frac{\left\{C^m_{H_2O}\right\}_{t=0,x=x_{mx+}} - \left\{C^m_{H_2O}\right\}_{t=0,x=x_{mx-}}}{x_{mx+} - x_{mx-}} (x - x_{mx-}) \qquad \text{.....(3.111)}$$

3.7.2.2 Temperature (*T(t,x)*).

The energy conservation equation requires two boundary conditions and one initial condition. Heat transport in the interface is assumed to take place due to conduction only. At the catalyst layer and polymer membrane interfaces, the interfacial heat flux is continuous. Thus,

$$\left\{\lambda_m \frac{\partial T}{\partial x}\right\}_{t,x=x_{mx-}} = \left\{\lambda^{eff} \frac{\partial T}{\partial x}\right\}_{t,x=x_{ccx-}} \quad \text{.....(3.112}a\text{)}$$

$$\left\{\lambda_m \frac{\partial T}{\partial x}\right\}_{t,x=x_{mx+}} = \left\{\lambda^{eff} \frac{\partial T}{\partial x}\right\}_{t,x=x_{cax+}} \quad \text{.....(3.112}b\text{)}$$

The initial condition for the temperature assumes a linear temperature profile across the membrane, i.e.

$$\{T\}_{t=0,x} = \{T\}_{t=0,x=x_{mx-}} + \frac{\{T\}_{t=0,x=x_{mx+}} - \{T\}_{t=0,x=x_{mx-}}}{x_{mx+} - x_{mx-}}(x - x_{mx-}) \quad \text{.....(3.113)}$$

Table 1 Initial and boundary conditions .

FIGURE	**5.27**	**5.28**	**5.29**	**5.30**	**5.31 , 5.32**
Initial condition					
Temperature(k)					
Anode	352.85	352.85	352.85	352.85	352.85
cathode	352.855	352.855	352.855	352.855	352.855
Gaseous water concentration (mol / m^3)					
Anode	5	5	5	5	5
cathode	9.5	9.5	9.5	9.5	9.5
Boundary hypothetical Conditions					
Gaseous water concentration (mol / m^3), Flux (mol/m^4)					
Anode	5	5	5	5	$(\partial c/\partial x)=0$
cathode	9.5	9.5	9.5	9.5	$\partial c/\partial x= 9.2*10^7$ $\partial c/\partial x= -9.2*10^7$
Temperature(k)					
Anode	352.85	352.85	352.85	352.85	352.85
cathode	$\partial T/\partial x=295$	$\partial T/\partial x=295$	$\partial T/\partial x=295$	$\partial T/\partial x=295$	$\partial T/\partial x=295$
Pressure (atm)					
Anode	1.86	1 , 1	1 , 1	1 , 1	1.86
cathode	2.56	3 , 1	3 , 1	3 , 1	2.56
Current density (A/cm^2)	0.1 0.4	0.6	0.1 , 0.5	0.1 , 0.5	0.6

3.7.3 Numerical Solution of the Membrane Model.

3.7.3.1 Finite Difference Approach.

The governing equations solved in the membrane are in the form of transient second order, parabolic, partial differential equations with variable coefficients. Because of the complexity of these equations, they cannot be solved analytically. However, they can be solved numerically using a finite difference method. The finite difference method used approximates each derivative and coefficient in each of the partial differential equations. This section describes the finite difference method used to solve the system of equations.

In finite difference methods, the derivatives that occur within the equation being solved are approximated using finite difference operators. In order to derive these operators, one must first partition the x (spatial direction) and the t (time dimension) plane into uniform cells Δx by Δt with cell spacing Δx =L/J and Δt = t/N, as shown in Fig.(3.2). where: L=Thickness of the membrane, t=Total time, J=Number of node.

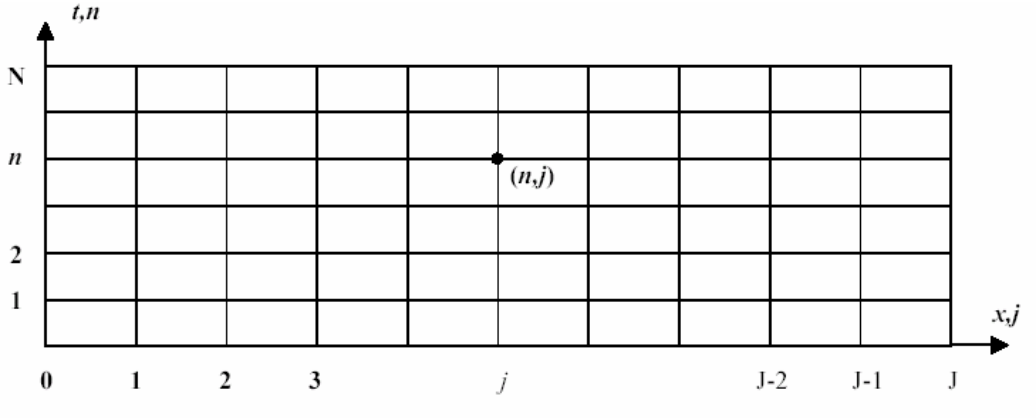

Figure (3.2): Grid Spacing.

After grid spacing has been established in the general terms depicted in Figure (3.2), derivatives are approximated using the system of line intersections (nodes) shown.

3.7.3.2 Approximation of the Variable Coefficients.

The details of the methods that using to approximate the variable coefficients which appear in the transient, second order, partial differential equations developed in Chapter 3, (section 3.7), are shown in Appendix D. These coefficients were approximated using methods described in ***Mitchel & Griffiths*** [46],

****From Appendix D:***

$$u_j^{n+1} = u_j^n + \Delta t\left[A_{j+1}(u_{j+1} - u_j) - A_j(u_j - u_{j-1}) + \left(\frac{b_j}{2\Delta x}(u_{j+1} - u_{j-1}) \right) + s_j \right]_j^n \qquad \text{.....(D.13)}$$

The final form of Eq.(3.89) and Eq.(3.93)becomes:

$$\frac{\partial C_{H_2O}^m}{\partial t} = \frac{\partial}{\partial x}\left[D_{H_2O}^m \frac{\partial C_{H_2O}^m}{\partial x} \right] - u^m \frac{\partial C_{H_2O}^m}{\partial x} - \frac{\partial}{\partial x}\left(\frac{2.5\lambda_{H_2O/SO_3} i_x}{22F} \right) \qquad \text{.....(3.117)}$$

$$\frac{\partial T}{\partial t} = \frac{\lambda_m}{\overline{\rho cp}} \frac{\partial^2 T}{\partial x^2} - \frac{\overline{McpN}}{\overline{\rho cp}} \frac{\partial T}{\partial x} + \frac{i_x^2}{\sigma_m \overline{\rho cp}} \qquad \text{.....(3.118)}$$

In the finite difference form Eq.(3.117) and Eq.(3.118) will become:

$$C(j,n+1) = C(j,n) + \Delta t\left[\begin{array}{l} CA(j+1,n)(C(j+1,n) - C(j,n)) - CA(j,n)(C(j,n) - C(j-1,n)) + \\ \left(\frac{Cb(j,n)}{2\Delta x}(C(j+1,n) - C(j-1,n)) \right) + Cs(j,n) \end{array} \right] \qquad \text{.....(3.119)}$$

$CA(j+1,n), CA(j,n), Cb(j,n)$ & $Cs(j,n)$ ...are Variable Coefficients *in* *Eq*(3.117) .

Where:

$$\rightarrow CA(j+1,n) = D^{'}\left\{ \exp\left[2476\left(\frac{1}{303} - \frac{1}{T(j+1,n)} \right) \right] \lambda_{H_2O/SO_3} \cdot \frac{1}{a} \frac{1}{17.81 - 78.9a + 108a^2} \right\} \qquad \text{...(3.120)}$$

$$\lambda_{H_2O/SO_3} = \frac{C(j+1,n)}{\frac{\rho}{M} - bC(j+1,n)} \qquad \text{....(3.121)}$$

$$\rightarrow Cb(j,n) = -\frac{Kk_r^g}{\mu}\left(\frac{\Delta p}{\Delta x} \right) \qquad \text{.....(3.122)}$$

$$\mu = \frac{M_{H^+} C_{H^+}}{\rho} \mu_{H^+} + \frac{M_{H_2O} C(j,n)}{\rho} \mu_{H_2O} \qquad \text{.....(3.123)}$$

$$\rightarrow Cs(j,n)=\frac{2.5i_x}{22F(2\Delta x)}\left[\frac{C(j+1,n)}{\frac{\rho}{M}-bC(j+1,n)}-\frac{C(j-1,n)}{\frac{\rho}{M}-bC(j-1,n)}\right] \quad .....(3.124)$$

$$T(j,n+1)=T(j,n)+\Delta t\left[\begin{array}{l}TA(j+1,n)(T(j+1,n)-T(j,n))-TA(j,n)(T(j,n)-T(j-1,n))+\\ \left(\frac{Tb(j,n)}{2\Delta x}(T(j+1,n)-T(j-1,n))\right)+Ts(j,n)\end{array}\right] \quad ....(3.125)$$

$TA(j+1,n), TA(j,n), Tb(j,n)\ \&\ Ts(j,n)$ ...are Variable Coefficients, $Eq(3.118)$.

Where:

$$\rightarrow TA(j+1,n)=\frac{\lambda_m}{\rho_m^{dry}c_{p_m}+M_{H_2O}C(j+1,n).c_{p_{H_2O}}+M_{H^+}C_{H^+}.c_{p_{H^+}}} \quad .....(3.126)$$

$$M_{H_2O}c_{p_{H_2O}}^m\left(\begin{array}{l}-C(j,n)\frac{Kk_r^g}{\mu}\left(\frac{\Delta p}{\Delta x}\right)-\left\{D'\left\{\begin{array}{l}\exp\left[2476\left(\frac{1}{303}-\frac{1}{T(j+1,n)}\right)\right]\lambda_{H_2O/SO_3}\cdot\\ \frac{1}{a}\frac{1}{17.81-78.9a+108a^2}\end{array}\right\}\right\}+\\ \frac{C(j+1,n)-C(j-1,n)}{2\Delta x}+2.5\frac{\lambda_{H_2O/SO_3}}{22}\frac{i_x}{F}\end{array}\right)+$$

$$\rightarrow Tb(j,n)=\frac{M_{H^+}c_{p_{H^+}}\left(-C_{H^+}\frac{Kk_r^g}{\mu}\left(\frac{\Delta p}{\Delta x}\right)-\frac{F}{RT}D_{H^+}C_{H^+}\left\{-\frac{i_x}{\sigma_m}-\frac{F}{\sigma_m}C_{H^+}\left(\frac{Kk_r^g}{\mu}\left(\frac{\Delta p}{\Delta x}\right)\right)\right\}\right)}{\rho_m^{dry}c_{p_m}+M_{H_2O}C(j,n).c_{p_{H_2O}}+M_{H^+}C_{H^+}.c_{p_{H^+}}}$$

.....(3.127)

$$\sigma_m=\left(0.5139\lambda_{H_2O/SO_3}-0.326\right)\exp\left[1268\left(\frac{1}{303}-\frac{1}{T(j,n)}\right)\right] \quad .....(3.128)$$

$$\rightarrow Ts(j,n)=\frac{i_x^2}{(\sigma_m)\left(\rho_m^{dry}c_{p_m}+M_{H_2O}C(j,n).c_{p_{H_2O}}+M_{H^+}C_{H^+}.c_{p_{H^+}}\right)} \quad .....(3.129)$$

CHAPTER 4

COMPUTATIONAL PROCEDURE AND COMPUTER PROGRAM

4.1 Introduction.

In this chapter, the two computer programs used to predict the behavior of PEM fuel cell are described. These programs are written in Quick Basic. Each program consists of the main program and four subroutines.

4.2 First Main Program (Calculation of losses in a PEMFC).

The different types of input data, required to run the computer program, are divided into the operating conditions, the current densities drawn from the cell and membrane thickness.

The computational procedure is as follows:

1 – Choose operating temperature.

2 – Choose Nafion thickness.

3 – Choose partial pressure of oxygen.

4 – Call the different subroutines to calculate the activation , ohmic and concentration losses.

5 – Calculate the cell voltage for current density greater than zero.

6 – Calculate the reversible voltage for current density equal zero.

7 – Open data file to save the program results in each step of program calculations.

8 – Print the results for each step of calculations.

9 – Choose another oxygen partial pressure and repeat steps 4 - 8 at the same thickness.

10 – Choose another thickness and repeat steps 3 – 8 at the same temperature.

11 – Finally choose another temperature and repeat steps 2 – 8 at the same procedure.

4.2.1 Description of Subroutines (First program).

The four subroutine used in the program are described as follows:

4.2.1.1 Subroutine Act.

This subroutne is developed to evaluate the activation loss by using Eqs.(3.27),(3.29) and (3.30) for different temperatures and current densities.

4.2.1.2 Subroutine Ohm.

This subroutine performs calculations related to Eq.(3.39)for different thicknesses, temperatures and current densities.

4.2.1.3 Subroutine Conc.

This subroutine calculates the concentration loss by using Eq.(3.51) for different current densities and temperatures.

4.2.1.4 Subroutine Rev.

Finally, this subroutine calculates the reversible voltage with different temperatures and partial pressures of oxygen (Eq(3.19)). Also, it calculates the electrical conductivity versus water content, water activity and the composition of the incoming gas streams.

4.3 Second Main Program (This program is used to solve the membrane model)

The computational procedure is as follows:

1 – Input anode and cathode boundary conditions (temperatures, pressures, gas concentrations, heat and water fluxes).

2 – Numerical solution parameters (Δt, total time, membrane thickness and number of nodes).

3 – Calling subroutine **INBTCV**, to determine the initial water concentration, voltage drop and temperature profiles across the membrane.

4 – Apply the finite difference algorithm in Eq.(3.126) to Eq.(3.128).

5 – Call subroutine ABSJ**T,** to calculate the coefficients Aj, Bj and Sj in Eq.(3.126).

6 – Repeat again, applying the finite difference algorithm in Eq.(3.126) to Eq.(3.127).

7 - Call subroutine ABSJ**C ,** to calculate the coefficients Aj, Bj and Sj in Eq.(3.126).

8 – After temperature and concentration profiles are set, voltage drop across the membrane is found as a function of temperature and concentration by calling the subroutine **VOLTAGE.**

9 – Finally, average resistance across the membrane is calculated and results are plotted.

4.3.1 Description of Subroutines (Second program).

Four subroutines are used in this program as described below:

4.3.1.1 Subroutine INBTCV.

It takes the boundary conditions from MAIN program and creates an initial temperature, concentration and voltage profile at time = 0. This initial profiles connect the anode and cathode temperatures, concentrations and voltages with a straight line (Eq.(3.111)& Eq(3.113)). When main program starts to loop through the time steps, subroutine **INBTCV** is called at the beginning of loop to set the temperature, concentration boundary conditions for that time step.

4.3.1.2 Subroutine ABSJT.

This subroutine is developed to calculate the variable coefficients for Eq.(3.128), $\lambda_m / \overline{\rho.cp}$, $\overline{McpN} / \overline{\rho cp}$.*and* $\frac{i_x^2}{\sigma_m . \overline{\rho cp}}$ at different nodes, which correspond Aj, Bj and Sj in Eq.(3.126), respectively.

The first term($\lambda_m / \overline{\rho.c_P}$) corresponds to the variable coefficient Aj in Eq.(3.126) is calculated at different nodes. It sets the node value and time step and proceeds to calculate $\overline{\rho.c_P}$ using Eq.(3.94) at that node and time step.

The second term ($\overline{Mc_PN} / \overline{\rho.c_P}$) corresponds to the variable coefficient Bj in Eq.(3.126) at different nodes. It sets the node value and time step and proceeds to calculate the molar flux $\overline{N}$. The variables(D_{H2O} , u^m) are calculated and then substituted according to Eqs.(3.94) and (3.98).

The third term($\frac{i_x^2}{\sigma_m . \overline{\rho cp}}$) at different node is calculated. In order to calculate the ohmic loss term, this subroutine must calculate $\overline{\rho.c_P}$ and the membrane conductivity (σ_m) at each node. Variables are calculated according to Eqs.(3.94),(3.99) and (3.100) and then substituted $\frac{i_x^2}{\sigma_m . \overline{\rho cp}}$ which corresponds to the variable coefficient Sj in Eq.(3.126).

4.3.1.3 Subroutine ABSJC.

This subroutine is developed to calculate the variable coefficients for Eq.(3.127), $D^m_{H_2O}$, u^m , $\frac{\partial}{\partial x}\left(\frac{2.5\lambda_{H_2O/SO_3} i_{mx}}{22F}\right)$ which correspond Aj, Bj and Sj in Eq.(3.126), respectively. The first term $D^m_{H_2O}$ at different nodes is calculated. It sets the node value and time step and proceeds to calculate water content and activity at that node and time step. $D^m_{H_2O}$ is then calculated using Eq.(3.84).

The second term u^m at different nodes for each time step is calculated. In order to calculate u^m , this subroutine calculate μ and pressure gradient at each node. Variables are calculated and then substituted according to Eq.(3.87), (3.88) and (3.105).

The third term, $\frac{\partial}{\partial x}\left(\frac{2.5\lambda_{H_2O/SO_3} i_{mx}}{22F}\right)$ at different nodes is calculated. This subroutine approximates the water drag term, and then calculate the water content λ_{H_2O/SO_3} at two adjacent nodes using Eq.(3.83). A forward difference approximation is then used to approximate $\frac{\partial}{\partial x}\left(\lambda_{H_2O/SO_3}\right)$.

4.3.1.4 Subroutine Voltage .

This subroutine is developed to calculate voltage gradient at each node after final water concentration and temperature profiles have been determined for a time step. Membrane conductivity and mixture velocity are calculated then substituted according to Eq.(3.103). The voltage at each node is calculated by taking the voltage at the previous node and adding the average of the voltage gradients of that node and the previous node, $V_{j+1}^{n+1} = V_j^{n+1} + \frac{\left[\left(\frac{\partial \phi}{\partial x}\right)_{j+1}^{n+1} + \left(\frac{\partial \phi}{\partial x}\right)_j^{n+1}\right]}{2}$. Voltage gradients are then sent back to Main program.

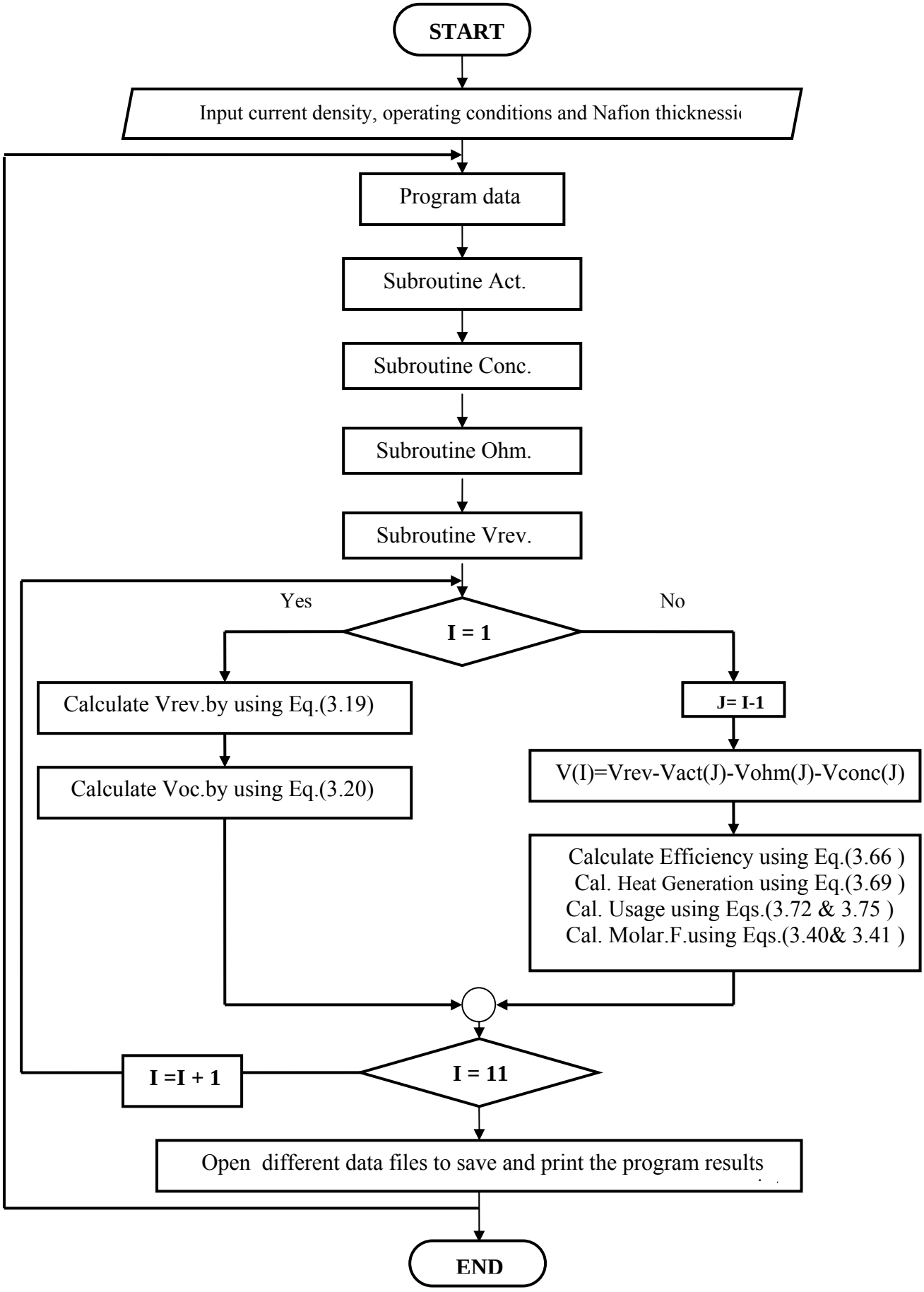

Fig.(4.1): Flowchart of the First Computer Program(Losses Model).

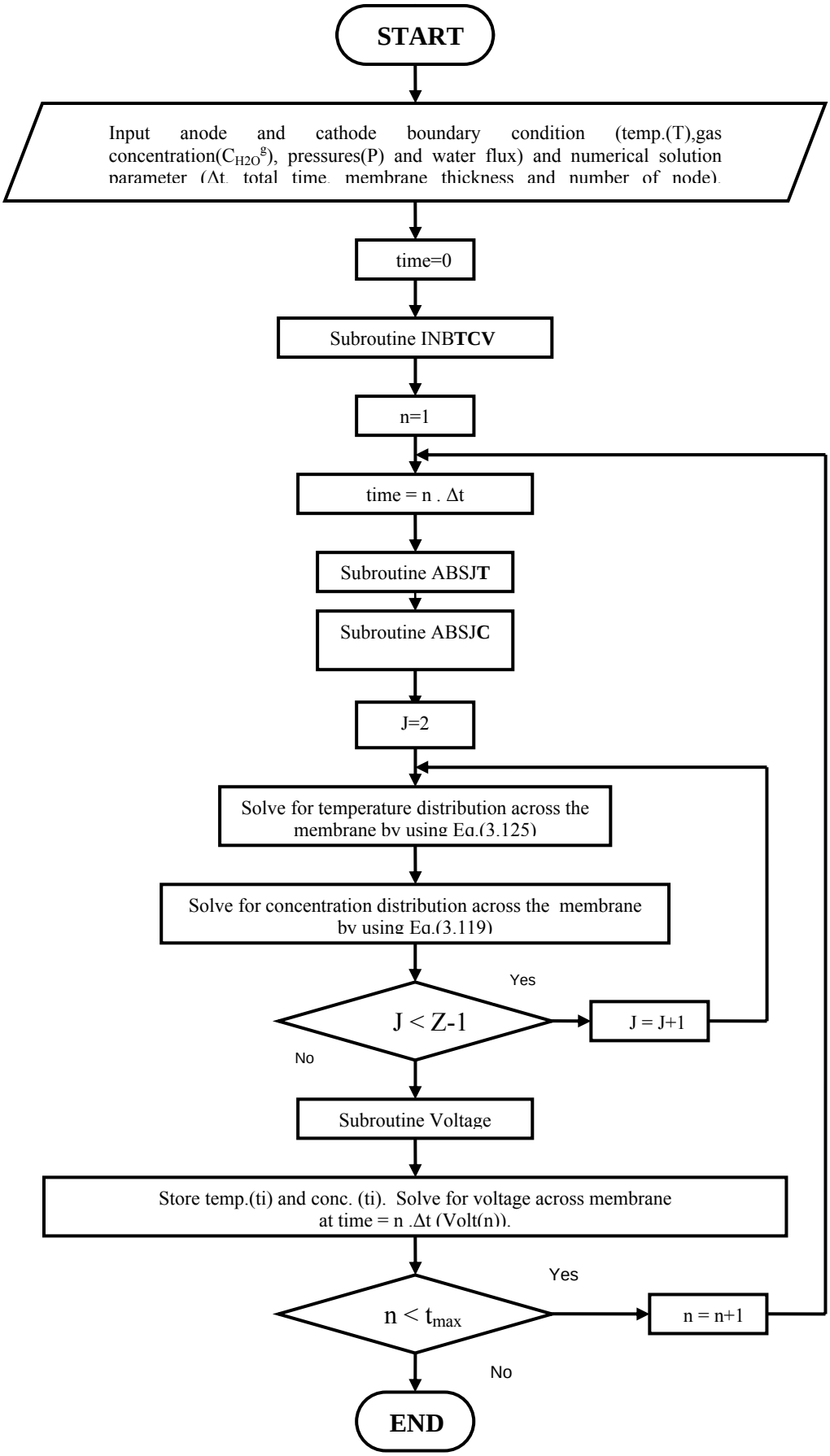

Fig.(4.2) : Flow Chart of the Second Program (Membrane Model).

Fig.(4.3): Subroutine ABCJT to find variable coefficients of Eq. (3.125)

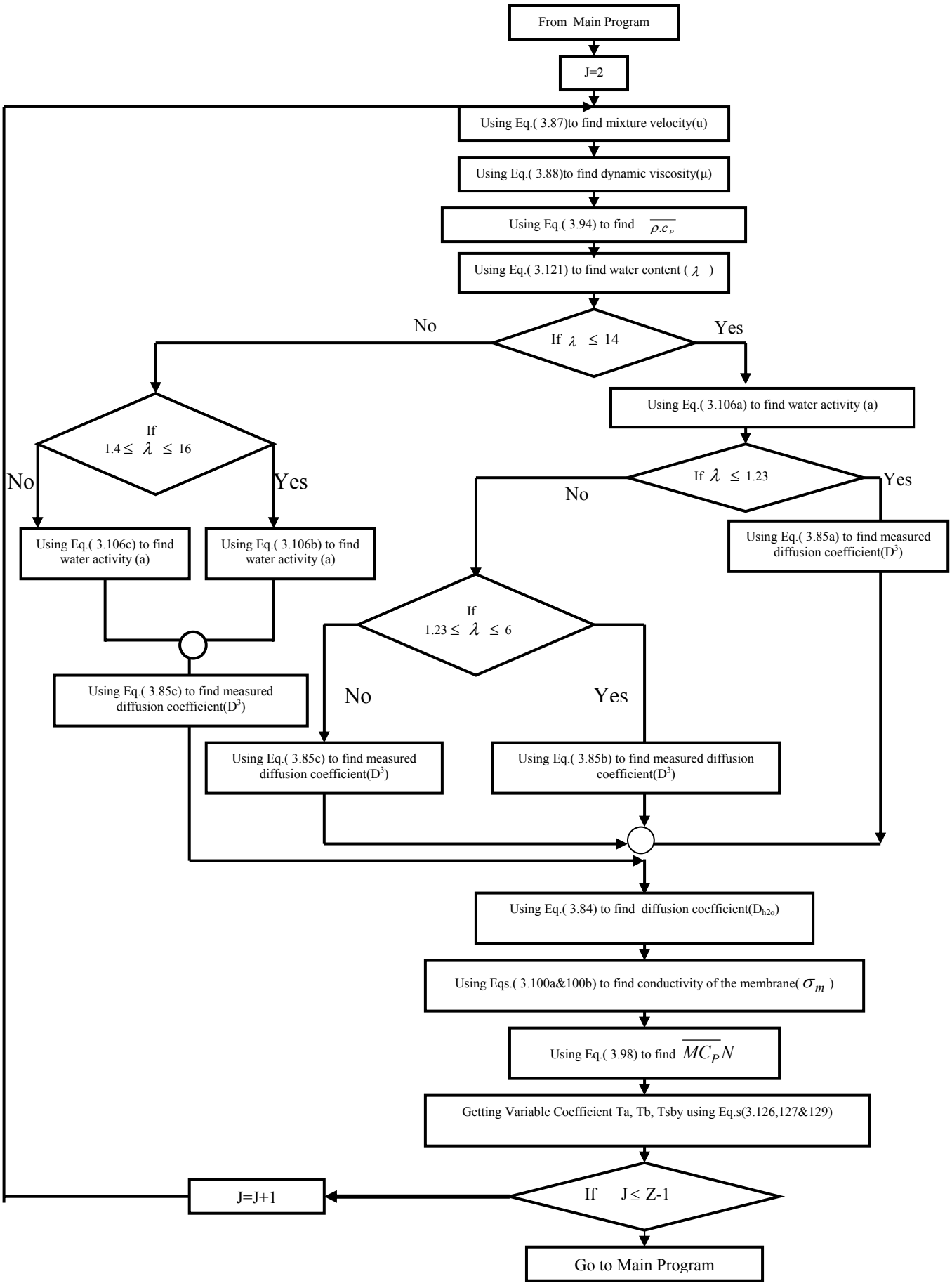

Fig.(4.4): Subroutine ABCJC to find variable coefficients of Eq. (3.119)

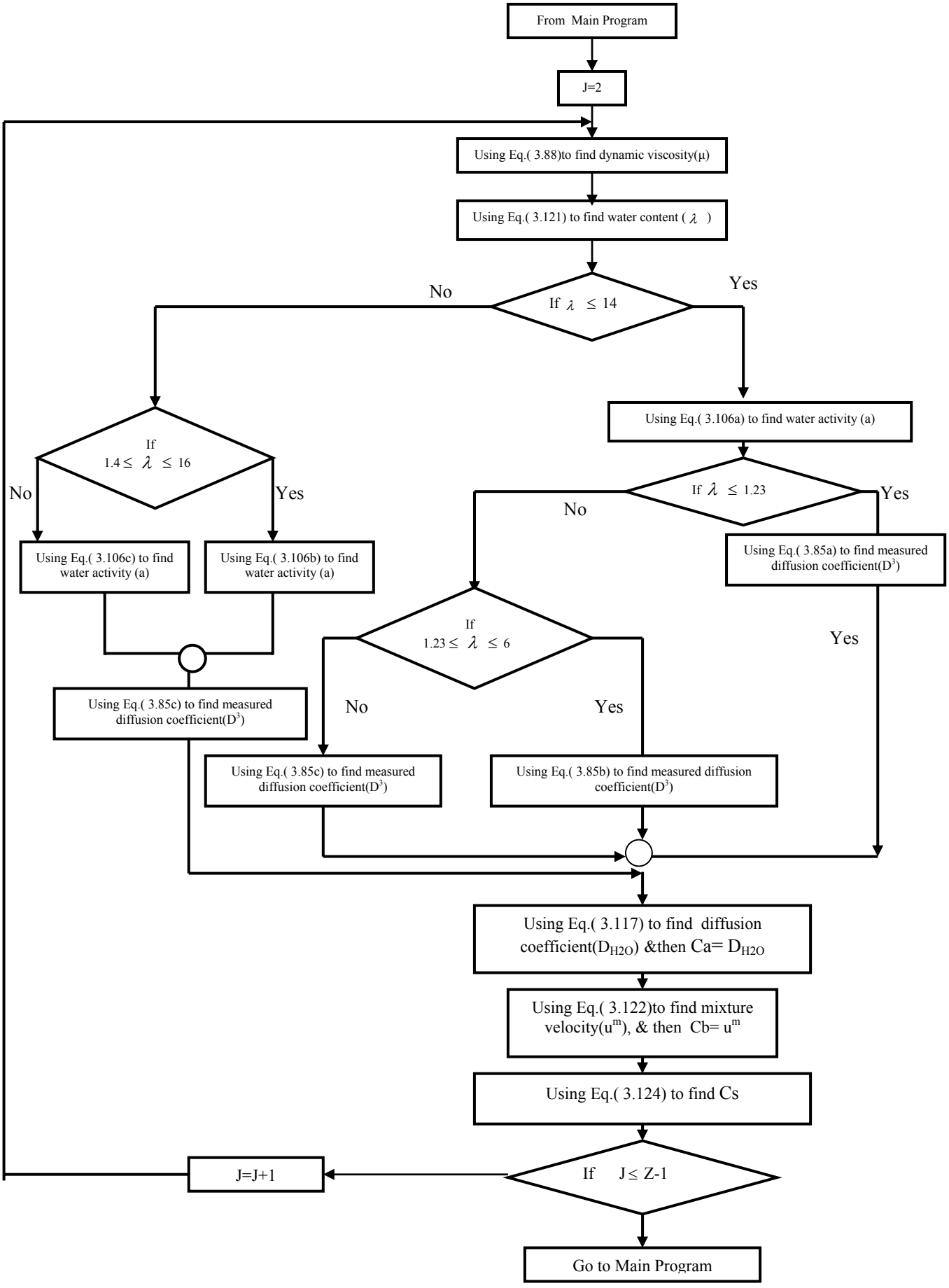

CHAPTER 5

RESULTS AND DISCUSSION

5.1 Introduction.

In this chapter, the results obtained from the computer programs consist of two parts. The first part studys the effect of various operating conditions and design parameters such as temperature, partial pressure, type and thickness of membrane, thickness of electrodes, and water content on the performance of Polymer Electrolyte Membrane Fuel Cell. The second part studys the effect of current density, pressure gradients and water flux on water concentration, temperature and voltage (proton potential) when the Nafion117 membrane is used.

5.2 Reversible Voltage.

Fig.(5.1) shows a linear relationship between the reversible voltage and the temperature. The reversible voltage of the hydrogen / oxygen fuel cell decreases with the increase in temperature because the water produced at the elevated temperature of the fuel cell contains the sensible heat at this temperature, which cannot be converted into electricity. This is due to the decrease in the change of Gibbs free energy with increasing temperatures.

The figure also shows that the increase in oxygen partial pressure leads to an increase in the reversible voltage according to the Nernst equation since it enhances the react between fuel and oxidant.

5.3 Air and Hydrogen Usage.

Fig.(5.2) illustrates a comparison between the predicted uasge mass flow rate of oxygen, air and hydrogen entering to cell. The flow rate of hydrogen on the fuel side and oxygen on the oxident side affects the performance of the polymer electrolyte membrane fuel cell. The current density increases as the flow rates of hydrogen and air or oxygen increases. The hydrogen / air cells have lower concentrations of oxygen on the cathode side than the hydrogen / oxygen cells.

5.4 Electrical Conductivity of the Membrane.

Fig.(5.3) shows that electrical conductivity of Nafion 117 is increasing linearly with membrane water content over the range of temperature from **20**^{0}C to **100**^{0}C.

At **40**^{0}C, for example, the value of electrical conductivity is **0.07** (S/cm, S= 1/Ω) for a water content **14** (mol H_2O/mol SO_3^-) whereas the value of electrical conductivity is **0.058** (S/cm) for a water of content **10** (mol H_2O/mol SO_3^-).

On the other hand, electrical conductivity also depends on temperature of the fuel cell. The electrical conductivity increases with increasing the operating temperature of fuel cell.

The conductivity of Nafion 117 membrane also increases with increasing water activity over the range of temperatures from **20**^{0}C to **100**^{0}C is shown in fig.(5.4).

This increases in electrical (proton) condictivity can be explained as follows. At low water activity the polymer electrolyte membrane adsorbs water that ionizes the sulfonic acid groups; which liberates protons that can hop between the fixed groups. The distance between ionized sites decreases with the increase in water content. Hopping frequency depends on distance so the electrical conductivity increases with water activity[47]. i.e with the decrease in distance between ionized sites.

5 . 5 Polarization Curves.

As mentioned earlier, the performance of fuel cell can be summarized in a plot of cell voltage versus current density called a polarization curve. In this section, the results of the study of effect of operating and design parameters such as temperature, partial pressure, thickness of membrane, thickness of electrode and water content are discussed.

5.5.1 Influence of Temperature.

Fig.(5.5)shows fuel cell polarization curves for Nafion112. The polarization curve is shifted upward as the fuel cell temperature increases until about 100 ^{0}C. The reason for this, is that higher temperatures improve mass transfer within the fuel cell and results in a net decrease in cell resistance (as the temperature increase, the electronic conduction in metals decreases but the ionic conduction in the membrane increases). Together, these effects improve the reaction rate. So, the net effect is that fuel cell voltage increases with temperature until the temperature approaches the boiling point of water (~**100** ^{0}C). At this temperature, the water boils and the resulting steam severely reduces the partial pressure of the oxygen, the voltage begins to decline and reduces cell performance.

On the other hand, the activation losses decrease with increasing the operating temperature (until ~**100**^{0}C) because the exchange current density of an electrochemical reaction increases with increasing the operating temperature. At this range, the effect of increasing the exchange current density is greater than the effect of increasing the Tafel slope, A_T ,(see Eq(3.22)), hence the cell performance is improved.

Above **100**^{0}C, an increase in operating temperature raises the activation losses because Tafel slope will be dominant compared with increase in the exchange current density, therefore, the cell performance is reduced.

The composition of the inlet gas streams are also affected by temperature since saturation pressure is a function of temperature. At **50** ^{0}C and **1** atm, for example, the molar fraction of water vapor in fully humidified gas streams is 13% whereas

the molar fraction of oxygen is **87%.** But, at **80** ^{0}C for the same pressure, the molar fraction of water vapor in fully humidified gas streams is **46%** and that for oxygen is **54%** . Therefore, the molar fraction of water vapor in fully humidified gas streams increases with temperature for a fixed total pressure, and the molar fraction of oxygen decreases with increasing temperature in a fully humidifed inlet stream with constant total pressure, as shown in Fig(5.6). This is in agreement with experimental parametric study of **Berning and Djilali**[40].

5.5.2 Influence of Partial Pressure of Oxygen.

Similar to the temperature, the operating pressure enhances transport properties in PEM fuel cell. Fig(5.7) shows the influence of partial pressure of oxygen on the performance of fuel cell at **80**^{0}C. An increase in the partial pressure of oxygen from **1.7** to **3.5** atm produces an increase of ***4.75* %** (**0.03V**) in the cell voltage at a current density of 1 A/cm^2.

As mentioned above, the fuel cell polarization curves typically increase with increasing partial pressure of oxygen. Conversely, the polarization curves decrease with decreasing operating pressure. The reason for this is that the rate of chemical reaction is proportional to the partial pressure of oxygen and hydrogen. Thus, the effect of increased pressure is most prominent when using a diluted oxidant (air) or a diluted fuel (reformate). In essence, higher pressures help to force the hydrogen and oxygen into contact with the membrane. This sensitivity to pressure is greater at high currents. Although an increase in pressure promotes the electrochemical reaction, it introduces other problems such as: Fuel cell stack flow field plates work better at low pressure since they exhibit smaller flow induced pressure losses. Fuel cell seals operate under additional stress. Additional air compression is required, which absorbs more of the gross power. Other system components must be re-designed accordingly; some components must increase in size and cost.

Fig.(5.5) shows that a temperature drop of approximately **20** ^{0}C (80^{0}C - 60^{0}C) will result in about a ***11.67%*** loss whereas reducing the partial pressure from **3.5** to **1.7** atm results in about a ***4.75 %*** loss (see Fig.(5.7)).

Fig.(5.8) shows a plot of molar oxygen and water vapor fractions versus pressures for the gas compositions of the cathode inlet stream. It can be seen that the change in inlet gas composition is particularly strong in the range from **1** atm to **3** atm. Above **3** atm, the composition changes only slightly with the pressure. Since the saturation pressure remains constant for constant operating temperature, the molar fraction of water vapor in fully humidified gas streams decreases with increasing the inlet pressure. On the other hand, the molar fraction of oxygen in fully humidified gas streams increases with increasing the operating pressure. This is agreement with experimental paramtric study [40].

5.5.3 Influence of Membrane Thickness.

Figs(5.9,10,11&12)show the comparison of polymer exchange membrane fuel cell performance with different Nafion types (Nafion112, Nafion1135, Nafion115 and Nafion117) at temperatures **60**, **70**, **80** and **100**^{0}C, respectively. The Nafion112 exhibits better cell performance compared to others at high current density and at all temperature.

The reason for this is that the resistance to charge transfer for Nafion112 is smaller, since it has thinner membrane. Therefore, the ohmic loss becomes less according to Eq.(3.39). The thinner membranes are also advantogeous because they keep the anode electrode wet by **back diffusion** of water from the cathode, where it is generated, towards the anode. However, there is a practical limit on the membrane thickness where it should not be less than **20**μm [48]. Below this thickness, mixing of reactant gases (hydrogen and oxygen) due to crossover through the membrane takes place and this reduces cell efficiency. For this reason, Nafion117 membrane is better than those of Nafion counterparts, especially for automotive applications.

Fig.(5.13) shows the electrical power density and waste heat versus current density at temperature **60**^{0}C . This figure shows that the electrical power density increases with increasing current density since the power density is directly proportional to the current density (the electrical power density is product of

voltage and current density). From the previous discussion it can be concluded, that the fuel cell which has lower thickness (Nafion112) gives maximum electrical power density. Worthwhile , the power density of fuel cell is usually stated in terms of cell area rather than volume. This is because the current density is directly related to the cell area.

In the same figure, the heat generated in the fuel cell increases with increasing in the current density. The reason for this is that the irreversible losses of the electrochemical reactions increase with current density.

Also, as previously discussed, the resistance of the membrane increases with increasing the thickness; therefore, the heat generated in the cell using Nafion117 greater than the rest of the fuel cells that uses other types of membrane.

Figs.(5.13, 14,15 and 16) show that, the electrical power density increases with increasing the operating temperature of the cell except Fig.(5.16). The reason of this is as discussed in figure(5.5). Conversely, the heat generated decreases with increasing in the temperature because the reversible heat (entropic heat) decreases with the increase in temperature.

Figs.(5.17,18,19 and 20) show the efficiency – power density relationship generated from the polarization curves of Figs.(5.9,10,11 and 12) respectively. The fuel cell efficiency is directly proportional to the cell voltage as shown in equation (3.66); therefore, the efficiency is inversely proportional to power density. In addition, these figures show that the efficiency of the fuel cell decreases when the power density increases. This is due to the mass transfer limitations which reduces the power density.

5.5.4 Influence of Electrode Thickness.

At high current densities, mass transport limitations become dominant. The diffusion of oxygen to the reaction site at the platinum surface, becomes a limiting factor for the current density. As described in Chapter Three, section 3.4, the limiting current density can be calculated as a function of the thickness of the

electrode. The influence of this parameter on the polarization curve is shown in Fig.(5.21). The figure shows that, increasing the thickness of the electrode results in poorer performance because of reactant transfer resistance.

5.5.5 Influence of Membrane Water Content.

Fig.(5.22) shows the influence of membrane water content in the catalyst on the polarization curve. Since membrane electrical conductivity increases with water content, the ohmic losses in the polymer membrane of the catalyst layer decreases with increased water content. Thus, better performance is obtained with higher water content. This result agree with **Genevey et al**.[25].

5.5.6 Electrode Losses.

Figs.(5.23, 24, 25 and 26) show contribution of anode and cathode voltages to fuel cell performance for different Nafion types at a temperature of **80**^{0}C.

At **80**^{0}C the voltage of the anode electrode and cathode electrode was nearly identical for all Nafion membranes, but the difference in ohmic losses voltage are apparent.

If the electrons flow from anode electrode to cathode electrode, the cell operates in its spontaneous change state, $\Delta G < 0$, and the voltage of the cathode electrode will be higher than that of anode (the standard electrode voltage for the anode is zero, whereas the standard electrode voltage for the cathode is 1.229). The cell voltage will be positive, but the anode voltage increases as electrons move to the cathode and the cathode voltage decreases as electrons begin to accumulate.

Also, Figs(5.23,24, 25 and 26) compare the ohmic losses which are obtained in four types of Nafion membranes. The ohmic losses of Nafion 112 is substantially less than those of Nafion counterparts, due to its smaller thickness.

However , the net result of current flow in fuel cell is to increase the anode voltage and to decrease the cathode voltage, thereby reducing the cell voltage.

5.6 Water Management Within the Membrane.

Within the membrane, water is transported as a result of a diffusive force, a convective force due to an applied pressure gradient, and an electric drag force imposed on the water molecules by the charged protons moving from anode to cathode. To demonstrate the electric drag force, the water concentration at both the anode and cathode interface is held constant and the current density is varied. By varying current density, the relative effect of moving more charged particles through the membrane is shown in Fig.(5.27).

To demonstrate the effect of the convective force on water transport in the membrane, different pressure gradients were applied across the membrane. The higher the gradient, the more water molecules are moved in the opposite direction to the gradient. These results are shown in Fig.(5.28).

Figs.(5.29) and (5.30) show the effect of the current density and the pressure gradient on the water concentration through both sides of the membrane (anode and cathode side) with time.

Also in this section on water management, the effects of water flux direction into and out of the membrane are shown in figures(5.31) and (5.32). It must be mentioned that all the results have the same initial and boundary hypothetical conditions of temperature and voltage. The coupling effects of water concentration on temperature and voltage are shown in Figs.(5.31) and (5.32).

5.6.1 Effect of Electric Drag.

Fig.(5.27)shows the effect of the electric drag force. As current density increases, more protons migrate from the anode where they are produced to the cathode where they are consumed. As they migrate, the charged protons drag the dipole water molecules with them from anode to cathode. Also, this figure shows how the water concentration in the membrane changes through the same time steps and the same applied boundary conditions but with different current density i.e **0.1**

A/cm^2 and **0.4** A/cm^2. The analyses the results, shows that water concentration on the anode side for a given time step is lower at the higher applied current density. This is because the higher current density drags more water molecules towards the cathode side. It is also seen that the water content in the membrane is lower with the higher current density because the increased protonic current is dragging more water molecules out of the membrane.

5.6.2 Effect of Pressure Gradients.

Fig.(5.28) illustrates the effect of pressure gradient in the membrane on water concentration. A positive pressure gradient can be established between the anode and cathode to force water molecules from cathode to anode.

This boundary condition can be established to help keeping the anode side of the membrane hydrated. Anode side drying is more important than cathode side drying because water content is usually higher on the cathode side. This is because water is produced at the cathode and water molecules are driven from the anode to the cathode due to the drag force as shown in Fig(5.27).

Fig.(5.28) shows how the water concentration in the membrane changes with time due to the applied pressure gradient between the anode and cathode. The pressure gradient of **2** atm between the anode and cathode i.e. a pressure of **1** atm was applied as a boundary condition at the anode membrane interface and pressure of **3** atm was applied at the cathode membrane interface. The other curves show water concentration at the same time steps with the same applied boundary conditions but with the pressures at the anode and cathode sides of the membrane set equal, i.e. no applied pressure gradient. This Figure also shows that the pressure gradient established helps to combat the lose of water brought about by protonic drag on the water molecules and therefore increasing the overall water content in the membrane compared to the case where no pressure gradient is applied.

5.6.3 Effects of Electric Drag and Pressure Gradients at both side of the Membrane with Time.

Fig.(5.29)shows the effect of the current density and the pressure gradient on the water concentration through the anode side of the membrane with time. This figure also shows that the water concentration increase with increasing pressure gradient due to the effect of the convective force. Conversely, the water concentration decreases with increasing the current density due to the effect of the electric drag force. It can be seen that the increase in the water concentration is particularly strong in the period from **0** to about **30 sec**. During the operation, all processes (electric drag force, convective force, back diffusion force) occur at the same time. Initially, both the convective and back diffusion forces are dominant compared to the electric drag force (direction of water flow from the cathode to the anode); therefore, the water concentration in the anode side of the membrane increases rapidly with time. After **30 sec** the water concentration increasing only slightly with time, especially at high current density. This phenomenon is caused by the increasing effect of the electric drag force which has an opposite effect on water flow direction. Therefore, little increasing in the water concentration occurs with time . Thereby the membrane showed good stability with time (the membrane is saturated).

Fig.(5.30)shows the effect of the current density and the pressure gradient on the water concentration through the cathode side of the membrane with time. This figure is identical to above figure, but the water concentration in the cathode side of the membrane is greater than the water concentration in the anode side. This event is caused by the production of the water in the cathode side of the catalyst layer.

5.6.4 Effects of Entering and Exiting Water Fluxes.

The effects of water fluxes at the boundaries of the membrane are shown in Figs(5.31)and (5.32). In first case, a zero flux condition (no water moves from the catalyst layer into the membrane) is applied at the anode and a positive flux

condition is applied at the cathode. The second case, a zero flux is applied at the anode and a negative flux (a flux of water out of the membrane) at the cathode.

Figs.(5.31) and (5.32) show the effect of membrane hydration on voltage losses and heating of the membrane, respectively. The figures show also the voltage and temperature across the membrane when either there is a water flux into or out of the membrane. When water flows **into** the membrane, the water content increases and membrane conductivity increases. As a result the voltage drop and ohmic heating in the membrane decrease. The decrease in ohmic heating which is a source term in the thermal energy conservation equation for the membrane is illustrated by the decrease in temperature inside the membrane, shown in Fig.(5.32). When water flows **out of** the membrane the opposite trends are illustrated. Water content in the membrane decreases and membrane conductivity decreases. As a result, larger voltage drops and ohmic heating across the membrane and higher temperatures inside the membrane take place.

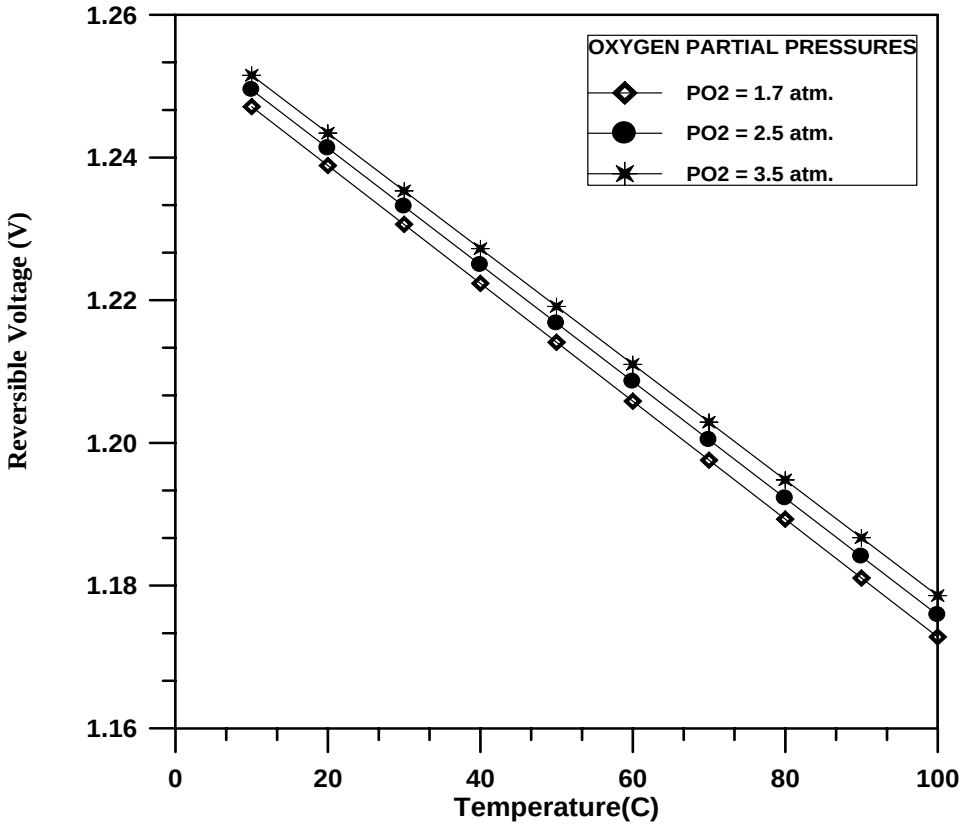

FIGURE(5.1):Reversible Voltage of the Hydrogen-Oxygen Cell with Different Oxygen Partial Pressures

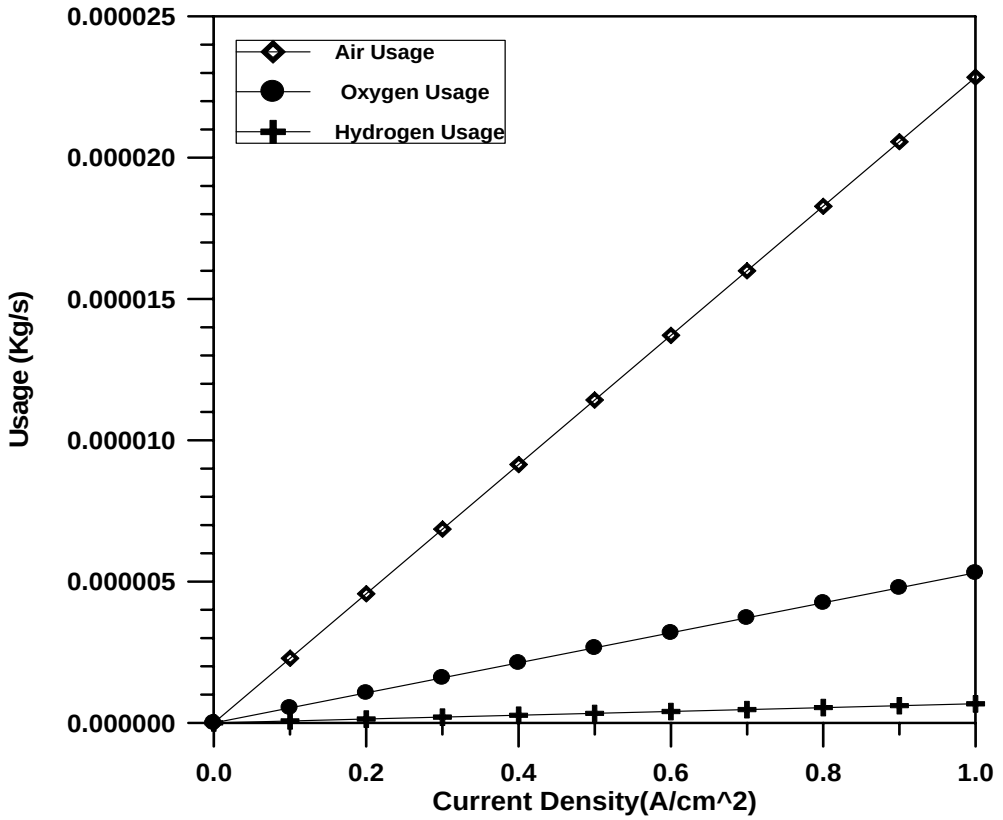

FIGURE(5.2):Hydrogen/Oxygen(or Air) Fuel Cell Usage

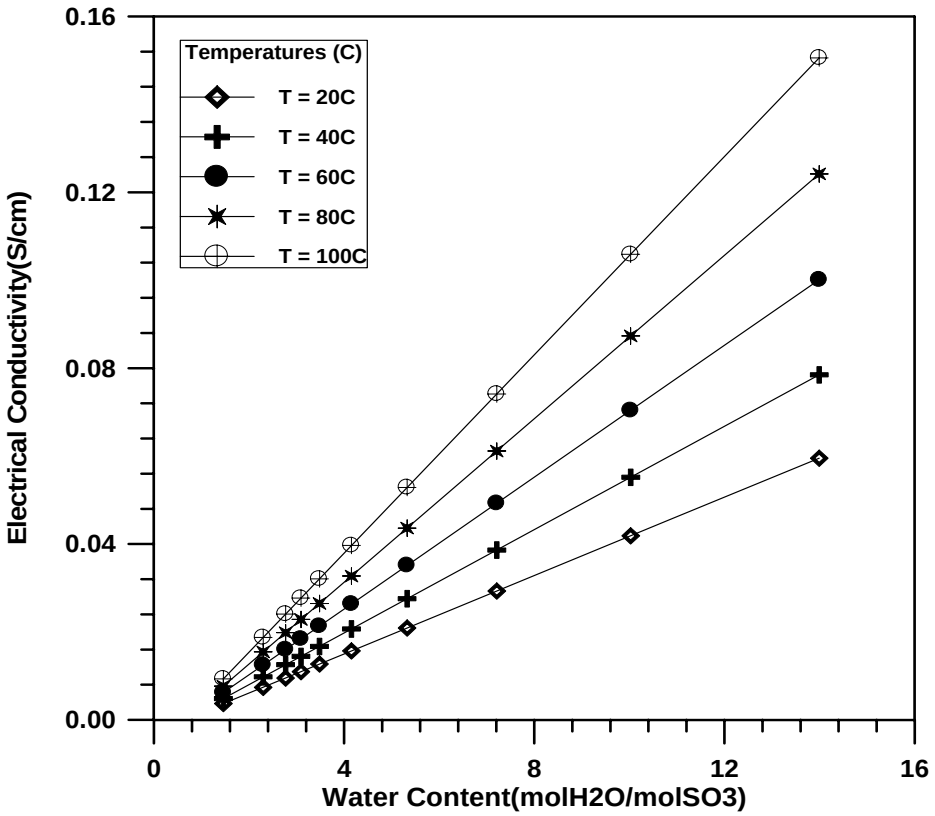

FIGURE (5.3): Nafion 117 Membrane Conductivity as a function of Water Content with different temperature.

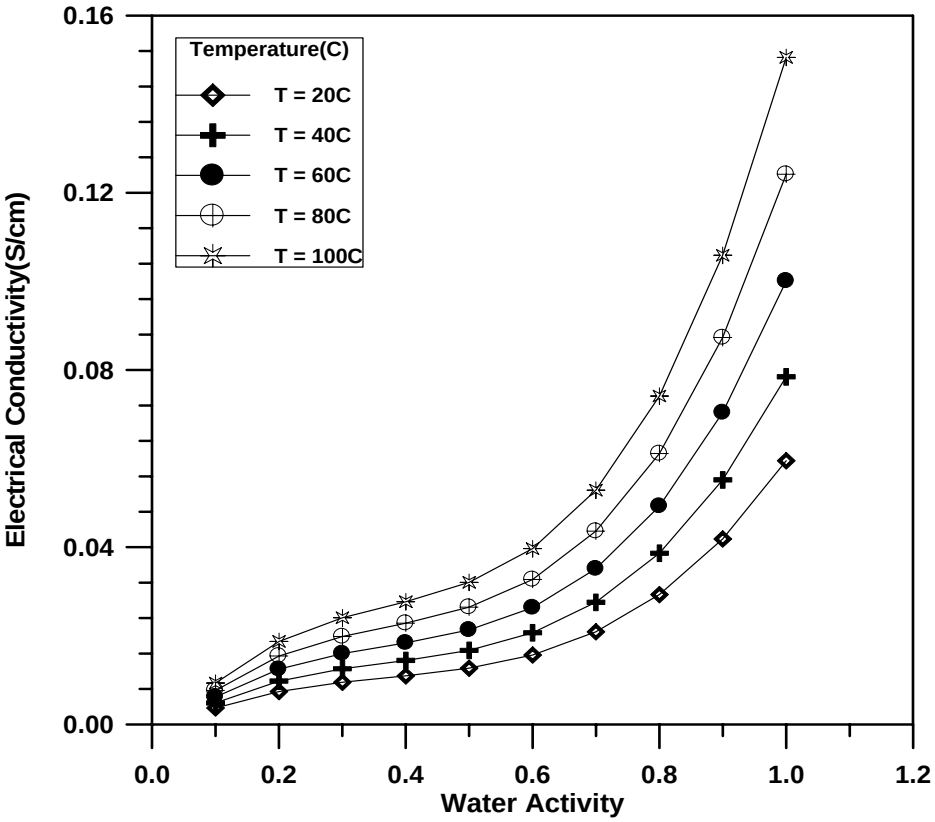

FIGURE (5.4): Nafion 117 Membrane Conductivity as a function of Water Activity with different temperature

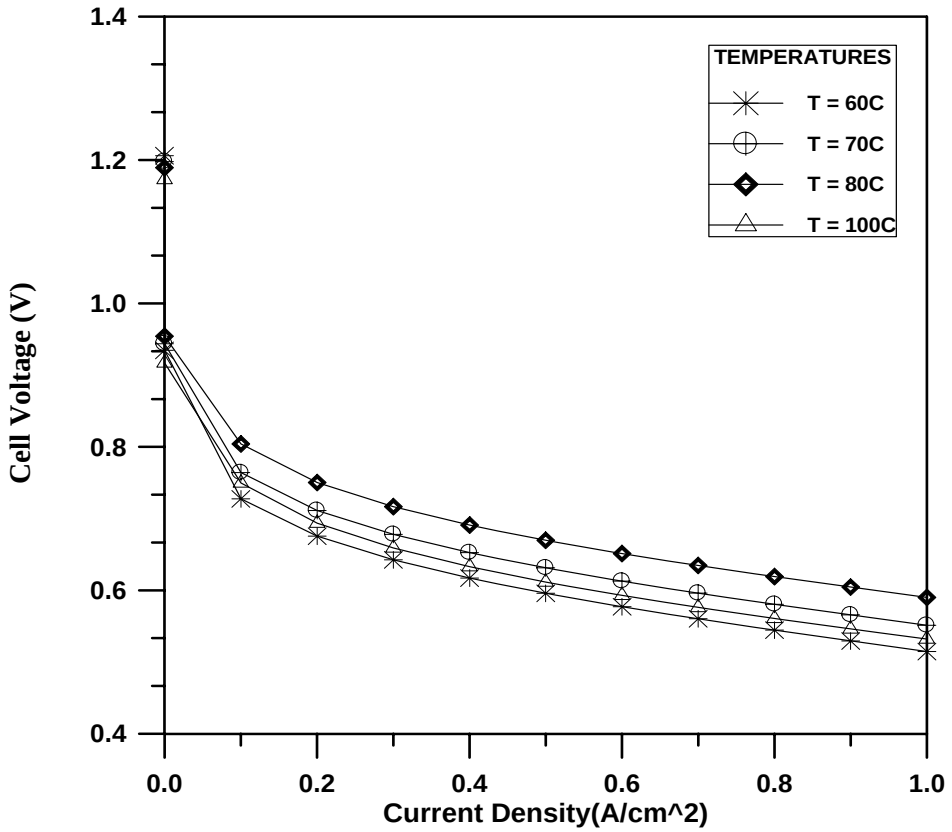

FIGURE (5.5):Polarization curve of Nafion112 for different Temperatures at PO2=1.7atm.

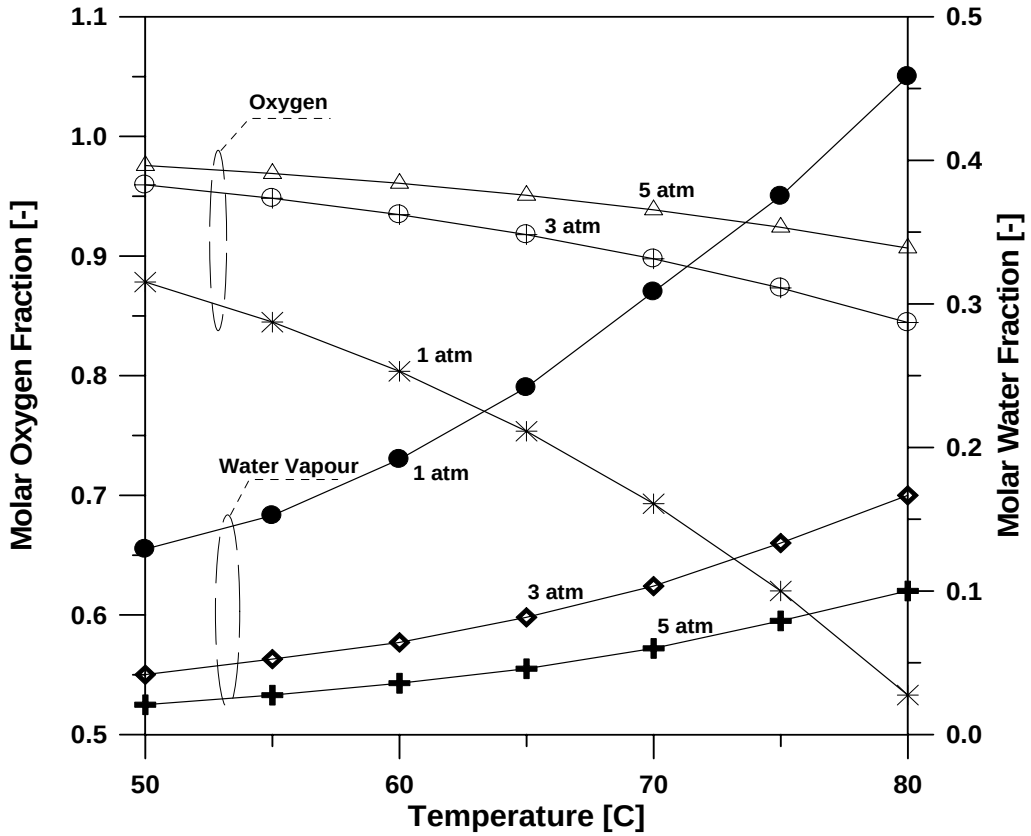

FIGURE (5.6): Molar inlet fraction of oxygen and water vapour as a function of temperature for three different pressures for fully humidified gas streams.

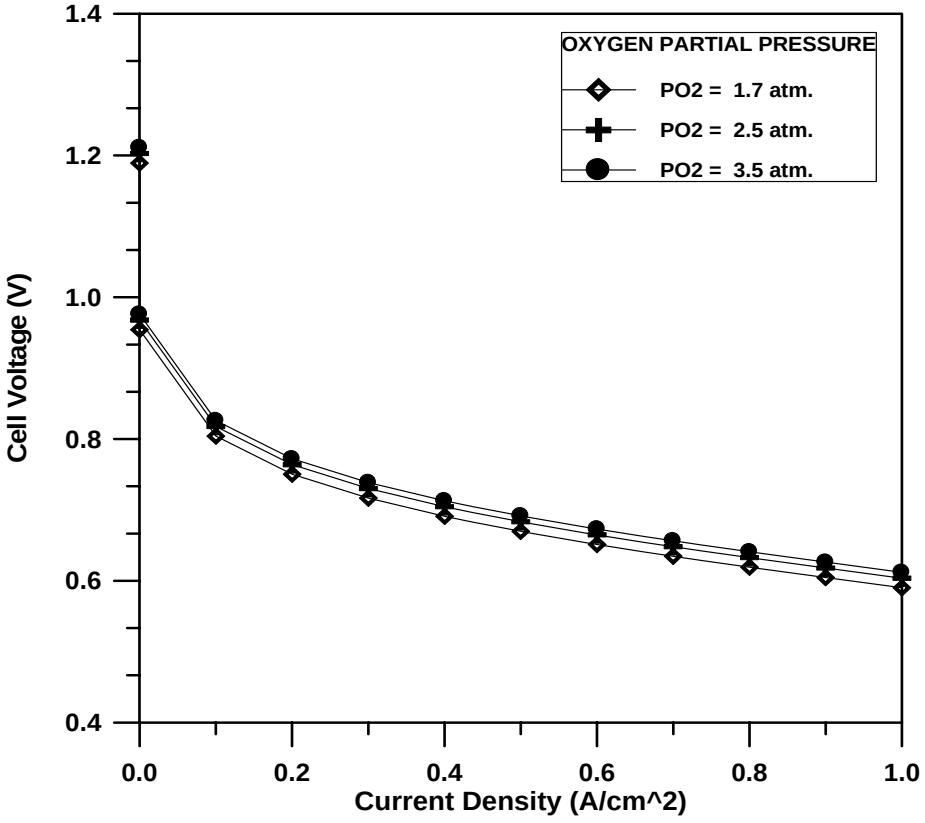

FIGURE (5.7):Polarization curve of Nafion112 for different oxygen partial pressures at 80°C

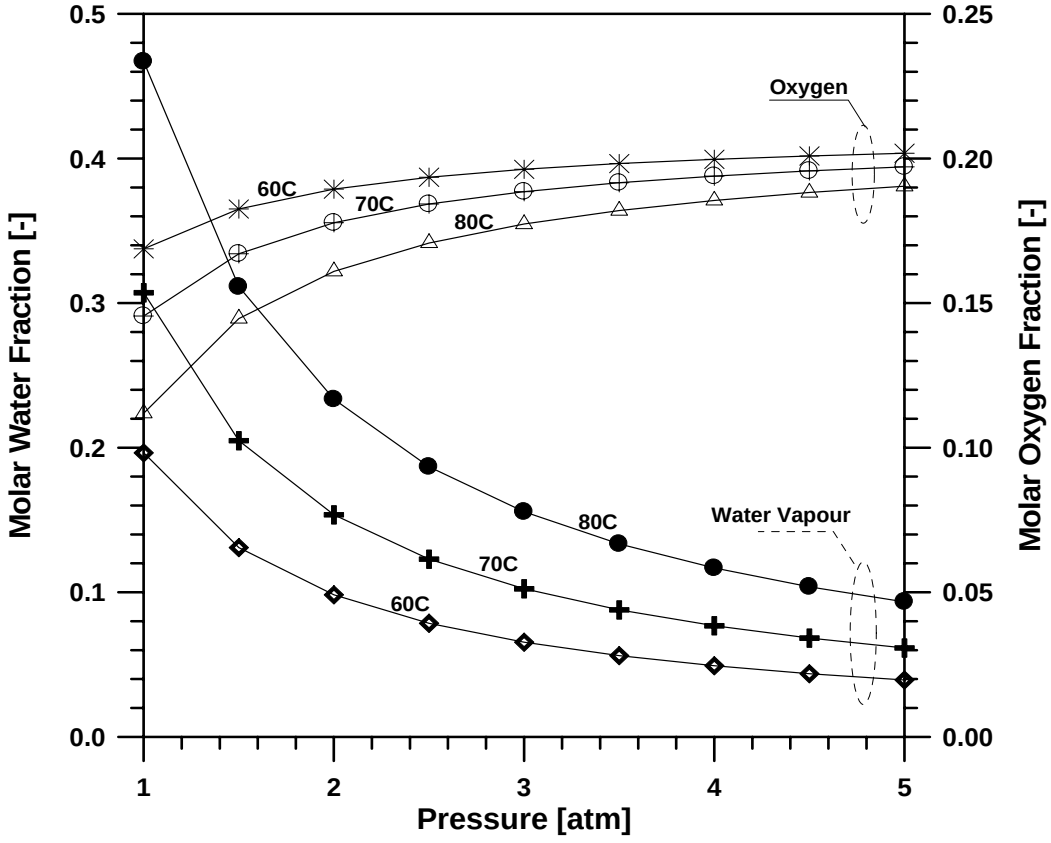

FIGURE (5.8):Molar oxygen and water vapour fraction of the incoming air as a function of pressure for three different temperatures for fully humidified gas streams.

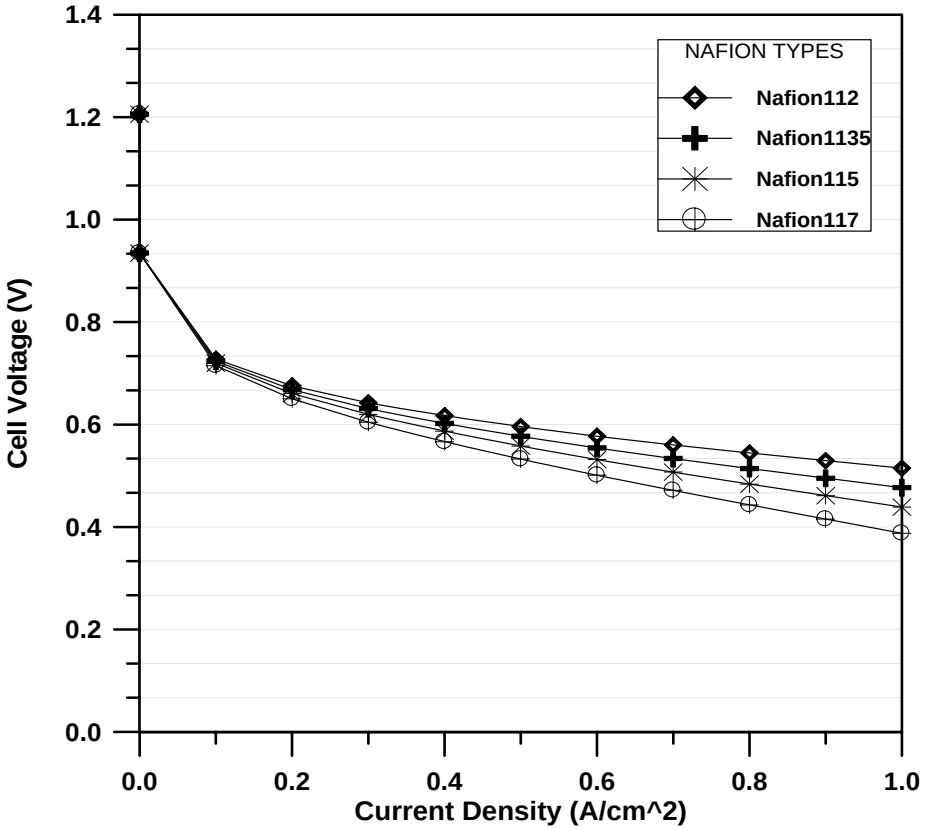

FIGURE (5.9):**Polarization Curves at T=60^{o}C**

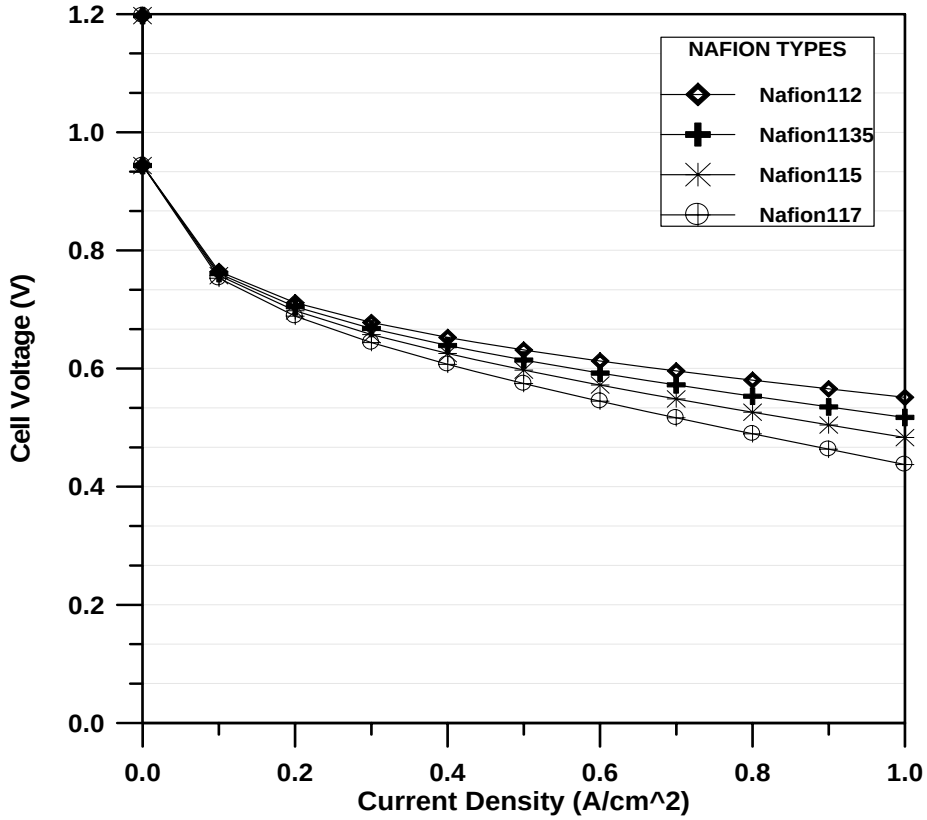

FIGURE (5.10):**Polarization Curves at T=70^{0}C**

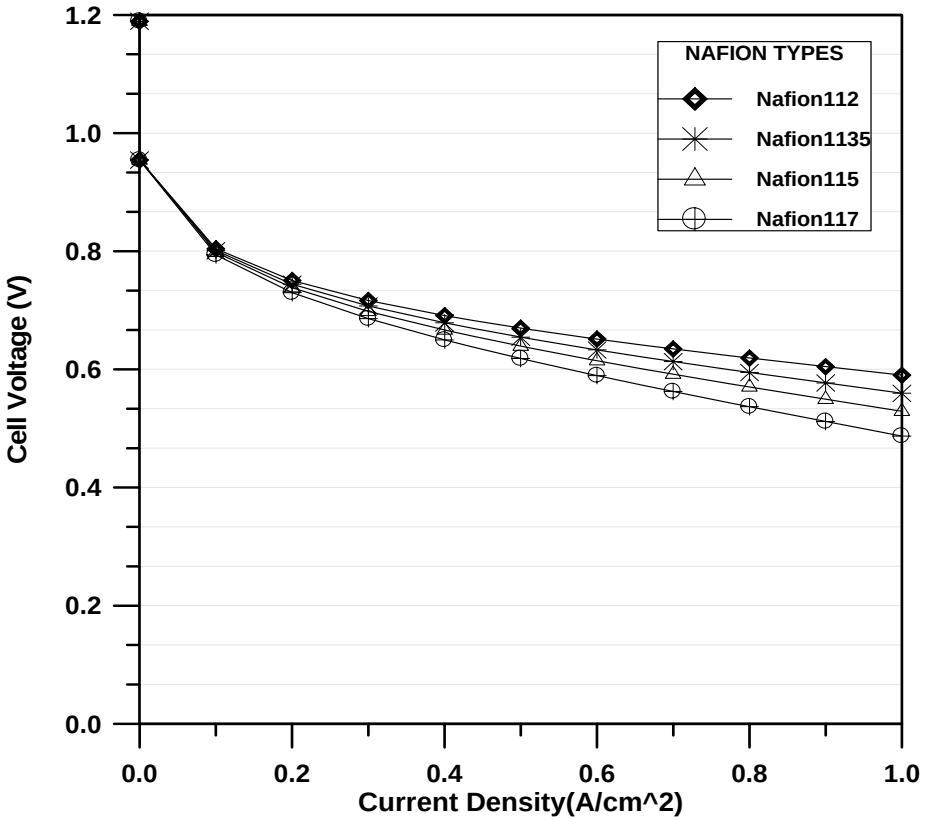

FIGURE (5.11):**Polarization Curves at T=80^{O}C**

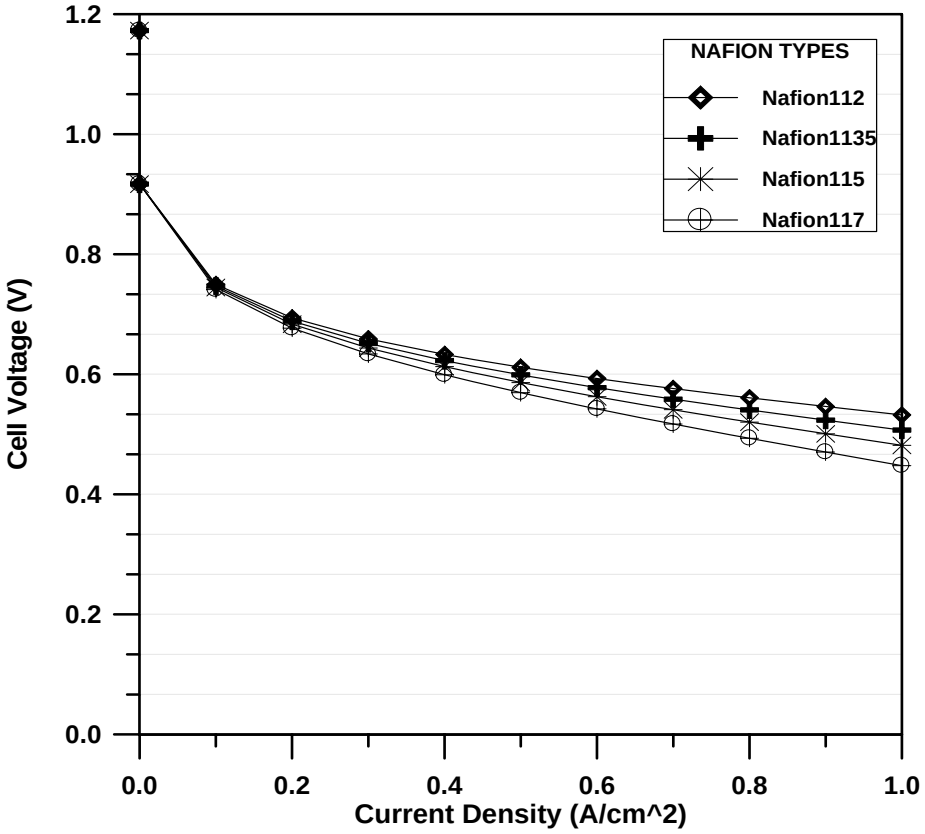

FIGURE(5.12):**Polarization Curves at T=100^{0}C**

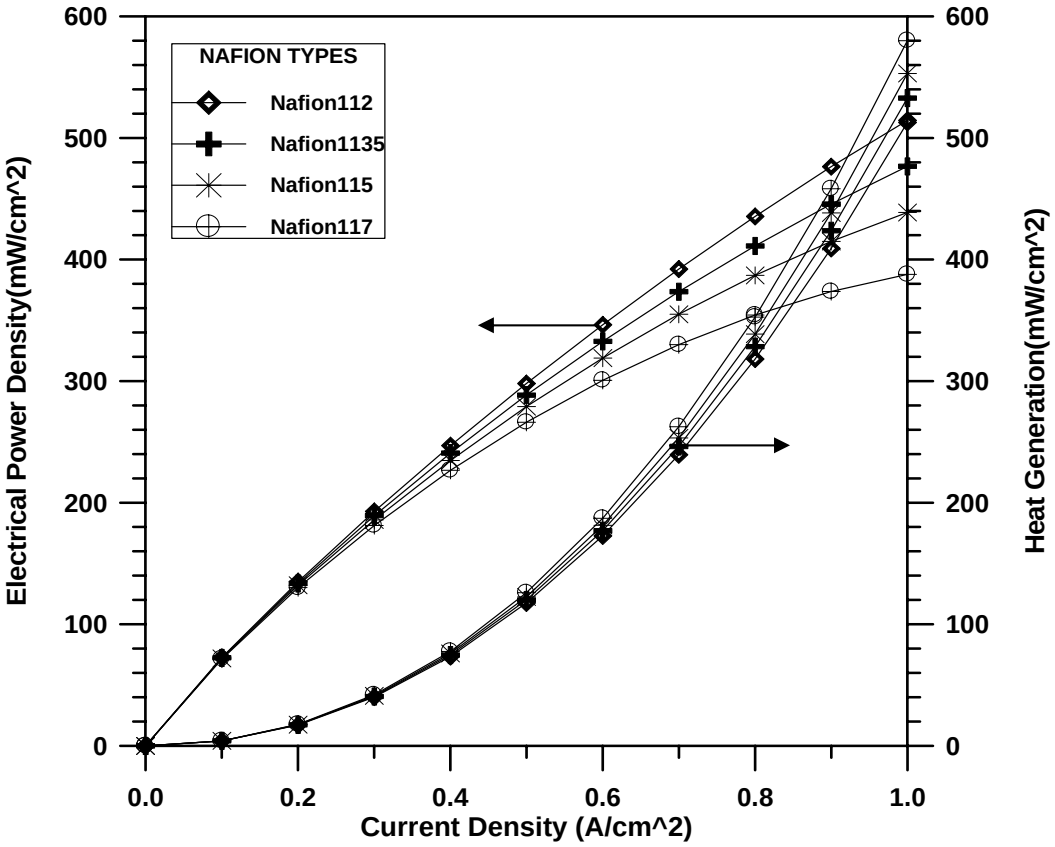

FIGURE (5.13): Electrical Power and Heat losses vs. Current Density at T=60^{O}C

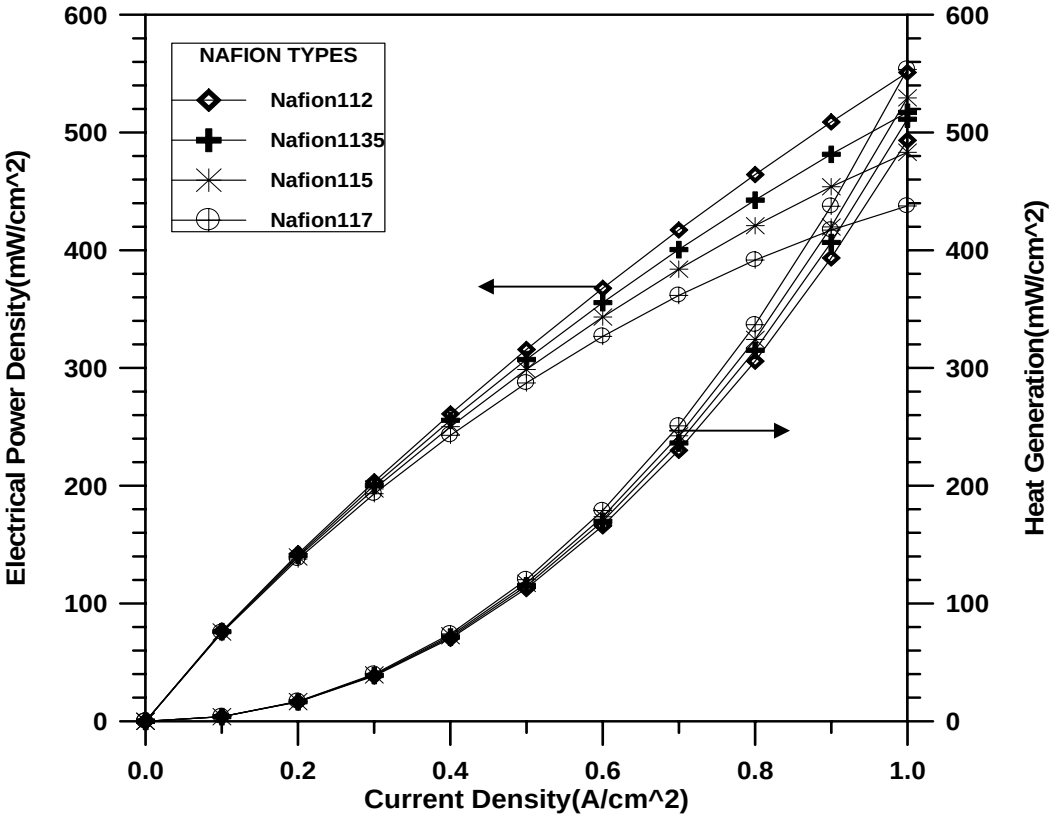

FIGURE (5.14): Electrical Power and Heat losses vs. Current Density at T=70^{0}C

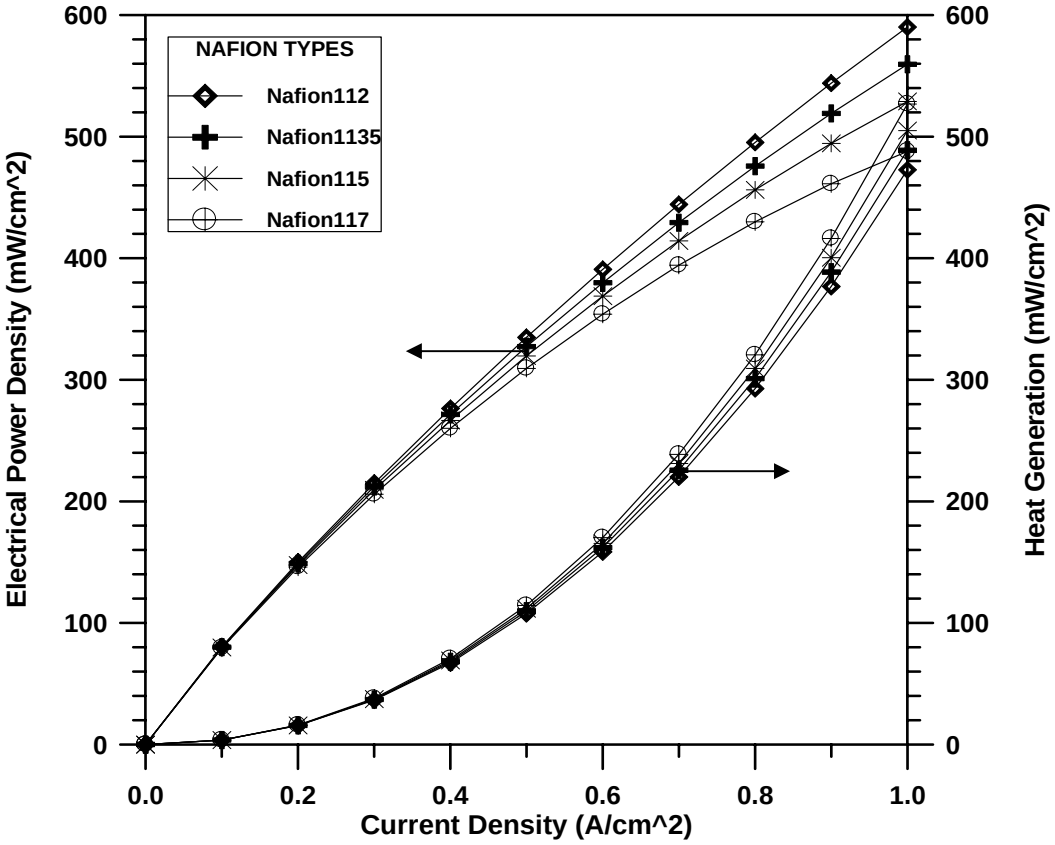

FIGURE (5.15): Electrical Power and Heat losses vs. Current Density at T=80^{O}C

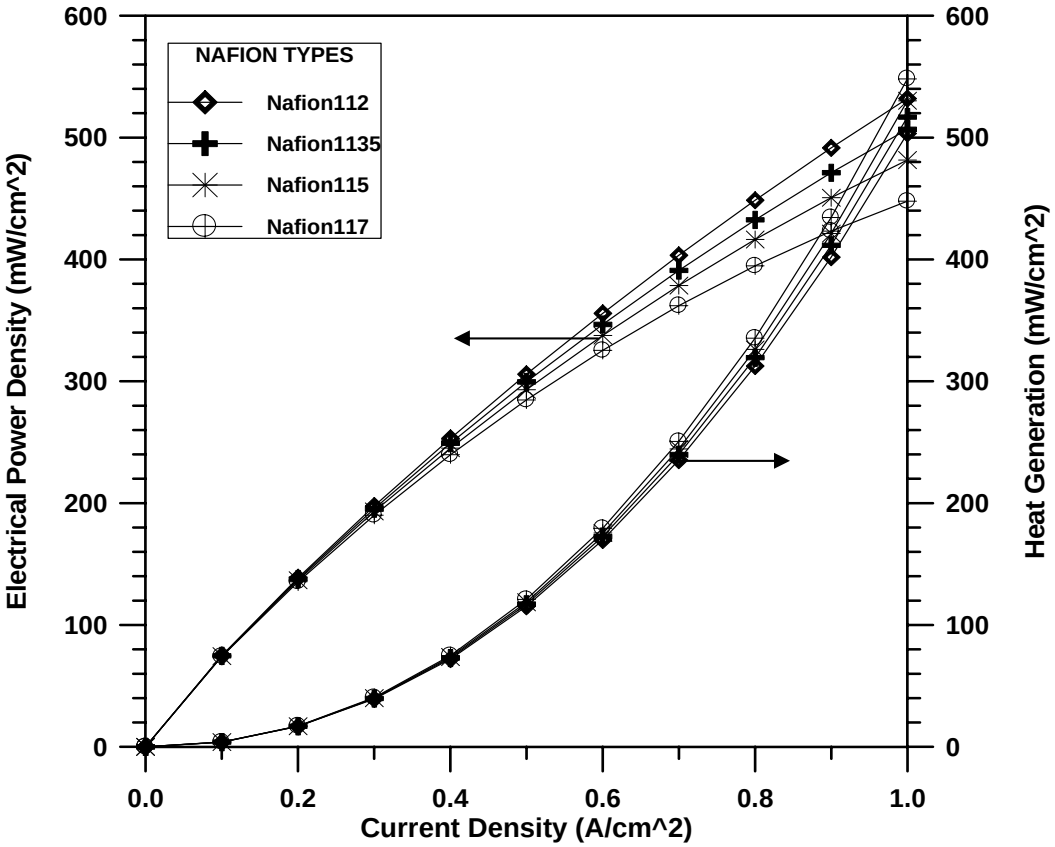

FIGURE (5.16): Electrical Power and Heat losses vs. Current Density at T=100^{O}C

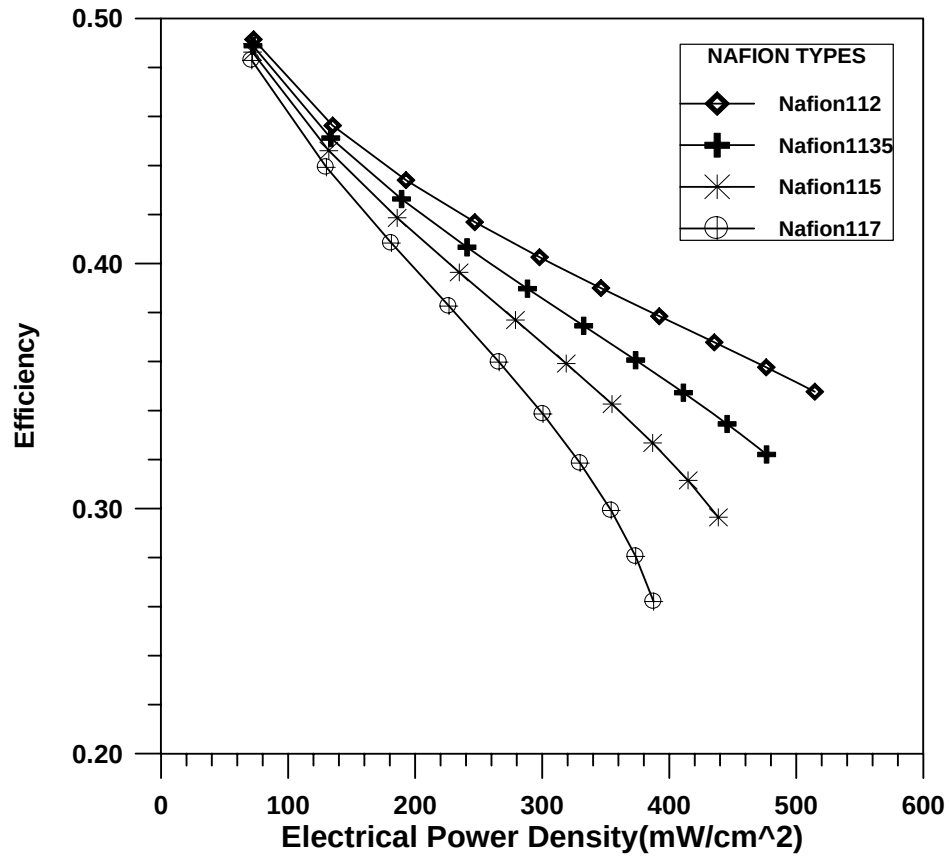

FIGURE (5.17): Efficiency versus Electrical Power Density at Temperature 60^{O}C

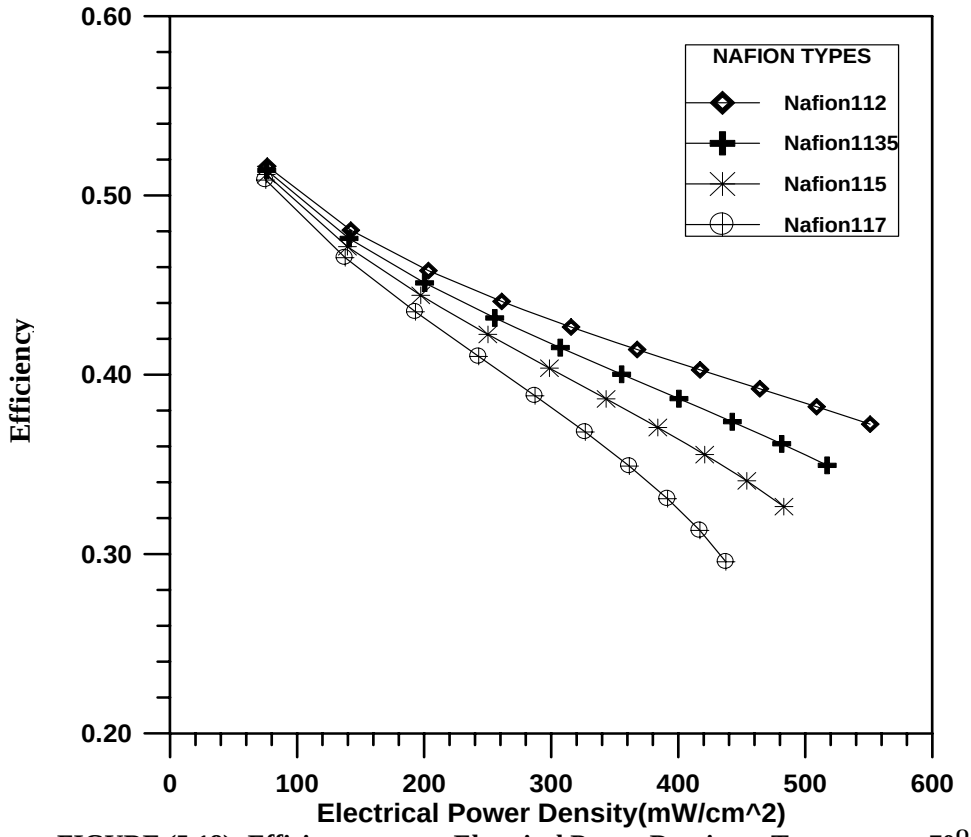

FIGURE (5.18): Efficiency versus Electrical Power Density at Temperature 70^{O}C

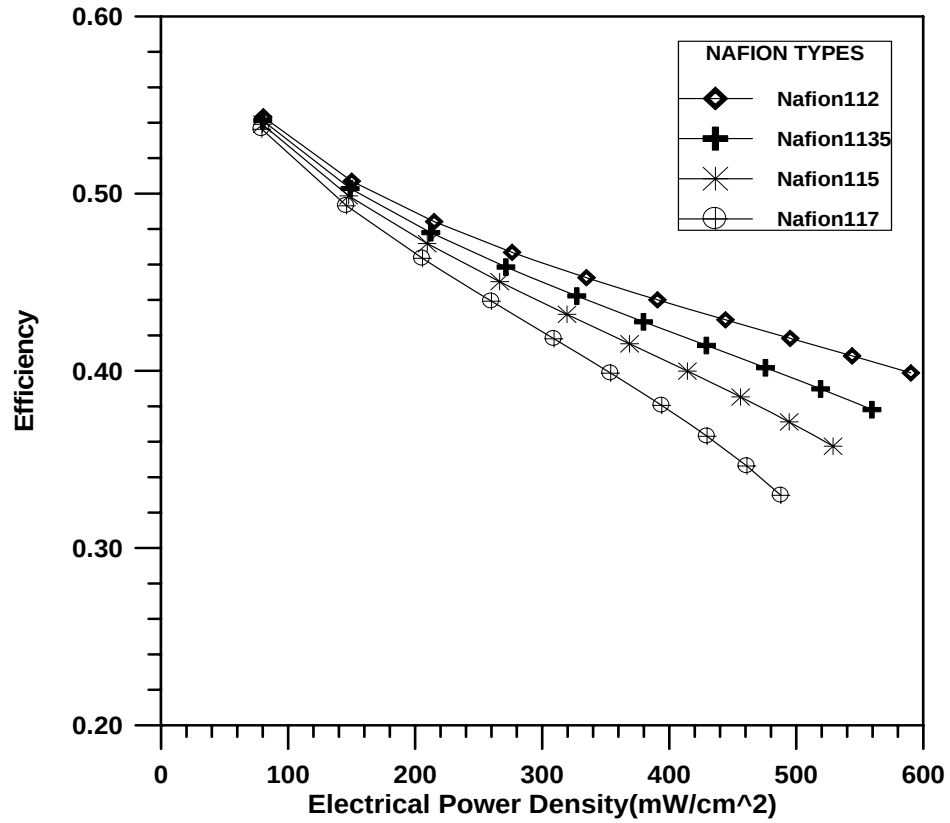

FIGURE (5.19) Efficiency versus Electrical Power Density at Temperature 80^{O}C

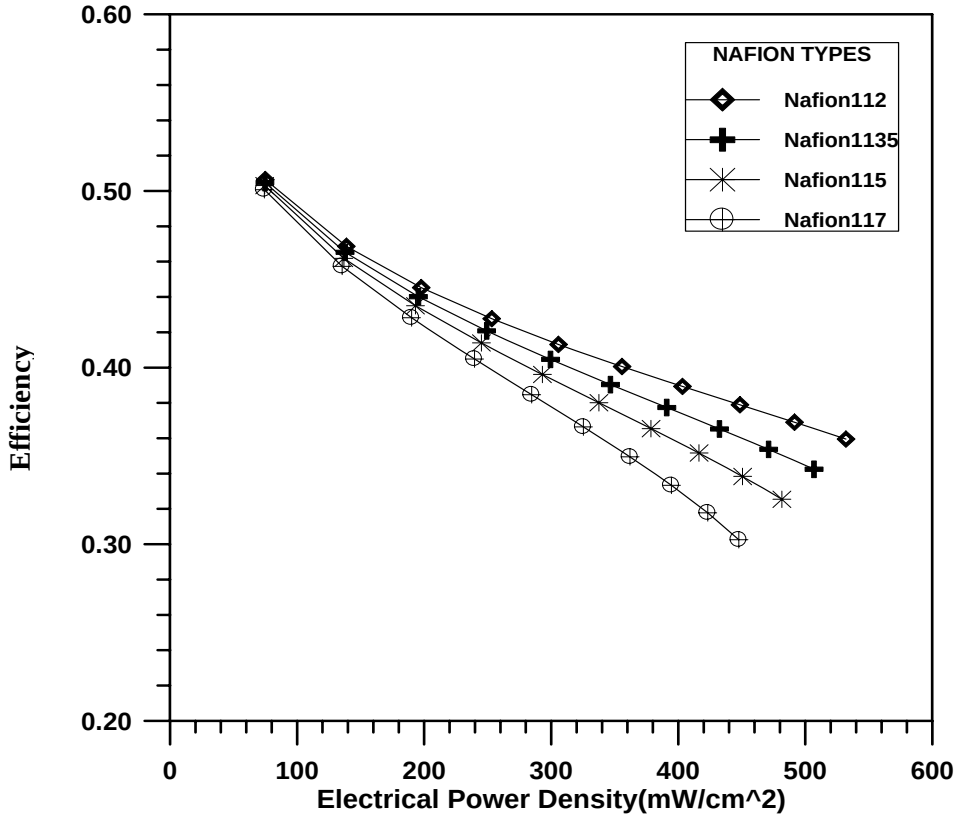

FIGURE (5.20) Efficiency versus Electrical Power Density at Temperature 100^{O}C

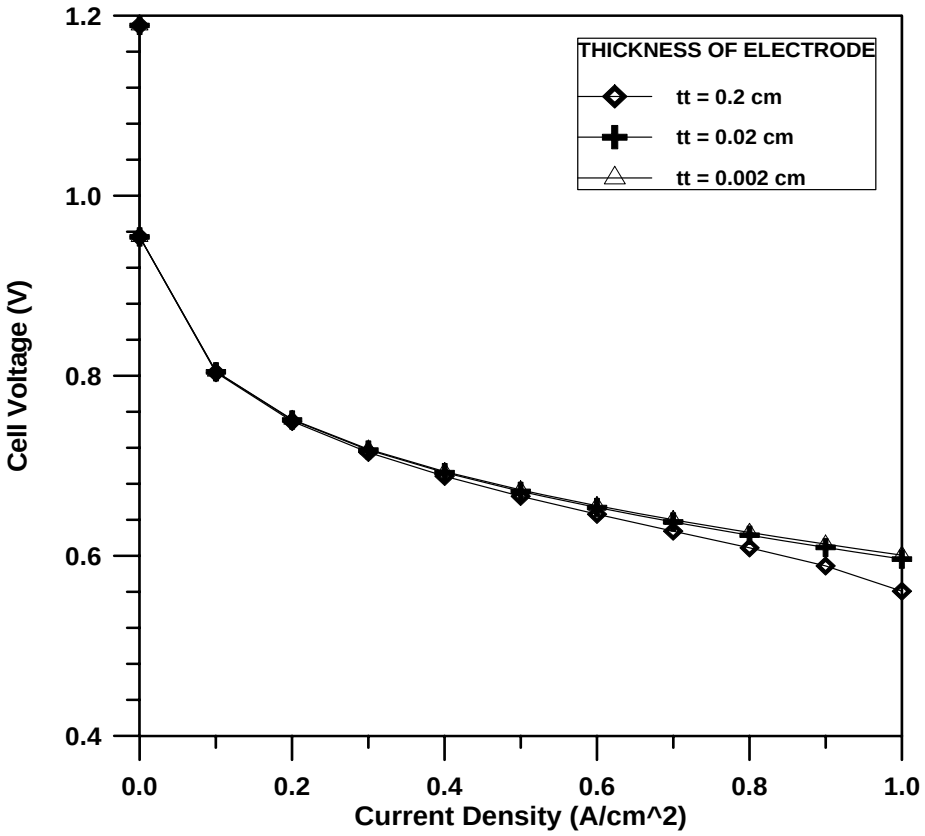

FIGURE (5.21): Polarization curve for three values of the electrode thickness for Nafion112 and temperature 80^{O}C

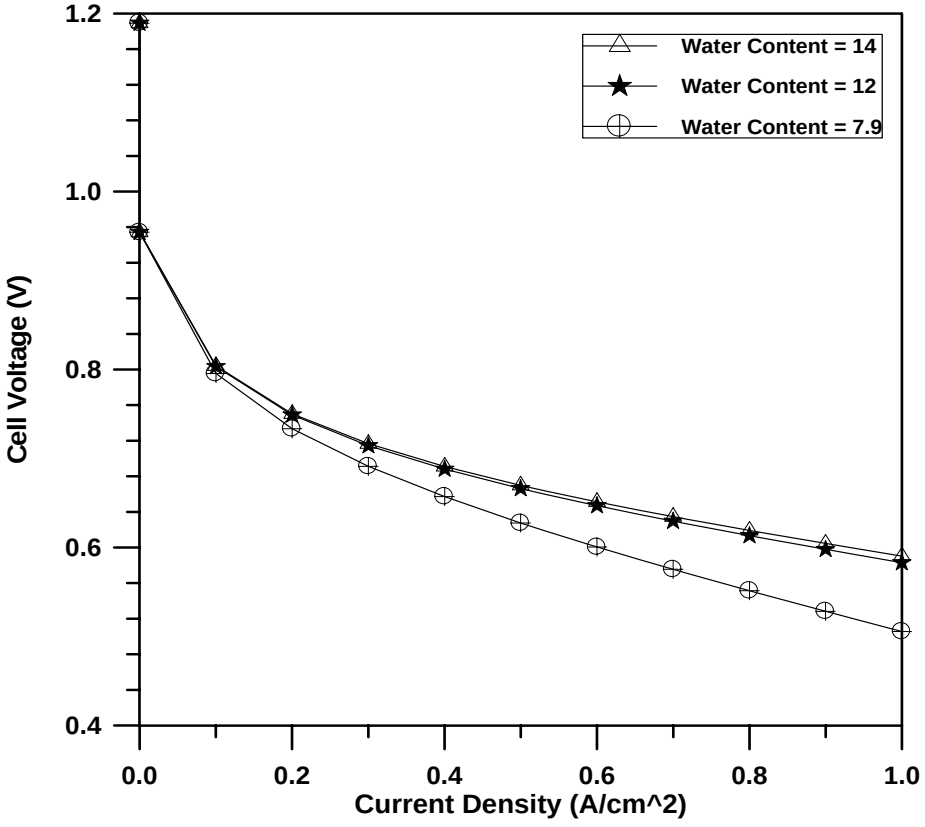

FIGURE (5.22)Influence of the membrane water content in the catalyst layer on performance.

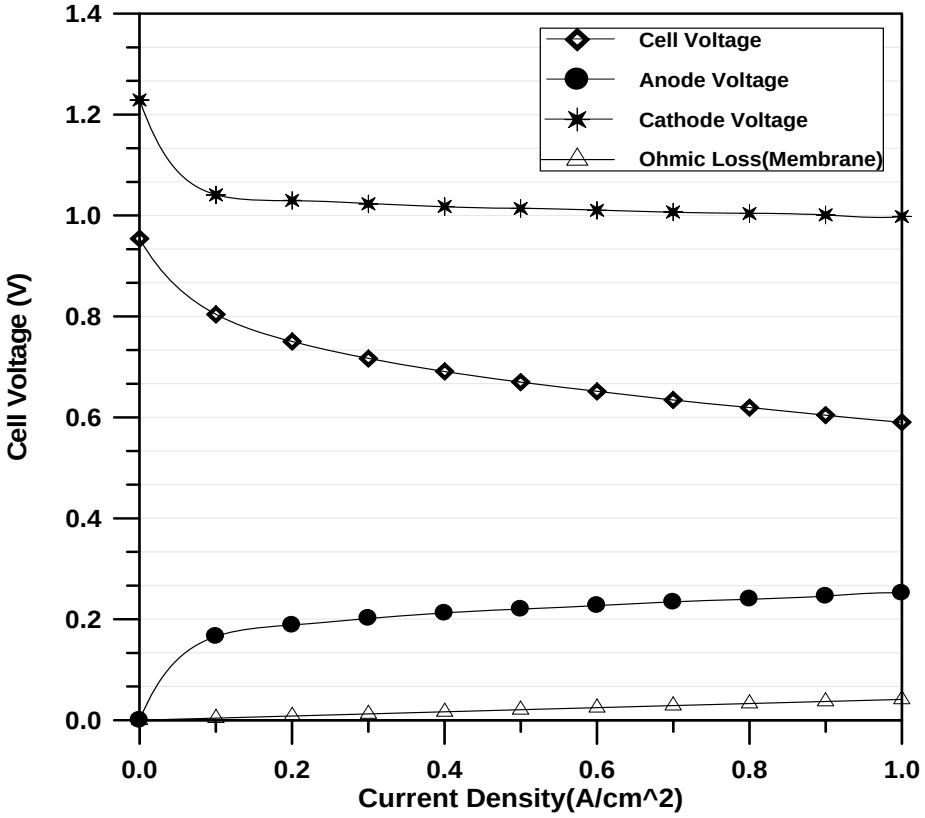

FIGURE (5.23):Contribution to Fuel Cell Performance (Polarization) of Anode and Cathode for Nafion 112 and Temperature 80 ^{0}C

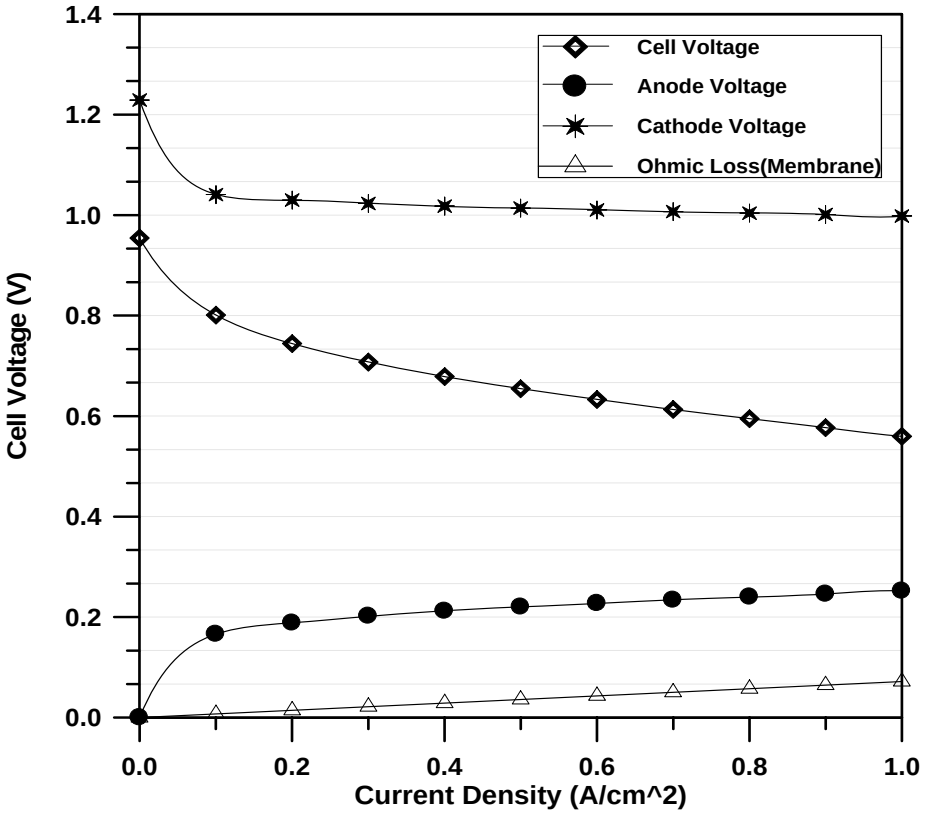

FIGURE (5.24):Contribution to Fuel Cell Performance (Polarization) of Anode and Cathode for Nafion 1135 and Temperature 80 ^{0}C.

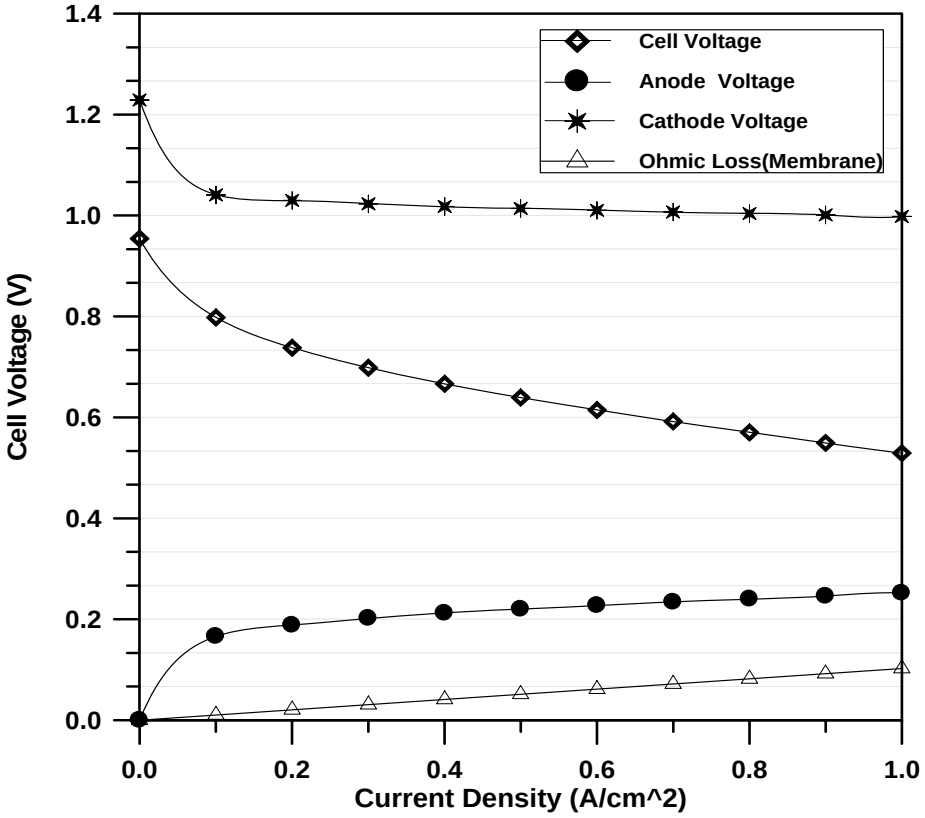

FIGURE (5.25):Contribution to Fuel Cell Performance (Polarization) of Anode and Cathode for Nafion 115 and Temperature 80 ^{0}C.

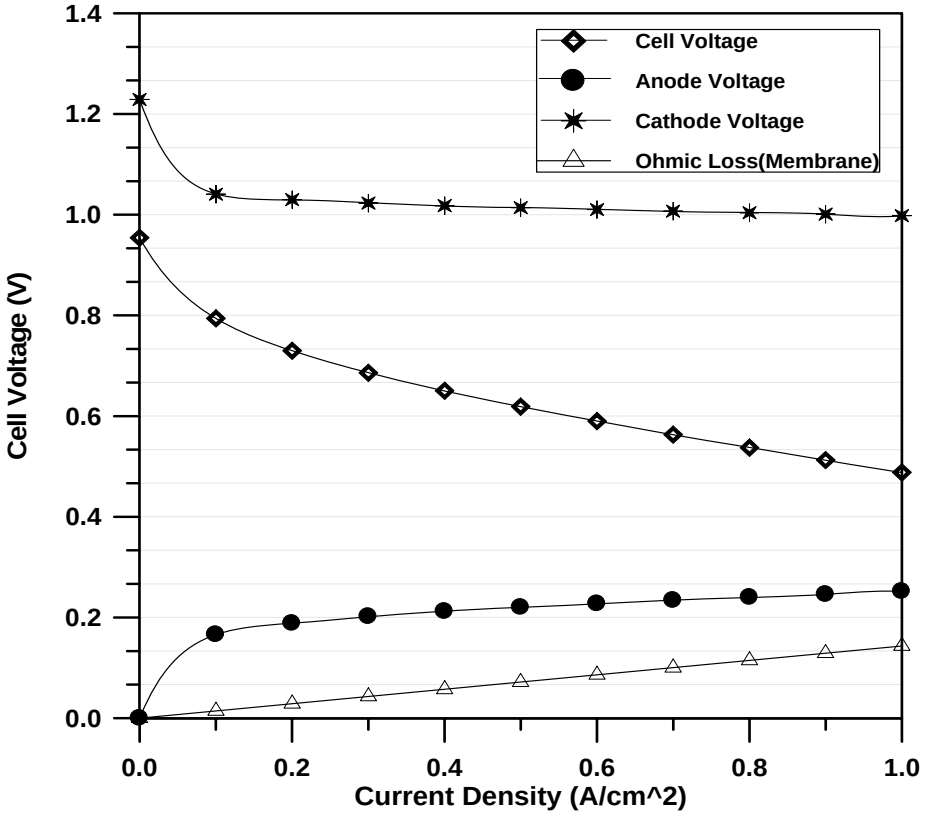

FIGURE (5.26):Contribution to Fuel Cell Performance (Polarization) of Anode and Cathode for Nafion 117 and Temperature 80 ^{0}C

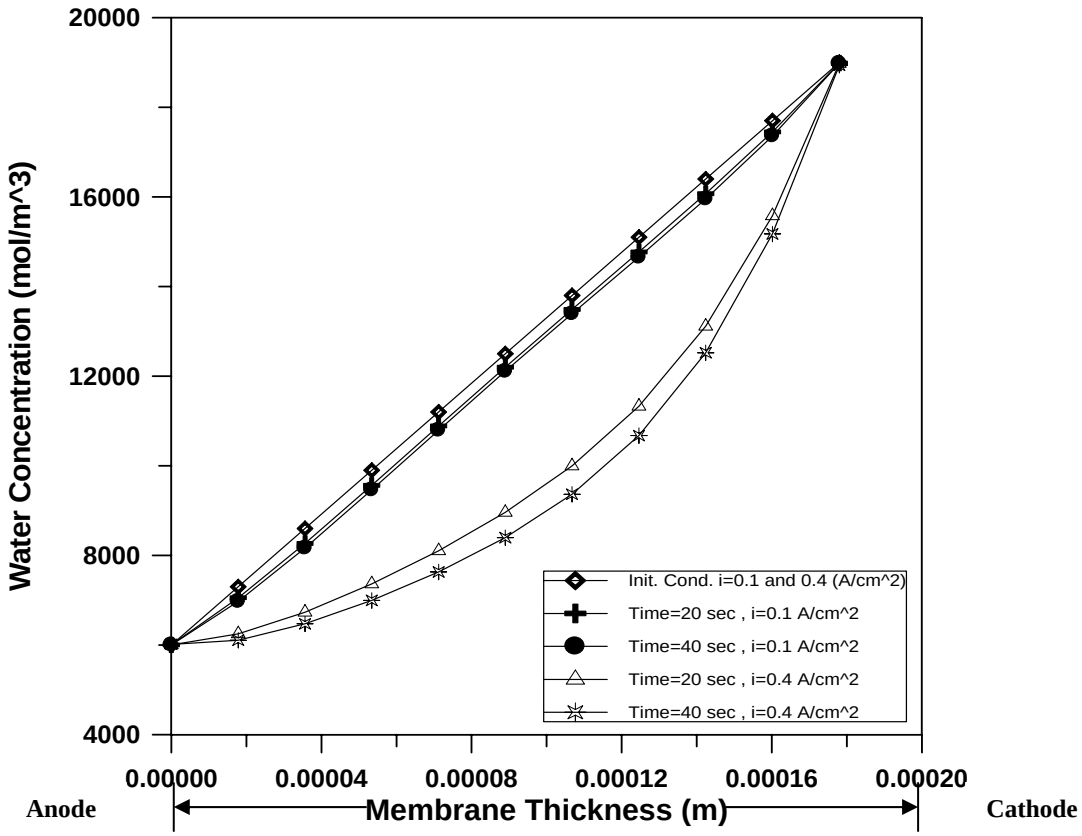

FIGURE (5.27):Effect of current density on water concentration through the membrane thickness at 80 ^{0}C.

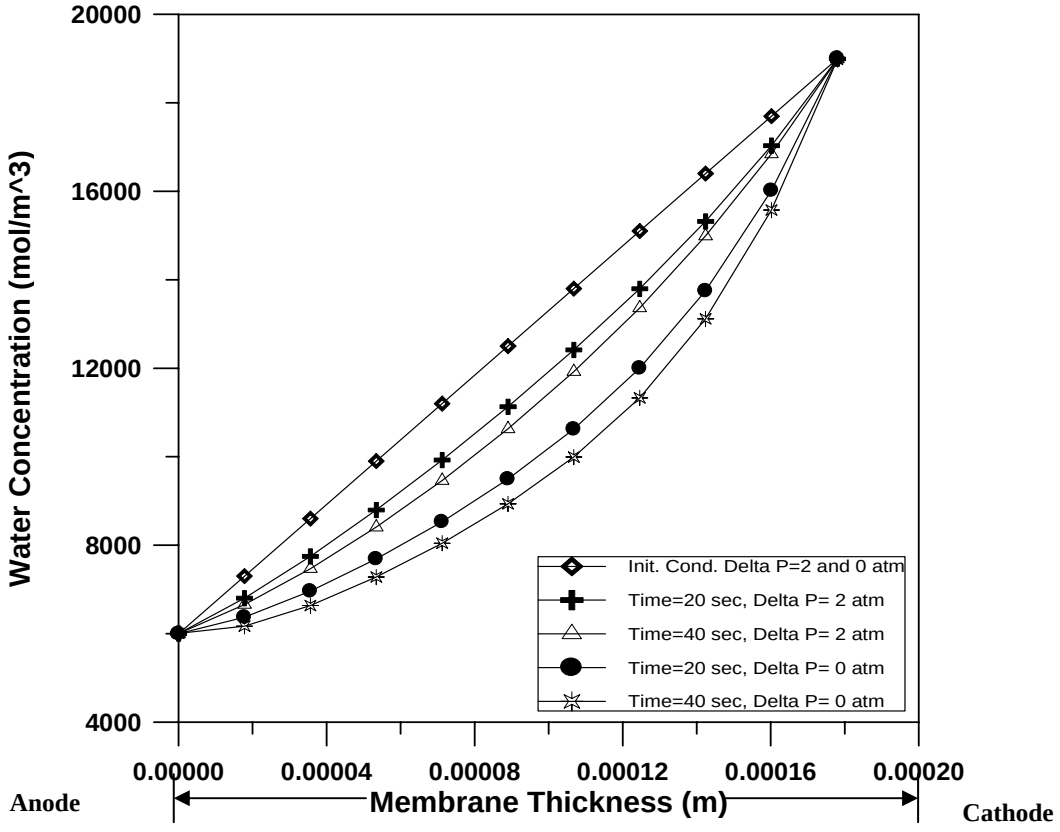

FIGURE (5.28):Effect of pressure gradient on water concentration through the membrane thickness at I=0.6 A/cm^2.

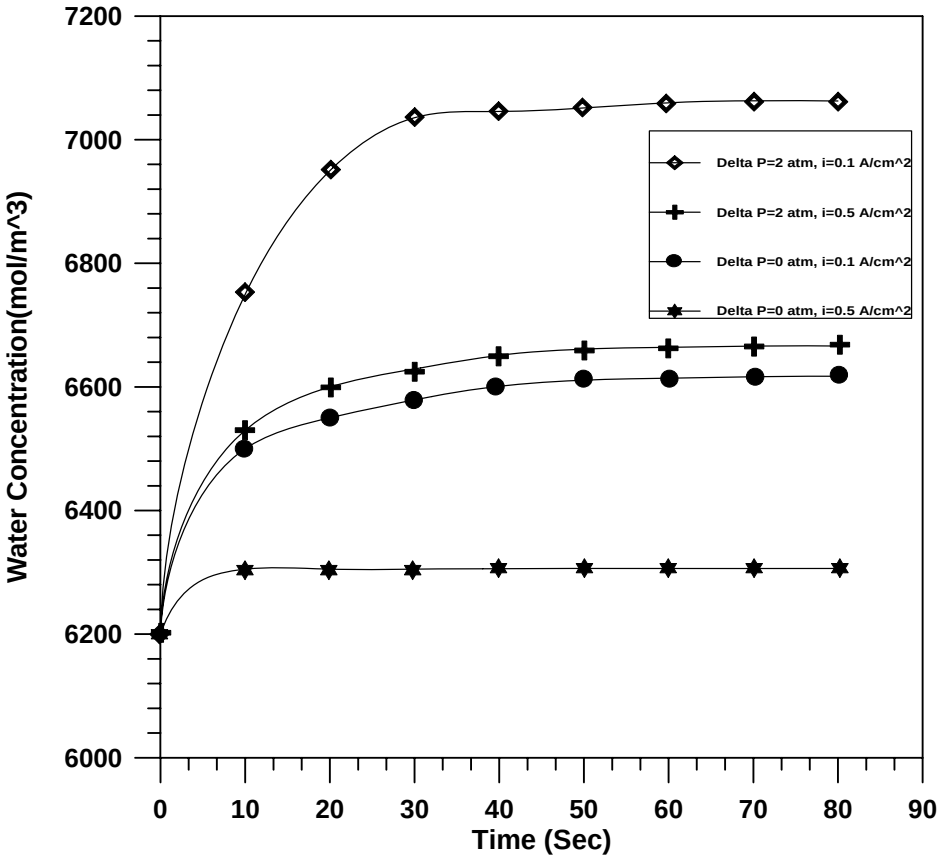

FIGURE(5.29): Effect of water concentration at (x=6.675*10^{-6}m) from the anode side of the membrane at 80 ^{0}C.

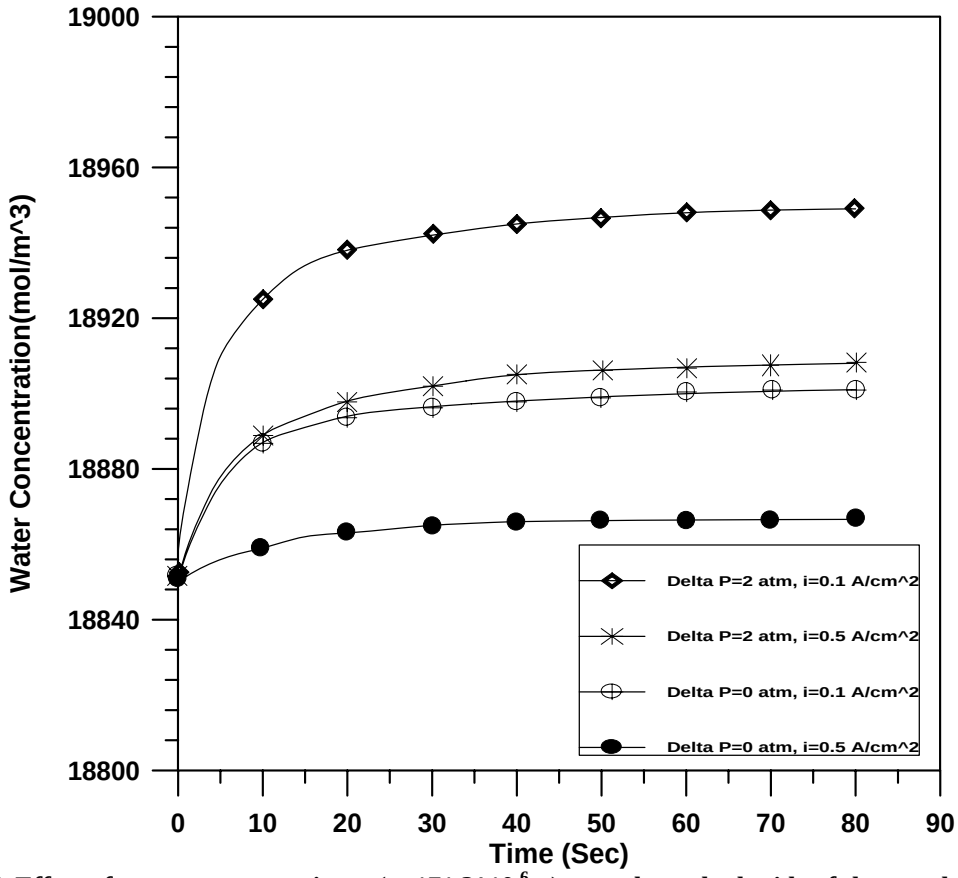

FIG.(5.30):Effect of water concentration at(x=171.2*10^{-6}m) near the cathode side of the membrane at 80 ^{0}C.

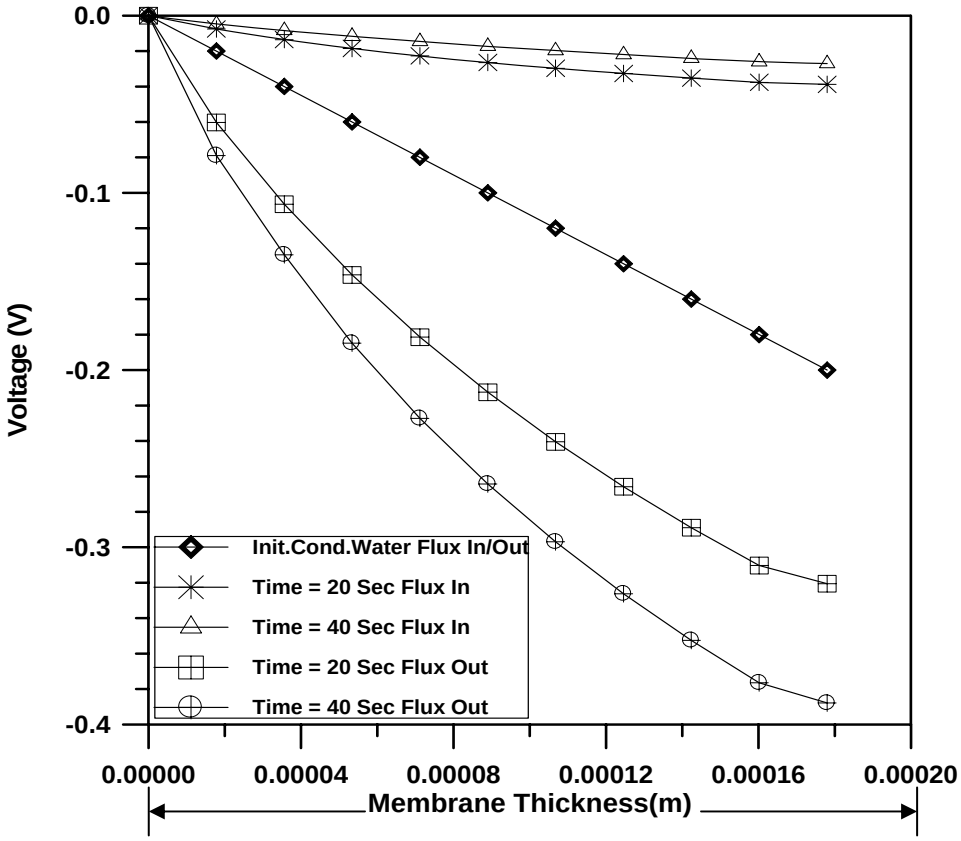

Figure(5.31):Effect of membrane hydration on voltage losses.

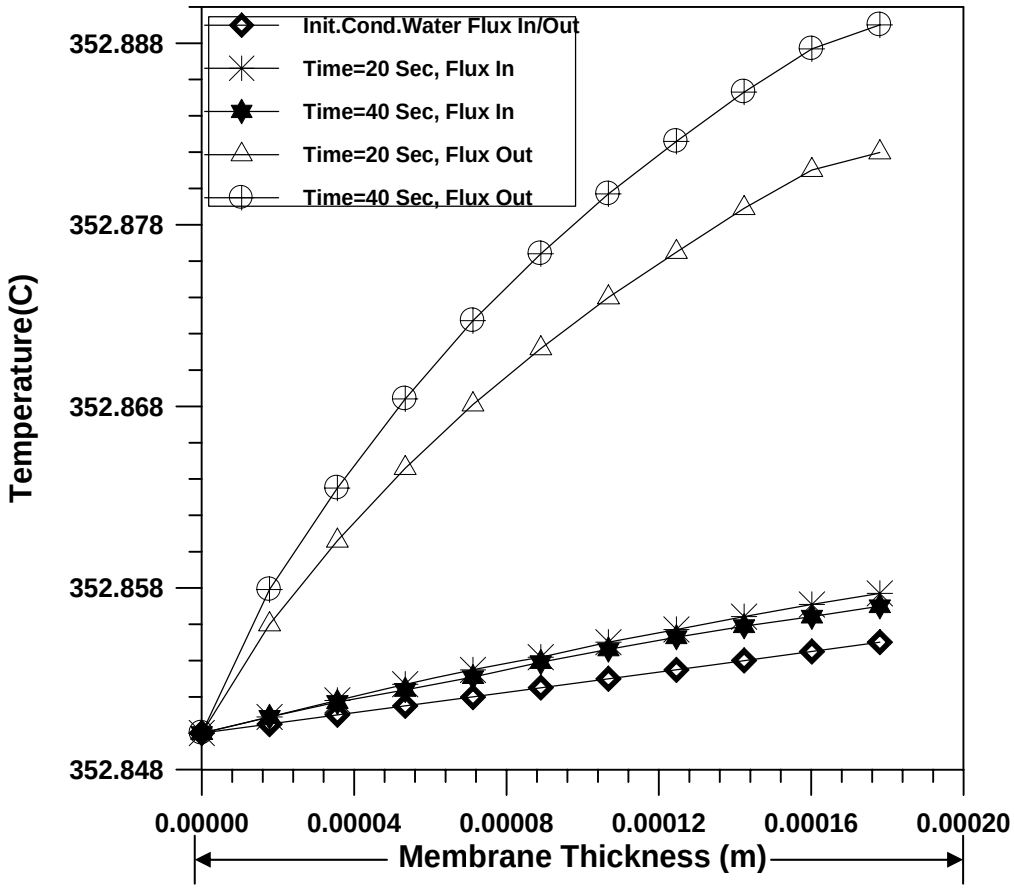

Figure(5.32):Effect of membrane hydration on temperature.

CHAPTER 6

CONCLUSIONS AND RECOMMANDATIONS

6.1 Conclusions.

The following conclusions can be drawn from this work:

1. Increasing water content causes an increase in the proton conduction thus improving the membrane performance in the fuel cell.

2. Cell performance drops as the temperature is decreased. This is due partly to a reduction in the exchange current density and the ionic conductivity with temperature. Also, it is clear from the results that the best working temperature is about ~80^0C for Nafion PEMFC which gives the maximum cell efficiency.

3. The increase of the oxygen partial pressure is helpful to increase the voltage of the cell for different current densities.

4. Increasing the electrode thickness reduces the limiting current densities at the anode and cathode, thereby reducing the cell voltage.

5. Ohmic losses increase with increasing membrane thickness, due to increase resistance of the membrane.

6. Activation losses decrease with increasing membrane operating temperature which causes an increase in exchange current density.

7. At very high current densities (concentration region), mass transfer causes a rapid drop off in the voltage, because oxygen and hydrogen simply cannot diffuse through the electrodes and ionize fast enough.

8. The heat generated in the PEM fuel cell decreases with increasing the operating temperature of the PEMFC.

9. The effect of an applied current density on water concentration demonstrated that the higher the current density, the more water is driven from the anode to the cathode and out of the membrane.

10.The effect of an applied pressure gradient on water concentration was to show that a positive pressure gradient from cathode to anode could be used to drive water toward the anode, hydrating the anode side which is more likely to dry out.

11.The effect of water flux into and out of the membrane illustrated that if too much water flows into the membrane, flooding may occur, whereas, if too much water is removed from the membrane drying may occur.

6.2 Recommendations for Future Work.

The following recommendations are suggested for future work:

1. Studying the thermodynamic analysis of a high temperature polymer electrolyte membrane fuel cell rather than a low temperature polymer electrolyte membrane fuel cell, which are considered in present work. The impetus for studying the higher temperature fuel cells are :

- faster reaction rates decrease or even eliminate the need for noble metal catalysts and should yield greater tolerance to co-poisoning at the anode.
- the higher proton mobility will increase the membrane conductivity, and
- water evaporation should mitigate the **flooding** problem at the cathode.

2. Using hydrocarbons as fuel instead of pure hydrogen, which are considered in the present work, such as natural gas, diesel, gasoline, propane, methanol and ethanol.

3. Study the effect of relative humidity of air and hydrogen on the polarization curve.

4. It is possible to improve the model by adding the internal current for all losses.
5. Study the effect of reactant gas stoichiometry on cell performance .
6. Performing a 3-D analysis of water flow in PEMFC.

APPENDIX A

Appendix A –Tables

Table A - Summary of Parameters Appearing in Equations

Symbol	*Parameter*	*Constant*	*Unit*	*Ref.*
F	Faraday's constant	**96485.3**	*C /mol*	**[31]**
N_A	Avogadro's Number	**$6.022*10^{23}$**	*$mole^{-1}$*	**[31]**
R	Universal gas constant	**8.314**	*J/mol.K*	
V^0	Reversible fuel cell voltage at STP	**1.229**	*volt*	**[16]**
L_v	Liquid gas enthalpy of vaporization	**$2310*10^3$**	*J/kg*	**[25]**
C_{H^+}	Proton concentration	**$1.2*10^{-3}$**	*mol/cm^3*	**[23]**
b	Membrane swelling coefficient	**0.0126**	-	**[39]**
D_{H+}	The proton diffusivity	**$4.5*10^{-5}$**	*cm^2 /s*	**[13]**
M^m	The membrane molecular mass	**1.1**	*Kg/mol*	**[39]**
Cp_m	Heat capacity of membrane	**852.63**	*J/ kg.K*	**[25]**
M_{H_2O}	The molecular weigh of water	**$18*10^{-3}$**	*kg/mol*	**[13]**
Cp_{H_2O}	Heat capacity of water	**4190**	*J/ kg.K*	**[25]**
M_{H+}	The molecular weigh of proton	**$1*10^{-3}$**	*kg/mol*	**[23]**
Cp_{H^+}	Heat capacity of proton	**20630**	*J/ kg.K*	**[23]**
x_{mx-}	Membrane thickness at x	**$1.78*10^{-4}$**	*m*	
x_{mx+}	Membrane thickness at x	**0**	*m*	
$K\,k_r^g$	Absolute Permeability * Relative Permeability	**$1.8*10^{-18}$**	*m^2*	**[25]**
g	The gravitational acceleration	**9.81**	*m/s^2*	
λ_m	Thermal conductivity coefficient	**100**	*W/m.K*	**[13]**
μ_{H2O}	Dynamic viscosity of the water	**$8.91*10^{-4}$**	*kg/m.s*	**[13]**
μ_{H^+}	Dynamic viscosity of the proton	**$98.8*10^{-7}$**	*kg/m.s*	**[13]**
$\rho^m{}_{dry}$	The dry membrane density	**2000**	*kg/m^3*	**[25]**
ρ_{H2O}	Density of the proton	**972**	*kg/m^3*	**[25]**

Table(1): Membrane Types by Dupont Corporation.

Nafion Type	Membrane Thickness
Nafion 112	51 µm
Nafion 1135	89 µm
Nafion 115	127 µm
Nafion 117	178 µm

Table(2):Gibbs free energy for water for various temperatures and states.

Form of water product	Temperature (C^0)	ΔG_f (KJ/mol)	Rev.Voltage (v)	Efficiency	ΔH_f (KJ/mol)
Liquid	25	-237.2	1.229	83%	-285.84
Liquid	80	-228.2	1.18	80%	-285.84
Vapor	100	-225.3	1.17	79%	-241.83
Vapor	200	-220.4	1.14	77%	-241.83
Vapor	400	-210.3	1.09	74%	-241.83
Vapor	600	-119.6	1.04	70%	-241.83
Vapor	800	-188.6	0.98	66%	-241.83
Vapor	1000	-177.4	0.92	62%	-241.83

Table(3):Standard thermodynamic values.

Species	(J/mol) $\Delta \bar{g}^0_f$	(J/mol.k) $\Delta \bar{s}^0$
$H_2o(l)$	$-237.2 * 10^3$	69.95
O_2 (g)	0	205.03
H_2 (g)	0	130.57

Table (4):Springer, Zawodzinski and Gottesfeld model.

Model	**Springer, Zawodzinski and Gottesfeld**
Assumptions	• Steady-state • Isothermal • One-dimensional • Catalyst is an interface • Polymer water content data at 30 C applies at 80 C • Liquid water effects neglected
Regions	• Membrane • Anode • Cathode
Investigated phenomena	• Water transport within the membrane • Influence of membrane conductivity
Main conclusions	• Net water flux across the membrane is less than that predicted by electro-osmotic drag alone • Thinner membranes offer advantages in decreased resistance and water flux from anode to cathode
Limits	Use of artificially fitted parameters (such as the cathode backing layer effective porosity) to predict water flooding

Table (5): Bernardi and Verbrugge model.

Model	**Bernardi and Verbrugge**
Assumptions	• Steady-state • Isothermal • One-dimensional • Pseudo-homogeneous model of the catalyst layers
Regions	• Membrane • Catalyst layers (anode and cathode) • Gas diffuser (cathode)
Investigated phenomena	• Limiting factors to cell performance • Species transport in the gas, liquid and solid phases • Influence of the porosity of the electrodes • Effects of membrane properties
Main conclusions	• Due to capillary forces, the liquid and the gas pressures are not in mutual equilibrium in the backing layer • The inefficiencies due to unreacted hydrogen or oxygen transport through the membrane are negligible • At practical operating current densities, catalyst utilization is low
Limits	•Valid only for fully hydrated membranes • Does not account for the drag force on water molecules. • Unable to predict flooding in the cathode backing layer due to water production • The polarization curve diverges from experimental data at high current densities

Table (6): Parthasarathy, Srinivasan, Appleby, and Martin model .

Model	**Parthasarathy, Srinivasan, Appleby, and Martin**
Regions	Temperature Dependence of the Electrode Kinetics of Oxygen Reduction at the Platinum/Nafion® Interface
Investigated phenomena	• Variation of kinetic parameters (exchange current density, Tafel slope, transfer coefficient) for oxygen reduction with temperature • Variation of open circuit potential with temperature • Solubility and diffusivity of oxygen in Nafion® as a function of temperature
Main conclusions	• The exchange current density varies with operating current density due to the presence of an oxide layer on the platinum at low current densities. • Oxygen diffusion in Nafion® increases with temperature while solubility decreases. • Transfer coefficient, exchange current density, and the open circuit voltage increase with temperature.

Table (7): Genevey et al model

Model	**Transient Model of Heat, Mass, and Charge Transfer as Well as Electrochemistry in the Cathode Catalyst Layer of a PEMFC .**
Assumptions	• Transient • Isotropic and homogenous • One-dimensional • Polymer water content data at 30 C applies at 80 C
Regions	• Cathode catalyst layer
Investigated phenomena	• Effect of catalyst layer porosity on oxygen transport, current production, and overall performance • Influence of cell temperature on catalyst layer performance • Transport effects associated with the presence of liquid water within the porous catalyst layer • The transient behavior of the transport processes associated with oxygen, liquid water, and thermal energy
Main conclusions	• An increase in the cell operating temperature leads to a decrease in the performance of the catalyst layer. • Large values of liquid water saturation lead to non-uniform current production across the catalyst layer and a decrease in overall catalyst utilization.
Limits	•The model requires the specification of a limiting current based solely on oxygen diffusion through the cathode catalyst layer. • Performance effects related to the occlusion of the reaction sites within the catalyst layer by liquid water are not included.

Table (8):Siegel et al model.

Model	**Siegel, Ellis, Nelson, and von Spakovsky.**
Assumptions	• Steady • Laminar flow • Incompressible • Ideal gases • Liquid water transport is neglected. • Agglomerate catalyst structure
Regions	• Gas channels, gas diffusers, catalyst layers, membrane
Investigated phenomena	• Physical structure of the catalyst layer • Effect of catalyst layer porosity on performance • Effect of agglomerate size on performance • Oxygen transport in the cathode
Main conclusions	• Scanning electron microscopy is a useful tool for a physical characterization of the catalyst layer. • An optimal catalyst layer void fraction can be calculated for a given operating voltage. • Agglomerates larger than 0.5 microns in radius decrease cell performance.
Limits	• Model does not include liquid water transport

APPENDIX B

Appendix B – Fuel Cell System & Direct Hydrogen fuel cell Vehicle

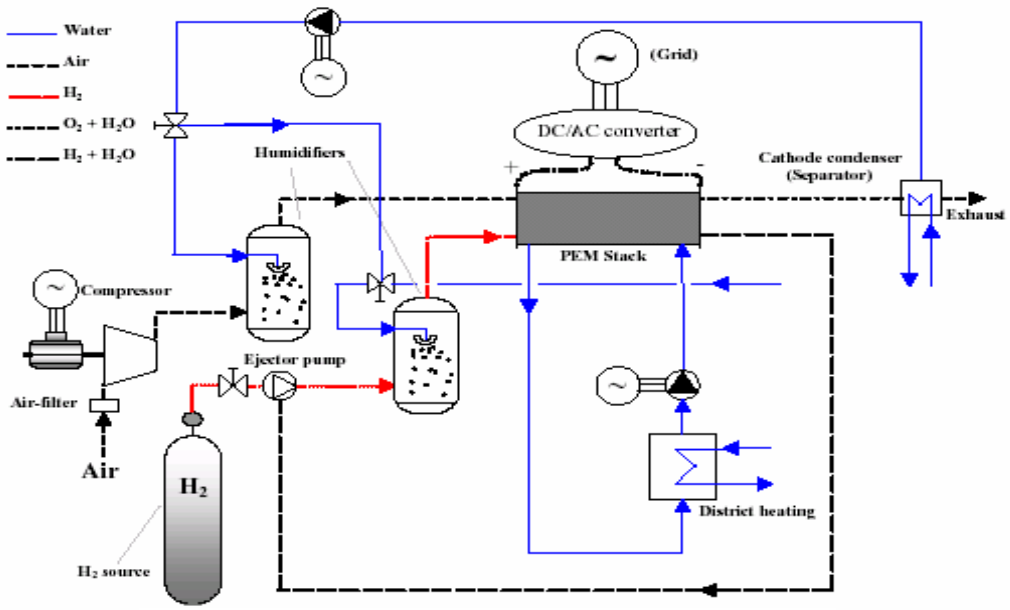

FIG.(B-1):Thermodynamic fuel cell system.

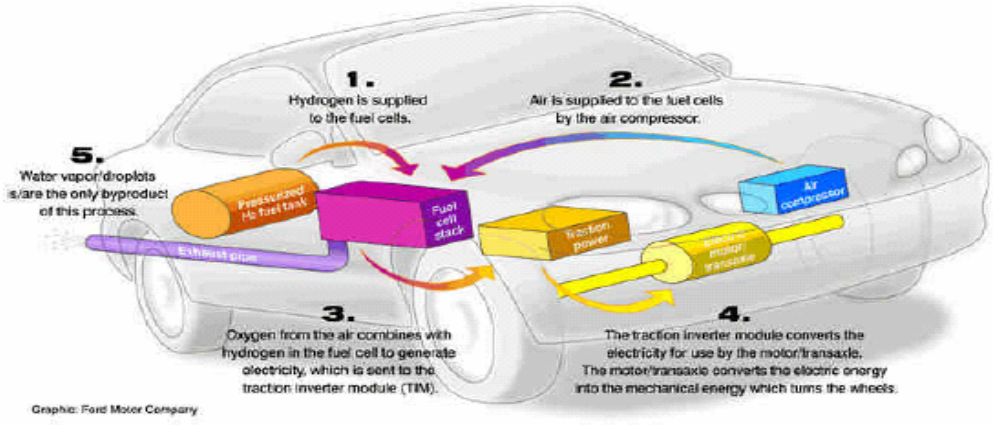

FIG.(B-2):Direct Hydrogen fuel cell Vehicle

APPENDIX C

Appendix C –Derivation of Activation Losses & Butler Volmer Equation.

The electrochemical reaction that takes place at the cathode, which is normally written as:

$$(Ox) \qquad O_2 + 4H^+ + 4e^- \underset{K_b \quad I_a}{\overset{K_f \quad I_c}{\longleftrightarrow}} 2H_2O \qquad (\mathrm{Re}d)$$

The theoretical current (i) is proportional to reaction velocity (v) as follows:

$$i = n\,F\,v \qquad \text{.....(C.1)}$$

For heterogeneous reaction (v) is proportional to the surface area(A) of the interface, so that the kinetics of the electrochemical reaction is better defined by:

$$\acute{v} = v/A \qquad \text{.....(C.2)}$$

And the theoretical current becomes:

$$i = n\,F\,\acute{v}\,A$$

Or

$$I = n\,F\,\acute{v} \qquad \text{. .....(C.3)}$$

From Fig(C) overleaf, introducting the exponential behavior of the rate constant with electrochemical activation energy, i.e.

$$\Delta G^{\#}_C = \Delta G^{\#}_{0,C} + n\,\alpha\,F\,(V - V^0) \qquad \text{reduction} \qquad \text{.....(C.4)}$$

$$\Delta G^{\#}_a = \Delta G^{\#}_{0,a} - n\,(1-\alpha)\,F\,(V - V^0) \qquad \text{oxidation} \qquad \text{.....(C.5)}$$

(Hint: V=E & $V^0=E^0$, as shown in Fig(c)).

which comprises two terms for each equation , the first one , $\Delta G^{\#}_{0,c}$ being the chemical energy of activation at the cathode , and the second one , $n\alpha\,(V\text{-}V^0)$, the electrical part of the activation energy, which is a fraction α($0 \le \alpha \le 1$)of the total electrical energy coming from the applied electrode voltage $(V\text{-}V^0)$.

For a typical chemical reaction , there is a relationship between rate constant and temperature represented by the Arrhenius equation:

$$K = B \cdot \exp\left(\frac{-\Delta G^{\#}}{RT}\right) \qquad \text{..... (C.6)}$$

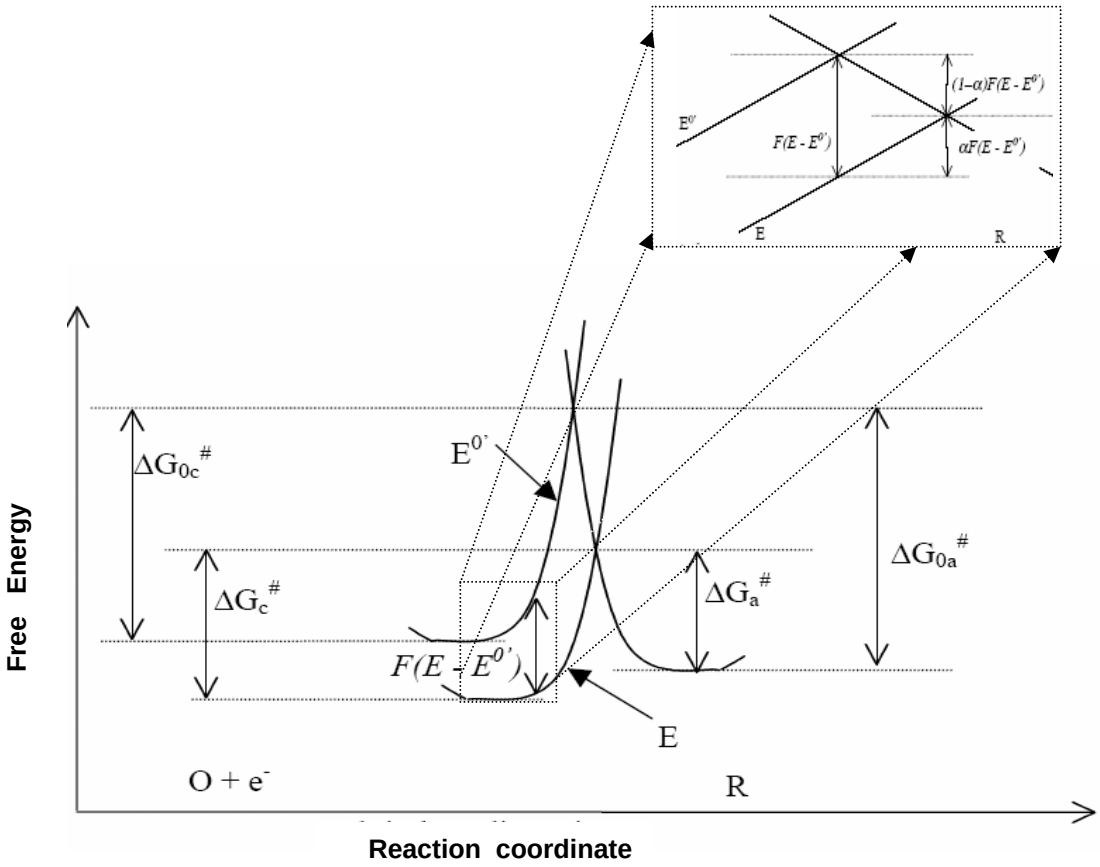

Figure(C):Energy diagram for electrochemical (redox) reaction

The rate constant(K) for the forward cathode reaction can be written as:

$$K_f = B_f \cdot \exp\left(\frac{-\Delta G_c^{\#}}{RT}\right) \qquad \text{.....(C.7)}$$

substituting Eq(C.4) into Eq(C.7) , we get :

$$K_f = B_f \cdot \exp\left(\frac{-\Delta G_{0,C}^{\#}}{RT}\right) \cdot \exp\left(\frac{-n.\alpha.F.\left(V - V^0\right)}{RT}\right) \qquad \text{..... (C.8)}$$

The cathode reaction velocity is defined as:

$$\nu_f' = K_f \cdot C_{OX} \qquad \text{.....(C.9)}$$

then by substituting Eq. (C.8) into Eq.(C.9) the following expression is obtained:

$$\nu'_f = B_f . \exp\left(\frac{-\Delta G^{\#}_{0,c}}{RT}\right).\exp\left(\frac{-n.\alpha.F.(V-V^0)}{RT}\right)C_{OX} \qquad \text{.....(C.10)}$$

Again,substituting Eq.(C.10)into Eq.(C.3), we get :

$$i_c = n\ .F.A.B_f . \exp\left(\frac{-\Delta G^{\#}_{0,C}}{RT}\right).\exp\left(\frac{-n.\alpha.F.(V-V^0)}{RT}\right)C_{OX} \qquad \text{.....(C.11)}$$

similarly,

$$\nu'_b = K_b . C_{\mathrm{Re}d}$$

$$\nu'_b = B_b . \exp\left(\frac{-\Delta G^{\#}_{0,C}}{RT}\right).\exp\left(\frac{n(1-\alpha).F.(V-V^0)}{RT}\right)C_{\mathrm{Re}d} \qquad \text{.....(C.12)}$$

finally ,

$$i_a = n\ .F.A.B_b . \exp\left(\frac{-\Delta G^{\#}_{0,a}}{RT}\right).\exp\left(\frac{n(1-\alpha).F.(V-V^0)}{RT}\right)C_{\mathrm{Re}d} \qquad \text{.....(C.13)}$$

At the open circuit, there is no current flow $\left(i = i_f - i_b = 0\right)$, but the reactions are proceeding at the anode and cathode . These reaction at anode and cathode occur in both the forward and reverse directions, but at equilibrium state. So $V = V_{eq}$ and $\acute{\upsilon}_f = \acute{\upsilon}_b$ as follows:

$$B_f . \exp\left(\frac{-\Delta G^{\#}_{0,c}}{RT}\right).\exp\left(\frac{-n.\alpha.F(V_{eq}-V^0)}{RT}\right)C_{ox} = B_b . \exp\left(\frac{-\Delta G^{\#}_{0,a}}{RT}\right).\exp\left(\frac{n.(1-\alpha)F(V_{eq}-V^0)}{RT}\right)C_{\mathrm{Re}d}$$

Also, the rate constants for the forward and backward are the same , i.e $K_f = K_b = K^0$, then:

$$\exp\left(\frac{-n.\alpha.F(V_{eq}-V^0)}{RT}\right)C_{OX} = \exp\left(\frac{n.(1-\alpha).F(V_{eq}-V^0)}{RT}\right)C_{\mathrm{Re}d}$$

or

$$\frac{C_{OX}}{C_{\mathrm{Re}d}} = \exp\left(\frac{n.F(V_{eq}-V^0)}{RT}\right) \qquad \text{.....(C.14)}$$

Again, at equilibrium, the anode current is exactly compensated by the cathode current, so that the overall current is zero, i.e, $i_c = i_a = i_0$, then Eq.(C.11) and Eq. (C.13) becomes :

$$i_{0,c} = n_c.F.A.B_f.\exp\left(\frac{-\Delta G^{\#}_{0,C}}{RT}\right).\exp\left(\frac{-n.\alpha.F(V_{eq}-V^0)}{RT}\right)C_{OX} \qquad \text{.....(C.15)}$$

$$i_{0,a} = n_a.F.A.B_b.\exp\left(\frac{-\Delta G^{\#}_{0,a}}{RT}\right).\exp\left(\frac{n(1-\alpha)F(V_{eq}-V^0)}{RT}\right)C_{\mathrm{Re}d} \qquad \text{.....(C.16)}$$

Substitution of Eq.(C.14)into Eq.(C.15) and Eq.(C.16)gives:

$$i_{0,c} = n_c.F.A.B_f.\exp\left(\frac{-\Delta G^{\#}_{0,C}}{RT}\right).\exp\left(-\alpha\ln\frac{C_{OX}}{C_{\mathrm{Re}d}}\right)C_{OX} \qquad \text{.....(C.17a)}$$

$$i_{0,a} = n_a.F.A.B_b.\exp\left(\frac{-\Delta G^{\#}_{0,a}}{RT}\right).\exp\left((1-\alpha)\ln\frac{C_{OX}}{C_{\mathrm{Re}d}}\right)C_{\mathrm{Re}d} \qquad \text{.....(C.17b)}$$

Now, Eq. (C.17) can be re-written as follows:

$$i_{0,c} = n_c.F.A.B_f(C_{OX})^{1-\alpha_c}(C_{\mathrm{Re}d})^{\alpha_c}\exp\left(\frac{-\Delta G^{\#}_{0,C}}{RT}\right) \qquad \text{.....(C.18a)}$$

$$i_{0,a} = n_a.F.A.B_b(C_{OX})^{1-\alpha_c}(C_{\mathrm{Re}d})^{\alpha_c}\exp\left(\frac{-\Delta G^{\#}_{0,a}}{RT}\right) \qquad \text{.....(C.18b)}$$

• For cathode reaction , $C_{OX} = C_{O_2} + C_{proton}$ and $C_{Red} = C_{H_2O}$. Eq.(C-18a)becomes:

$$i_{0,c} = n_c.F.A.B_f(C_{proton})^{1-\alpha_c}(C_{O_2})^{1-\alpha_c}(C_{H_2O})^{\alpha_c}\exp\left(\frac{-\Delta G^{\#}_{0,C}}{RT}\right) \qquad \text{..... (C.19)}$$

The constants *F, R,* n_c, C_{H_2O} and $\Delta G^{\#}_{0,C}$ are known . The parameters α_c , B_f and C_{H^+} are approximately constant for the reaction and are assumed to be constant as in [20]. The exchange current for the cathode is a function of T, C_{O_2} and the quoted constants *F, R* , n_c , C_{H_2O} , $\Delta G^{\#}_{O_2}$, α_c , B_f and C_{H^+} .

The value of $i_{0,c}$ can then be placed into the cathode activation loss Eq.(3.24) and after rearrangement it becomes:

$$V_{act,c} = \left(\frac{RT}{2\alpha_c F}\right)\ln i + \left(\frac{\Delta G^{\#}_{0,C}}{2\alpha_c F}\right) - \left(\frac{RT.\ln(n_c.F.A.B_f)}{2\alpha_c F}(C_{proton})^{1-\alpha_c}(C_{H_2O})^{\alpha_c}\right) - \frac{RT(1-\alpha_C)}{2\alpha_c F}\ln(C_{O_2}) \qquad \text{...(C.20)}$$

Or $\qquad V_{act,c} = \zeta_1 T\ln i + \zeta_2 + \zeta_3 T + \zeta_4 T\ln(C_{O_2})$ $\qquad$ ....(C.21)

• For anode reaction $C_{OX} = C_{H_2}$ and $C_{Red} = C_{H_2}$, Eq.(C.18b) becomes:

$$i_{0,a} = n_a.F.A.B_b.C_{H_2}.\exp\left(\frac{-\Delta G^{\#}_{0,a}}{RT}\right) \qquad \text{…….(C.22)}$$

The constants F, R, n_a and $\Delta G^{\#}_{0,a}$ are known. The parameters α_a , B_b are approximately constant for the reaction and assumed to be constant.

The value of $i_{0,a}$ can then be placed into the anode activation loss Eq(3.25). This re-arranged gives the activation loss at the anode as ,

$$V_{act,a} = \left(\frac{RT}{2\alpha_a F}\right)\ln i + \left(\frac{\Delta G^{\#}_{0,a}}{2\alpha_a F}\right) - \left(\frac{R.T.\ln(n_a.F.A.B_b)}{2\alpha_a F}\right)\ln(C_{H_2}) \qquad \text{……(C.23)}$$

Or $$V_{act,a} = \zeta_5 T\ln i + \zeta_6 + \zeta_7 T\ln(C_{H_2}) \qquad \text{……...(C.24)}$$

The activation loss for the cathode and the anode can now be combined in the form of a semi-empirical equation.

$$V_{act} = \delta_1 T\ln i + \delta_2 + \delta_3 T + \zeta_4 T\ln(C_{O_2}) \qquad \text{……..(C.25)}$$

The physical meaning of δ_1, δ_2, δ_3, δ_4 are

$$\delta_1 = \frac{R}{2\alpha_c F} + \frac{R}{2\alpha_a F} \qquad \text{……(C.26a)}$$

$$\delta_2 = \frac{\Delta G^{\#}_{0,C}}{2\alpha_c F} + \frac{\Delta G^{\#}_{0,a}}{2\alpha_a F} \qquad \text{……(C.26b)}$$

$$\delta_3 = -\left(\frac{R\ln(n_c FAk^0)}{2\alpha_c F} C_{proton}{}^{1-\alpha_c} C_{H_2O}{}^{\alpha_c}\right) - \frac{R}{2\alpha_a F}\left[\ln\left(n_a FAk^0 C_{H_2}\right)\right] \qquad \text{……(C.26c)}$$

$$\delta_4 = -\frac{R(1-\alpha_C)}{2\alpha_c F} \qquad \text{……(C.26d)}$$

The values used here for the coefficients δ_i are the ones proposed in [18]and is shown in Table(C1).

Table C1: Values for the constants used in the activation loss expressions

δ_1	***-0.9514***
δ_2	***0.00312***
δ_3	***$7.4*10^{-5}$***
δ_4	***-0.000187***

The concentration of oxygen at the catalyst interface (mol/cm^3) can be defined by **Henry's Law** expression of the form [20].

$$C_{O_2} = \frac{P_{O_2}}{5.08 * 10^{-6} \exp\left(\frac{-498}{T}\right)} \qquad \text{……(C.27)}$$

Re-arranging Eq.(C.18a) or Eq.(C.18b) gives:

$$i_0 = n\ F\ A\ K^0 (C_{OX})^{1-\alpha}\ (C_{Red})^{\alpha} \qquad \text{……..(C.28)}$$

The theoretical current of the fuel cell can be expressed as :

$$i = i_c - i_a \qquad \text{……... (C.29)}$$

By substituting Eq.(C.11) and Eq.(C.13) into Eq.(C.29) and doing some re-arrangements , Eq.(C.25)becomes :

$$i = n\ .F.A.K^0 \left[C_{OX} \exp\left(\frac{-n.\alpha.F(V - V^0)}{RT}\right) - C_{OX} . \exp\left(\frac{n(1-\alpha)F(V - V^0)}{RT}\right)\right] \qquad \text{…….(C.30)}$$

The above Eq. (C.30) divided by the Eq. (C.28) , we get :

$$\frac{i}{i_0} = \left(\frac{C_{OX}}{C_{Red}}\right)^{\alpha} \exp\left(\frac{-n.\alpha.F(V - V^0)}{RT}\right) - \left(\frac{C_{Red}}{C_{ox}}\right)^{1-\alpha} \exp\left(\frac{n(1-\alpha)F(V - V^0)}{RT}\right) \qquad \text{……..(C.31)}$$

Recall Eq.(C.14):

$$V^0 = V_{eq} - \frac{RT}{nF} \ln\left(\frac{C_{OX}}{C_{Red}}\right)$$

Offsetting of Eq.(C.14) into Eq(C.31) then Eq(C.31)becomes after simplification [38]:

$$i = i_0 \left[\exp\left(\frac{-n.\alpha.F.(V - V_{eq})}{RT}\right) - \exp\left(\frac{n(1-\alpha).F.(V - V_{eq})}{RT}\right)\right] \qquad \text{……(C.32)}$$

The final form of the equation above is often written as [36]:

$$i = i_0 \left[\exp\left(\frac{-n.\alpha.F.V_{act}}{RT}\right) - \exp\left(\frac{n(1-\alpha).F.V_{act}}{RT}\right)\right] \qquad \text{……..(C.33)}$$

Where V_{act} , is the activation polarization loss. This is the ***Butler - Volmer equation***.

APPENDIX
D

Appendix D – Finite Difference Approach

Taylor's formula or series expansion is used to express the value of some dependent variable u at node n, $j+1$(u^n_{j+1}) in terms of its adjacent node n, j (u^n_j) and its spatial derivatives, where $t^n = n.\Delta t$ and $x_j = j.\Delta x$. Thus,

$$u^n_{j+1} = u^n_j + \left(\frac{\partial u}{\partial x}\right)^n_j \Delta x + \frac{1}{2i}\left(\frac{\partial^2 u}{\partial x^2}\right)^n_j \Delta x^2 + \ldots\ldots + \frac{1}{ki}\left(\frac{\partial^k u}{\partial x^k}\right)^n_j \Delta x^k + \frac{1}{(k+1)i}\left(\frac{\partial^{k+1} u}{\partial x^{k+1}}\right)^n_{j+\delta} \Delta x^{k+1} \qquad \ldots\ldots\ldots(D.1)$$

Eq.(D.2) demonstrates how this weighted method can be used to approximate Eq.(D.1).

$$\frac{u^{n+1}_j - u^n_j}{\Delta t} = \theta\alpha \frac{u^{n+1}_{j-1} - 2u^{n+1}_j + u^{n+1}_{j+1}}{\Delta x^2} + (1-\theta)\alpha \frac{u^n_{j-1} - 2u^n_j + u^n_{j+1}}{\Delta x^2} \quad for\ \ 0 \le \theta \le 1 \qquad \ldots..(D.2)$$

- if θ = 0, Eq. (D.2) is an explicit method
- if θ= 1, Eq. (D.2) is a fully implicit method
- if θ = 1/2, Eq. (D.2) is a Crank-Nicolson method

The method depicted in Eq. (D.2) can be written in the following more common form, grouping nodes at similar time steps and using $s = \alpha\,\Delta t/\Delta x^2$:

$$-\theta s u^{n+1}_{j-1} + (1+2\theta)u^{n+1}_j - \theta s u^{n+1}_{j+1} = (1-\theta)s u^n_{j-1} + (1-2(1-\theta)s)u^n_j + (1-\theta)s u^n_{j+1} \qquad \ldots(D.3)$$

The finite difference method used to solve for temperature and water concentration in the membrane is a weighted or theta method. This allows the change

from fully implicit to fully explicit or any fraction of either depending on the value of theta. In this study, the explicit method is adopted (i.e. θ = 0).

The first step was to start with a general equation of the form which describes the thermal energy conservation equation (Eq.(3.93)) and the water concentration conservation equation (Eq.(3.89)) in the membrane. Such a general equation is expressed as:

$$\frac{\partial u}{\partial t} = \frac{\partial}{\partial x}\left(a(x,t)\frac{\partial u}{\partial x}\right) + b(x,t)\frac{\partial u}{\partial x} + s(x,t) \qquad \text{.....(D.4)}$$

This equation is made up of a second order term multiplied by a variable coefficient *a(x,t)*, a first order term multiplied by a variable coefficient *b(x,t)*, and a source term, *s(x,t)*. The next step in approximating Eq.(D.4) using finite difference methods is the application of a weighting method to the spatial terms and a forward difference methods to the transient term. Once that has been done, the spatial terms containing variable coefficients (on the right hand side of Eq.(D.5) inside the square brackets) can be properly approximated and substitutions made. Consider Eq.(D.5) to be located at time $t = (n+\theta)\Delta t$, and $x = j\Delta x$. Thus.

$$\left(\frac{u_j^{n+1} - u_j^n}{\Delta t}\right) = \theta\left[\frac{\partial}{\partial x}\left(a(x,t)\frac{\partial u}{\partial x}\right) + b(x,t)\frac{\partial u}{\partial x} + s(x,t)\right]_j^{n+1} + (1-\theta)\left[\frac{\partial}{\partial x}\left(a(x,t)\frac{\partial u}{\partial x}\right) + b(x,t)\frac{\partial u}{\partial x} + s(x,t)\right]_j^{n} \qquad \text{.....(D.5)}$$

To approximate the first order term and its variable coefficient, a first centered finite difference approximation is used,

$$b(x,t)\frac{\partial u}{\partial x} = b_j\frac{u_{j+1} - u_{j-1}}{2\Delta x} + O(\Delta x^2) \qquad \text{.....(D.6)}$$

Notice that the value of *b(x,t)* is taken at node u_j and the time step at which u_{j+1} , u_{j-1}, and b_j are taken is not specified. In the final finite difference method, u_{j+1}, u_{j-1} , and b_j will be taken at both t = (n+1)Δt and t = n Δt and weighted by theta.

To approximate the second order term and its variable coefficient (*a(x,t)*), a more complicated approach is needed. First, the time derivative and second order term are written in the following form:

$$\frac{\partial u}{\partial t} = -\frac{\partial w}{\partial x} \qquad \text{.....(D.7)}$$

where

$$w = -a(x,t)\frac{\partial u}{\partial x} \qquad \text{.....(D.8)}$$

Eq.(D.8)is now rewritten in the form given below and integrated with respect to *x* over the intervals $[(j\text{-}1)\Delta x\ ,\ j\Delta x]$ and $[j\Delta x, (j+1)\Delta x]$, assuming $w = w_{j-\frac{1}{2}}$ over the first interval and $w = w_{j+\frac{1}{2}}$ over the second interval. The result is:

$$\frac{w}{a(x,t)} = -\frac{\partial u}{\partial x}$$

$$w_{j+1/2}\int_{j\Delta x}^{(j+1)\Delta x}\frac{dx}{a(x,t)} = u_j - u_{j+1}$$

$$w_{j-1/2}\int_{(j-1)\Delta x}^{j\Delta x}\frac{dx}{a(x,t)} = u_{j-1} - u_j \qquad \text{.....(D.9)}$$

Eq.(D.7) is then approximated using a first forward approximation for $\partial u/\partial t$ and a centered finite difference approximation (the derivation of which is detailed on page 23 in Mitchell and Griffiths (1981)) for $\partial w/\partial x$. This yields:

$$\frac{u_j^{n+1}-u_j^n}{\Delta t}+O(\Delta t)=\frac{w_{j-1/2}-w_{j+1/2}}{\Delta x}+O(\Delta x^2)=A_{j+1}(u_{j+1}-u_j)-A_j(u_j-u_{j-1})+O(\Delta x^2)\ldots\text{(D.10)}$$

where

$$A_j=\frac{1}{\Delta x}\left[\int_{(j-1)\Delta x}^{j\Delta x}\frac{dx}{a(x,t)}\right]^{-1} \qquad \ldots\text{(D.11a)}$$

$$A_{j+1}=\frac{1}{\Delta x}\left[\int_{j\Delta x}^{(j+1)\Delta x}\frac{dx}{a(x,t)}\right]^{-1} \qquad \text{.....(D.11b)}$$

The advantage of the approximation described in Eqs. (D.7) through (D.11) is that it does not destroy the self adjoint nature of the operator $\partial/\partial x\ [\ a(x,t).\ \partial u/\partial x\ ]$ (Mitchell and Griffiths, 1981). Having used Eqs.(D.10) and (D.11) to relate the

approximation of the second order spatial term to the transient term, only the source term in Eq.(D.4) is left to approximate. The source term s will be approximated by evaluating it at $t = (n+\theta)\Delta t$, $x = j\Delta x$.

Now substituting the approximations Eqs.(D.6) and (D.10) as well as that for the source term into Eq. (D.5)**,** the resulting finite difference approximation for Eq.(D.4) is obtained and expressed by

$$\frac{u_j^{n+1}-u_j^n}{\Delta t}=\theta\left[A_{j+1}(u_{j+1}-u_j)-A_j(u_j-u_{j-1})+\frac{b_j}{2\Delta x}(u_{j+1}-u_{j-1})+s_j\right]_j^{n+1}+$$
$$(1-\theta)\left[A_{j+1}(u_{j+1}-u_j)-A_j(u_j-u_{j-1})+\frac{b_j}{2\Delta x}(u_{j+1}-u_{j-1})+s_j\right]_j^{n} \qquad \text{…….(D.12)}$$

Let θ =0, the final form of Eq.(D.12) becomes:

$$\frac{u_j^{n+1}-u_j^n}{\Delta t}=\left[A_{j+1}(u_{j+1}-u_j)-A_j(u_j-u_{j-1})+\frac{b_j}{2\Delta x}(u_{j+1}-u_{j-1})+s_j\right]_j^{n}$$

or $$u_j^{n+1}=u_j^n+\Delta t\left[A_{j+1}(u_{j+1}-u_j)-A_j(u_j-u_{j-1})+\left(\frac{b_j}{2\Delta x}(u_{j+1}-u_{j-1})\right)+s_j\right]_j^{n} \qquad \text{…..(D.13)}$$

Abstract

Polymer Electrolyte Membrane Fuel Cells **(PEMFC's)** have recently been the focus of intense research and development for powering the next generation of road vehicles, for distributed power generation as well as for powering small portable devices such as cellular phones and laptop computers.

Fuel Cells are electrochemical devices that directly convert the chemical energy of reactants into electricity and heat. In contrast to batteries, which are energy storage devices, fuel cells operate continuously as long as they are provided with reactant gases. In the case of a hydrogen/oxygen fuel cell, the only reaction product is water. The different types of fuel cells are distinguished by the type of electrolyte used. The Proton Exchange Membrane Fuel Cell, which is the focus of this thesis, is characterized by the use of a polymer electrolyte membrane.

In this thesis, a theoretical model is developed for the various processes that are related to the performance of a single **PEMFC**, and to study the effect of various designs and operating parameters on the fuel cell performance. A model is also developed to determine the different losses of fuel cell such as activation, ohmic, and concentration losses. The equilibrium voltage is calculated using the Nernst equation, and reaction kinetics is determined using the Butler Volmer equation. Four kinds of Nafion membranes were studied in this thesis, under same conditions for the purpose of comparison. The results are presented in the form of polarization curves.

Also, an analysis of water transport process in the membrane **(Nafion117)** of a polymer electrolyte membrane fuel cell is presented, and a model to describe this process is developed. This model takes into account the diffusion due to concentration gradients, migration due to electric gradients and convection due to pressure gradients within a membrane. This model is capable of predicting transient water concentration, voltage, and temperature profiles. The phenomena of the water transport over time is analyzed using ***a fully explicit finite difference***

method. It is found that the best working temperature is about **80 ^{0}C** for Nafion membrane PEMFC which gives the maximum cell performance. The increase of oxygen partial pressure is helpful to increase the voltage of the cell for different current intensities because of increasing the chemical activity of the reactants on the surface of the electrodes. Where, the drop in temperature of approximately **20** ^{0}C will result about a ***11.67%*** loss whereas reducing the partial pressure from **3.5** to **1.7 atm** results about a ***4.75 %*** loss. Ohmic losses increase with increasing membrane thickness due to increase the resistance of the membrane. As well as the electrical power intensity increases with increasing the operating temperature of the cell. Conversely, the heat generated decreases with increasing in the temperature because the reversible heat decreases with an increase in temperature.

In the second model, that described the water transport process in the membrane, it is found that the positive pressure gradient from cathode to anode could be used to drive water toward the anode . furthermore, the electro-osmotic drag could decrease water content and conductivity at the anode.

REFERENCES

[1] Michel A.Saad," ***Thermodynamic Principle and Practice***", pp. 694 – 697, 1994.

[2] Fuel cells 2000(online). Web: www.fuelcells.org .

[3] EG&G Services Parsons, Inc.,"***Fuel Cell Handbook*** **",** Fifth edition, Department of Energy, Office of Fossil Energy, National Energy Technology Laboratory, USA, 2000. Web: http://www.fuelcells.org /fchandbook.pdf .

[4] Mennola T.," ***Design and Experimental Characterization of Polymer Electrolyte Membrane Fuel Cells*** ", Helsinki University of Technology, Department of Engineering Physics and Mathematics, Master's Thesis, 2000.
Web: http://www.tkk.fi/Units/AES/studies/theses/mennola.pdf

[5] Richard A.," ***Modeling A 500W Polymer Electrolyte Membrane Fuel Cell*** ", Sydeny University, Master's Thesis, 2002 .

[6] Wang H., Sweikart M.A., and Turner J.A.," ***Stainless steel as bipolar plate material for polymer electrolyte membrane fuel cells*** ", J. Power Sources **,**Vol 115, PP. 243-251, 2003.

[7] Nielsen M. P., Bang M. and Bach I.," ***Modelling of Thermodynamic Fuel Cell Systems*** ", Paper, Aalborg University, Denmark, 2001.

Web: www.iet.auc.dk/~mba/papers/PaperSIMS2001.pdf

[8] Mikkola M.," ***Experimental studies on polymer electrolyte membrane fuel cell stacks*** ", Helsinki University of Technology, Master's Thesis, 2001.
Web: http://www.hut.fi/Units/AES/studies/dis/mikkola.pdf .

[9] Ritzmann A.,"***Fuel Cells: Environmentally Friendly Power for the Future***", Technical Report, Cornell University, 2003.

[10] Parthasarathy A., Srinivasan S., Appleby A. J., and Martin C. R.. "***Pressure Dependence of the Oxygen Reduction Reaction at the Platinum***

Microelectrode /Nafion Interface: Electrode Kinetics and Mass Transport ". J. Electrochemical Society, 139(10): 2856-2862, 1992.

[11] Easton E.B.," ***Chemical Modification of Fuel Cell Catalysts and Electro-chemistry of Proton Exchange Membrane Fuel Cell Electrodes*** ", PhD Thesis in Chemical Engineering, Newfoundland, Canada , 2003.

[12] Thomas S., , and Zalbowitz M.," ***Fuel Cells Green Power*** ", Los Alamos National Laboratory in Los Alamos, New Mexico, 1998.

Web: http://www.education.lanl.gov/resources/fuelcells

[13] Eaton B. M.," ***One Dimensional, Transient Model of Heat, Mass, and Charge Transfer in a Proton Exchange Membrane*** ", International Mechanical Engineering Congress and Exposition (IMECE), 2001.

[14]Wakefield E.," ***History of the Electric Automobile, Battery-Only Powered Cars*** ", Society of Automobile Engineers, USA, 1994.

[15] Berger C." ***Handbook of Fuel Cell Technology*** ", Prentice-Hall, NJ New York, 1968 .

[16] Hoogers G." ***Fuel Cell Technology Handbook*** " CRC Press, Boca Raton, FL, USA, 2003.

[17]Maggio G., Recupero V.and Pino L.," ***Modeling polymer electrolyte membrane fuel cells: an innovative approach*** ", Journal of Power Sources Vol 101, pp. 275-286, 2001.

[18] Kim J., Lee S, Srinivasan S. and Chamberlin C.E.," ***Modelling of Proton Exchange Membrane Fuel Cell Performance with an Empirical Equation*** ", Journal of the Electrochemical Society Vol 142, pp.2670-2674, 1995.

[19] Shapiro, Howard N., Michael J.Moran," ***Fundamentals of Engineering Thermodynamics*** ", John Wiley and Sons, Ltd., New York, 1995.

[20] Amphlett J.C., Baumert R.M., Mann R.F., Peppley B.A.,"***Performance Modeling of the Ballard Mark IV Solid Polymer Electrolyte Fuel Cell II. Empirical Model Development*** ", Journal of the Electrochemical Society, Vol 142, pp.9-15, 1995.

[21] Mennola T., Mikkola M., Noponen M., Hottinen T., Lund P.," ***Measurement of ohmic voltage losses in individual cells of a PEMFC stack*** ", Journal of Power Sources, Vol 112, pp 261–272, 2002.

[22] Springer T.E., Zawodzinski T.A. and Gottesfeld S.," ***Polymer Electrolyte Fuel Cell Model*** ", Journal of the Electrochemical Society, Vol 138, pp.2334-2342, 1991.

[23] Bernardi D.M. and Verbrugge M.W. " ***Mathematical Model of a Gas Diffusion Electrode Bonded to a Polymer Electrolyte*** ", Journal of AIChE, Vol 37, pp.1151-1163, 1991.

[24] Parthasarathy A., Srinivasan S., Appleby A.J., Martin C.R.,"***Temperature Dependenceof the Electrode Kinetics of Oxygen Reduction at the Platinum/Nafion® Interface – A Microelectrode Investigation*** " J. Electrochem. Soc., Vol. 139, No. 9, pp. 2530-2537, 1992.

[25] Genevey D., von Spakovsky M.R., Ellis M.W., Nelson D.J., Olsommer B., Topin F., Montel N., Siegel N.P.," ***Transient Model of the Heat, Mass and Charge Transfer as well as Electrochemistry in the Catalyst Layer of a PEMFC*** " International Mechanical Engineering Congress and Exposition (IMECE), 2002.

[26] Siegel N. P., Ellis M., Nelson D.J. and Spakovsky M.," ***Development and Validation of a Computational Model for a Proton Exchange Membrane Fuel Cell*** ", PhD Thesis in Mechanical Engineering, Virginia University, 2003.

[27] Amphlett J.C., Baumert R.M., Mann R.F., Peppley B.A. and Roberge P.R., "***Performance Modeling of the Ballard Mark IV Solid Polymer Electrolyte Fuel Cell I. Mechanistic Model Development*** ", Journal of the Electrochemical Society Vol 142, pp.1-8, 1995.

[28] Larminie J.E. and Dicks A.," ***Fuel Cell Systems Explained*** ", John Wiley & Sons, Chichester, England, 2000.

[29] Mozurkewich M.," ***Introduction to Thermodynamics: Gibbs Free Energy Changes and Chemical Equilibrium Constants*** ", Report, 2003.

[30] Rayment C., Sherwin S.," ***Introduction to Fuel Cell Technology*** ", University of Notre Dame, USA, 2003.

[31] Le Chateliers," ***The hydrogen fuel cell power system*** ", 1999.
Web: < www.spinglass.net/scooters/pdf/ch3c.pdf >.

[32] Brady J.E. and Holum J.R.," ***Chemistry, The Study of Matter and Its Changes***", John Wiley & Sons, Brisbane, Australia, 1996.

[33] Benson R.S," ***Advanced Engineering Thermodynamics*** ", Second Edition, 1976.

[34] Bockris J., Srinivasan S.," ***Fuel cells, their electrochemistry*** ", McGraw-Hill Book Co., New York, 1969.

[35] Ryan O'Hayre,Tibor Fabian, Sang Joon Lee, and Fritz B. Prinza, "***Lateral Ionic Conduction in Planar Array Fuel Cells*** ", Journal of The Electrochemical Society,Vol. 150(4), pp 430-438 , 2003.

[36]Canaday J.D., Wheat T.A., Kuriakose A. K. and Ahmad A.," ***A polarization Model for Solid Electrolyte Fuel Cell*** ", International Journal of Hydrogen Energy, Vol 12, No.3, pp151-157, 1987.

[37] Appleby A., Foulkes F., " ***Fuel Cell Handbook*** ", Van Nostrand Reinhold, New York, USA, 1989.

[38] Tanja K.," ***Electrode Kinetics*** ", Helsinki University of Technology, Department of Chemical Technology, pp 1-18, 2001(written in Finnish)

[39] Sukkee Um., Wang C.Y., and Chenb K. S.," ***Computational Fluid Dynamics Modeling of Proton Exchange Membrane Fuel Cells*** ", Journal of the Electrochemical Society, Vol. 147, No. 12, pp. 4485-4493, (2000).

[40] Berning T., and Djilali N., "***Three-Dimensional Computational Analysis of Transport Phenomena in a PEM Fuel Cell*** ", J. Power Sources ,Vol 116 , 2002.

[41] Hyunchul J., Hua M., Wang C.Y.,"***A single-phase non-isothermal model for PEM fuel cells***", International Journal of Heat and Mass Transfer, Vol.48, pp1303-1315, 2005.

[42] Musser J., Wang C.Y.," ***HEAT TRANSFER IN A FUEL CELL ENGINE***", Proceedings of the ASME Fuel Cell Division, 34th National Heat Transfer Conference, 2000.

[43] Candusso D., Rullière E. and Toutain E., "***A Fuel Cell Hybrid Power Source for a Small Electric Vehicle*** ", Rev. Energ. Ren. , Power Engineering, pp 85-92, 2001.

[44] Bird R. B., Stewart W. E., and Lightfoot E. N., "***Transport Phenomena***", Wiley International Edition, New York, 1960.

[**45**] Sui,P.C. and N. Djilali, " **Analysis of Water Transport in Proton Exchange Membranes using a Phenomenological Model**", ASME J. Fuel Cell Science & Technology, in print 2005.

[46] Mitchell A.R., Griffiths D.F.," ***The Finite Difference Method in Partial Differential Equations*** ", John Wiley & Sons, NY, 1981.

[47] Benziger J.B., Moxley J., Tulyani S., Turner A.," ***The Autohumidification Polymer Electrolyte Membrane Fuel Cell*** ", Journal of AICHE, 2003.

[48] Fuqiang Li., Baolian Yi., Danmin Xing, Jingrong Yu, Huamin Zhang," ***Nafion/PTFE composite membranes for fuel cell applications*** " Journal of Membrane Science Vol.212, 213–223, 2003.

الخلاصة

لقد تركزت البحوث مؤخرا حول خلايا وقود غشاء التبادل ألبروتوني(PEMFC's) لتشغيل الجيل القادم من سـيارات الطريق، محطات التوليد بالإضافة إلى الأجهزة الصغيرة كالهواتف الخلوية وأجهزة الحاسوب النقال والمركبات الفضائية.

أن خلايا الوقود هي عبارة عن أجهزة كهر وكيميائية تقوم بتحويل الطاقة الكيميائية للمتفاعلات إلى كهرباء وحرارة بصورة مباشرة، بالمقارنة مع البطاريات، والتي هي بدورها أجهزة خزن للطاقة. أن خلايا الوقود تعمل باستمرار طالما يـتم تزويدها بالغازات المتفاعلة. أن الماء هو الناتج الوحيدة لخلية الوقـود التـي تعمـل بغـازي الأوكـسجين والهيـدروجين (Hydrogen/Oxygen Fuel Cell). تختلف خلايا الوقود عن بعضها البعض حسب نوع الالكتروليت المستخدم (صـلب أو سائل). وقد تركزت هذه الدراسة على خلية الوقود ذات غشاء التبادل ألبروتـوني (Proton Exchange Membrane Fuel Cell).

في هذا البحث، تم تطوير الموديل النظري ليتعامل مع العمليات المختلف والمتعلقة بأداء خليـة الوقـود ذات الغـشاء التبادل ألبروتوني المنفردة ، ولدراسة العوامل التشغيلية والتصميمية المختلفة والتي تؤثر على أداء خلية الوقود. بالإضـافة إلى ذالك، تم تطوير موديل الخسائر لكامل خلية الوقود والذي يأخذ بنظر الاعتبار خسائر التنشيط ، خسائر الأومية ، وخسائر الانتشار. أن فولتية الخلية تحسب باستخدام معادلة نرنست (Nernst)، أما حركيات التفاعل فتحسب باستخدام معادلة بوتلر فولمر (Butler Volmer Equation). تحت نفس الظروف ولغرض المقارنة، استخدمت أربع أنواع من أغشية من نوع النافيون (Nafion) في هذه الدراسة.

بالإضافة إلى ذالك، تم تحليل عمليات نقل الماء والبروتون داخل الغشاء (Nafion117) لخلية الوقود غشاء التبـادل لبروتوني، وتم وصف هذه العمليات ضمن الموديل. هذا الموديل يأخذ بنظر الاعتبار الانتشار الناتج عن تدرج التركيـز بـين الأنود والكاثود ، الارتحال الأيوني الناتج عن التدرج الكهربائي، والحمل الناتج عن تدرج الضغط . أن هذا الموديـل يحـل عدديا معادلات الطاقة و التركيز باستخدام طريقة الاخـتلاف الواضـح المحـدد (a fully explicit finite difference method) مع الزمن.

وجد ان افضل درجة حرارة حوالي ٨٠ ^{0}م لخلية الوقود ولتي تعطي أفضل أداء. ان زيادة ضغط الأوكسجين ألجزيئي يساعد على زيادة فولتية الخلية عند مختلف التيارات بسبب زيادة الفعالية الكيميائية للمتفاعلات على سطح الأقطـاب. فمـثلا عند زيادة درجة حرارة بحدود ٢٠ ^{0}م سوف يؤدي الى ربح بالفولتيـة بحـدود ١١,٦٧% فـي حـين ان ارتفـاع ضـغط الأوكسجين ألجزيئي من ١,٧ - ٣,٥ جوي يؤدي الى ربح بحدود ٤,٧٥ % . ان الخسائر الأومية تزداد مـع زيـادة سـمك الغشاء نتيجة لزيادة مقاومته. بالإضافة إلى ذالك، تزداد شدة القدرة الكهربائية مع زيادة درجة الحرارة التشغيلية وبالعكس تقل الحرارة المتولدة مع زيادة درجة الحرارة بسبب نقصان الحرارة الرجوعية.

الموديل الثاني، والذي يصف عملية انتقال الماء خلال الغشاء من نوع النـافيون ١١٧، وجـد ان تـدرج الـضغط الموجب(من الكاثود الى الأنود) يسحب جزيئة الماء باتجاه الانود وبالتالي يزداد محتوى الماء الغـشائي والنتيجـة زيـادة موصليه . بالإضافة إلى ذالك، ان زيادة التيار المسحوب يزيد من الإعاقة الكهروتناضية ولتي بدورها سوف تقلل من محتوى الماء الغشائي وبالتالي تقليل موصليه.

جمهورية العراق
وزارة التعليم العالي
والبحث العلمي

تطوير موديل للتحليل الثرموديناميكي لخلية الوقود التي تعمل على الهيدروجين-الأوكسجين

رسالة
مقدمة إلى كلية الهندسة في جامعة بابل
كجزء من متطلبات نيل درجة ماجستير علوم
في الهندسة الميكانيكية

أعدت من قبل
المهند س

قصي رشيد عبد الأمير الحجاج
بكالوريوس هندسة ميكانيكية

مايس، ٢٠٠٥